XFEL.EU TR-2024-001

INSTRUMENT REVIEW REPORT

High Energy Density *and* Helmholtz International Beamline for Extreme Fields (HED-HIBEF)

February 2024

U. Zastrau

for the HED-HIBEF team

at European XFEL

European X-Ray Free-Electron Laser Facility GmbH

Holzkoppel 4

22869 Schenefeld

Germany

Contents

Preamble

This instrument review report describes the status of HED-HIBEF, the High Energy Density (HED) instrument at the European X-Ray Free-Electron Laser (EuXFEL) facility in Schenefeld, Germany, augmented and completed by the contributions of the Helmholtz International Beamline for Extreme Fields (HIBEF). While EuXFEL obtained first X-ray lasing in May 2017, HED-HIBEF only started user operation in May 2019 and will be reviewed for the first time in March 2024. The review report follows a standard template describing the instrument features, specifications, and performance. The staff profile and scientific output are outlined as well as the user statistics. Future development plans and directions are also discussed. A thorough review article of the HED-HIBEF instrument was published three years ago (U. Zastrau *et al.*, 2021 [1]). Consequently, this report concentrates only on new developments, recent scientific output and performance, open issues, and the future strategy with respect to the scientific landscape at EuXFEL and worldwide.

HIBEF is an international user consortium led by the Helmholtz-Centre Dresden-Rossendorf; additional funding members are DESY and the Central Laser Facility (CLF), UK. HIBEF contributes experimental drivers to the HED beamline such as the optical laser ReLaX and DiPOLE-100X, the diamond anvil cell setup, and the pulsed magnetic field experiment. Additionally, HIBEF personnel are responsible for the operation and maintenance of these devices and also participate in normal EuXFEL user operation. In return, HIBEF members are eligible for priority access to HED-HIBEF to advance their programmatic scientific research and community building.

The report can be downloaded from the links below:

- **HED-HIBEF review report**
  https://syncandshare.xfel.eu/index.php/s/HWoN9yaQWpaM6p3
- **European XFEL website**
  https://www.xfel.eu/
- **HED-HIBEF instrument pages**
  https://www.xfel.eu/facility/instruments/hed/
- **European XFEL publication database**
  https://xfel.tind.io/record/3346

Additional information regarding EuXFEL and HED-HIBEF are also available.

Versions

This document is written in LaTeX following the European XFEL common style and report class, and using the Overleaf™ editor.

For further information, please contact Ulf Zastrau <ulf.zastrau@xfel.eu>.

Version 0.1

Release date: 12 Sep. 2023

Improvements and changes:

- Started the project in Overleaf
- Set up the chapter structure of the report as given in the template

Version 0.5

Release date: 3 Dec. 2023

Improvements and changes:

- Chapters 1, 2, 6, 7 written
- Shared draft with HED-HIBEF group

Version 1.0

Release date: 19 Dec. 2023

Improvements and changes:

- Finished all chapters
- Asked group for feedback by 20 Jan. 2024

Version 2.0

Release date: 25 Jan. 2024

Improvements and changes:

- HED-HIBEF group made changes and improvements
- Revision by Toma Toncian
- Incorporated remarks by EuXFEL Scientific Director Sakura Pascarelli

Version 2.5

Release date: 16 Feb. 2024

Improvements and changes:

- proof-read by Kurt Amend, improved formatting and indexing
- Incorporated remarks by EuXFEL department heads Steve Aplin and Harald Sinn.

Version 3.0

Release date: 18 Feb. 2024

Improvements and changes:

- final touches by Ulf Zastrau

1 HED-HIBEF overview

This chapter describes the High Energy Density (HED) instrument, including its HIBEF User Consortium (UC) contributions (HED-HIBEF) [1; 2; 3], at the European XFEL (EuXFEL) [4; 5]. HED-HIBEF is located at the SASE 2 undulator beamline and started user operation in May 2019. The instrument specializes in applications of hard X-ray FEL pulses in the investigation of dynamics of extreme high energy-density states, addressing a multitude of science questions, ranging from femtosecond laser plasma science in bulk and on surfaces, to X-ray isochoric heating and atomic physics in warm dense matter, to high-pressure phenomena in shock waves and under hydrodynamic compression, to cryogenic materials in strong pulsed magnetic fields.

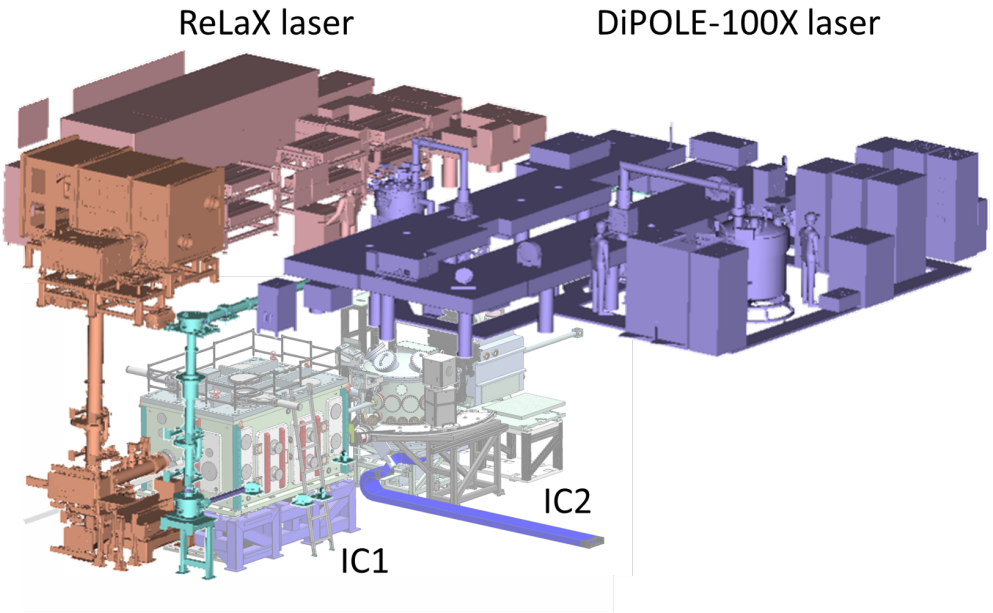

Figure 1.1: Schematics showing the HED-HIBEF instrument. The ReLaX and DiPOLE 100-X lasers are located above the experiment hutch with the interaction chambers IC1, 2 (walls not shown).

The X-ray techniques used at HED-HIBEF are often based on using intense X-rays to pump or probe samples, or on exploiting the unique capability of MHz pulse trains at hard X-ray energies to time-resolved sub-millisecond phenomena. The experimental X-ray techniques comprise pump–probe imaging, small- and wide-angle diffraction, emission spectroscopy, and inelastic scattering. These are complemented by optical techniques, such as streaked optical pyrometry (SOP), the velocity interferometer

system for any reflector (VISAR), or Fourier-Domain Interferometry (FDI). The main setups at the HED-HIBEF instrument are first a target chamber (IC1) where all drivers can be combined, and a versatile second interaction area, optimized for X-ray diffraction, where a second chamber (IC2) can be set up for either diamond anvil cell (DAC) or laser shock experiments. Alternatively to IC2, user-supplied equipment or a goniometer for pulsed magnetic field experiments can be fielded. The setup in the IC1 and IC2 chambers can be all-in-vacuum with no windows, or featuring a sample environment in air with beam transparent diamond or Kapton windows to separate the vacuum sections. An extensive overview of HED's instrumentation and capabilities are given in Ref. [1].

1.1 X-ray beam transport

The main outline of the SASE 2 beamline and HED instrument shown in Fig. 1.2 are described in the Technical Design Report (TDR) from 2014 [3] and in the recent instrument review article from 2021 [1]. Here, we focus on updates of components and functionalities that we have developed in the last three years.

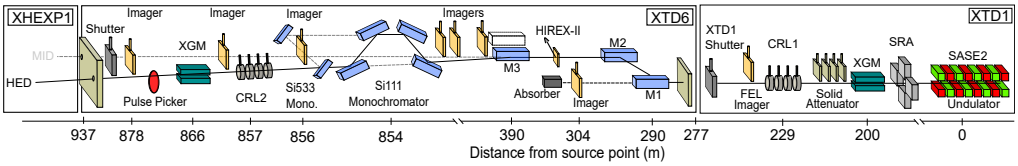

Figure 1.2: Beam transport in the XTD1 and XTD6 underground tunnels up to EuXFEL Experiment Hall 1 (XHEXP1). The X-rays enter from the right. Not all components are shown. A detailed list of devices and distances can be found in [1].

1.1.1 Horizontal offset mirrors and beam stabilization

Ultrabright femtosecond (fs) X-ray pulses are generated via self-amplified spontaneous emission (SASE) in the SASE 2 undulator system consisting of 35 insertion devices of 5 m magnetic length each. The nominal source point defining distances along the photon beamline is set to the middle of 33^{rd} insertion device.

Since 2022, reference marks exist at the FEL imager right after the undulators, to which the X-ray beam pointing is adjusted before the X-rays are handed over to the instruments for further beamline alignment. This should allow the instrument to arrive at standard positions of mirrors and beamline optics.

After exiting the SASE 2 undulator, the beam passes the spontaneous radiation

aperture (SRA), the X-ray gas monitor (XGM), a solid-state attenuator, and compound refractive lens unit 1 (CRL1), all located in the XTD1 tunnel. Further beam transport towards the HED instrument is performed by the horizontal offset mirrors M1 and M2 located at 290 m and 301 m from the source in the XTD6 photon tunnel, as well as the M3 deflection mirror. The offset mirrors are part of the radiation safety concept of the EuXFEL. Their purpose is to separate the SASE beam from the bright spontaneous background and bremsstrahlung radiation that also can be generated in the undulator, as well as to reject higher harmonics of the fundamental SASE depending on angle of incidence. The X-ray mirrors are aligned to a grazing incidence angle in a range of 1.1 – 3.6 mrad which results in a horizontal beam offset between 25 mm and 85 mm that is required to bypass a safety absorber. Each Si mirror has 0.9 m optical length (polished surface) and features both Pt and B_4C coated stripes [6]. The B_4C stripe is used to transport the X-ray FEL beam in a 5 – 14 keV photon energy range, while Pt is suited for a harder X-ray range of 14 – 25 keV, and is reflective even above 50 keV [7] (see Section 4.1.4). The second mirror M2 is equipped with mechanics for a slight meridional bending to enable adjustment of the horizontal beam size at the instrument.

After M1 and M2, a third mirror, M3, can be inserted to switch the beam to the HED branch with a fixed incidence angle of 1.3 mrad set by the offset of the MID and HED hutches. To ensure a consistent beam axis downstream of M3 towards the HED instrument, the lateral position of the M3 mirror is fixed regardless of the angle settings of M1 and M2, and the beam is brought to HED by pitching M2 slightly. Due to the large distances involved (~ 100 m), the difference in incidence angles on M1 and M2 from this process is negligible .

A mirror feedback system keeps the beam stable by monitoring beam motions on a transmissive beam imager based on a thin diamond screen positioned between M2 and M3 [8] and by acting on a piezo motor that adjusts the pitch angle of M2 slightly to counteract long-term drifts. This beam motion is even smaller if subsequent 10 Hz pulses or even pulses within a train are considered because an electron feedback mechanism of the linear accelerator (linac) is acting within the train. The horizontal jitter of the unfocused beam is of order 100 µm rms with peak values of 0.5 to 1 times its diameter of typically 0.5 mm. When focused tightly, the jitter is practically suppressed. In the vertical direction, the beam pointing fluctuation is about a factor of 10 smaller than that in the horizontal, so no feedback system is implemented.

We suspect that the horizontal beam pointing fluctuation could originate from several sources, including the M3 mirror. The attempt to compensate all horizontal drifts solely with the M2 pitch can lead to beam clipping on M3, which decreases transmission and introduces diffraction from the edge. Therefore, we also operate

independent feedback on the M3 mirror using an imager much further downstream. This scheme is adopted from the optical alignment scheme with two mirrors and two apertures and shows superior performance compared to single feedback on M2.

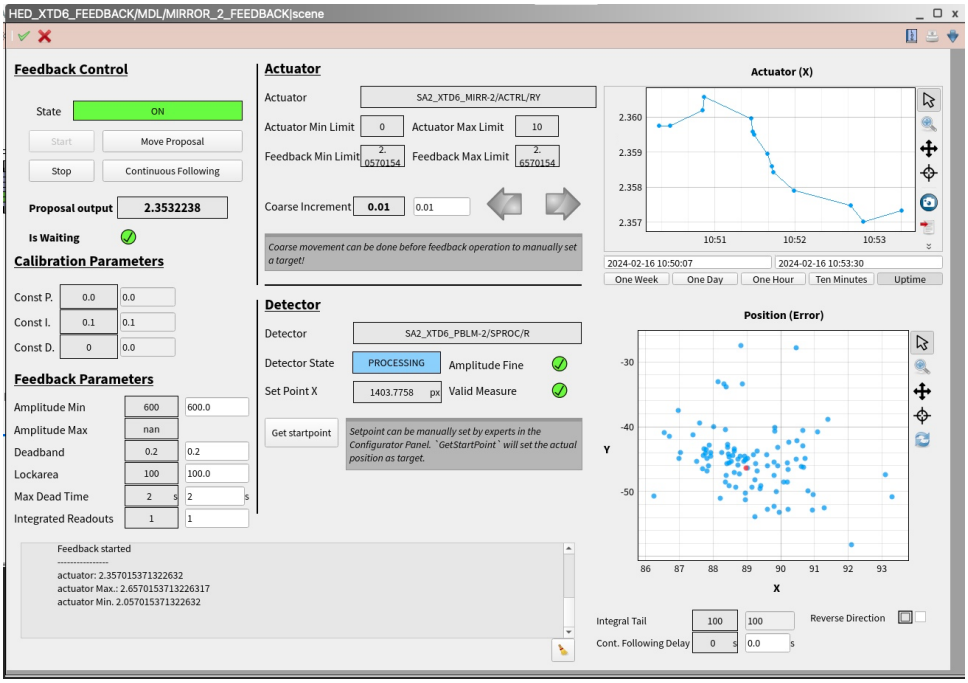

Figure 1.3: Screenshot of the GUI for active M2 beam stabilization at HED, showing how piezo actuators act on the M2 mirror to compensate for beam movements. A similar feedback exists for the M3 mirror stabilization.

1.1.2 Beam imagers

Beam transport and alignment of optical components require high-resolution monitoring of the position and profile of the SASE beam. Therefore, imaging tools are necessary at different locations along the beam path to provide time-resolved images of the beam cross-section. The imagers have to be removable and provide large enough field of view to measure beam offsets after optical elements, such as offset mirrors, monochromators, etc. The concept of retractable imagers, known as *pop-in* monitors, has been implemented at the EuXFEL featuring an optical camera recording images of the beam produced by a scintillator screen. Yttrium aluminium garnet (YAG) as well as boron-doped chemical vapour deposited (CVD) diamond are commonly utilized screen materials since they yield an almost linear optical response to the X-ray beam intensity. Thin diamond screens provide only little beam attenuation and can be kept in during operation, enabling for instance the mirror feedback loop described in Section 1.1.1.

1.1.3 X-ray attenuators

The HED beamline includes two attenuator units—in the XTD1 tunnel (Fig. 1.2) and the HED optics hutch (Fig. 1.8)—which serve to adjust the X-ray FEL beam intensity on the downstream optical components and/or on the sample. They are based on foils and thin plates of Si, B_4C, and diamond that can be inserted in the beam. Upgrade of the devices to better attenuate high photon energies (above ~20 keV) is beneficial if this operation mode becomes more demanded. If the SASE 2 undulator is upgraded with an afterburner to provide SASE beams up to ~70 keV [9], an attenuator upgrade is mandatory (see Section 4.1.4).

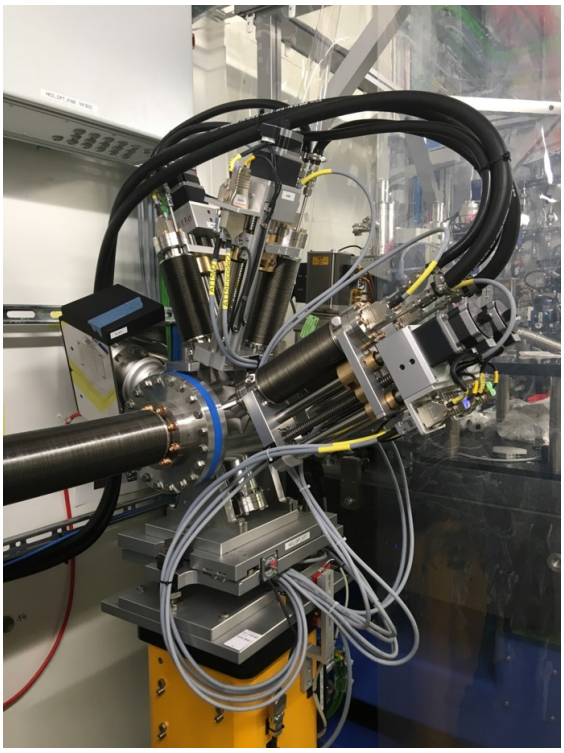

Figure 1.4: Photograph of an attenuator vessel in the HED optics hutch. Visible are the three water-cooled actuator arms. The box in the left-back is an ion pump.

Initially, we used the upstream attenuators right after the undulators in the XTD1 tunnel, as they react fast via pneumatic actuators. However, attenuating the beam so early in the beamline causes the active beam stabilization to fail. By improving the motor speed in the HED optics hutch attenuators (Fig. 1.4), optimizing their choice of filters (now only silicon and diamond of thicknesses between 3.2 mm and 25 µm, see Fig. 1.5), and developing a smart control panel where the user can simply select the attenuation level, we now use this attenuator ~ 10 m upstream of the experiment chamber and maintain active beam stabilization (see Section 1.1.1).

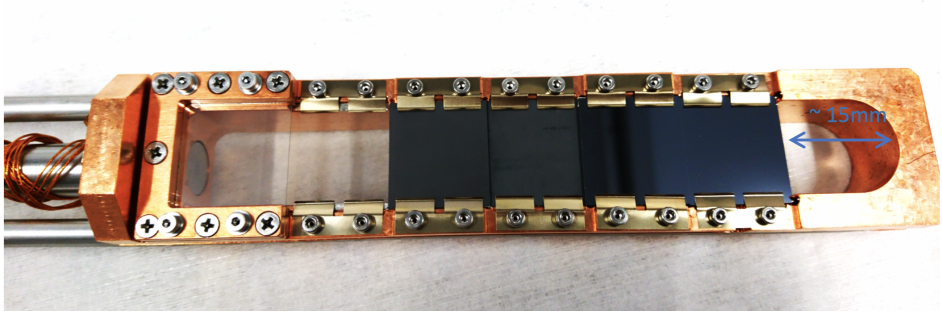

Figure 1.5: Photograph of an attenuator arm in the HED optics hutch. Three of these arms are installed.

1.1.4 Slit systems

The water-cooled power slits (PSLITs) at the beginning of the optics (Fig. **??**) hutch reduce stray light and allow proper filling of the subsequent CRL aperture without beam leakage around the CRLs.

The clean-up slits (CSLITs) that are installed in the experiment hutch right before the IC1 chamber are regularly used to clean up diffraction from upstream slits, lenses, and attenuators. After the beam axis and focusing is optimized, they are closed just around the wings of the primary beam.

In order to clean up the small angle scattering signal in related experiments (ReLaX standard configuration, Section 1.3.1), another slit system can be installed even closer to the target (SmarAct slits, SSLIT). It is mounted on a movable post in IC1 when needed.

1.1.5 Pulse and train on demand

The linac delivers single pulses or bunch trains at 10 Hz, and the driver lasers run at a fixed repetition rate (PP laser 10 Hz, ReLaX 5 Hz, Dipole 1–10 Hz). As both X-rays and drive lasers are destructive for the sample, we needed to develop a scheme to deliver a single pulse (or train) together with the ability to trigger the lasers, detectors, and other drivers to that event. While it is possible to deliver single X-ray bunches by interrupting the injection of electrons into the accelerator, the lack of feedback for the electrons in the undulators rapidly causes drifts of several parameters, in particular in case of relative low duty cycles, as in most of our experiments. A single pulse triggered after several minutes of “zero bunches” is therefore likely weak in pulse energy and off in pointing.

To mitigate this issue, we have a pulse picker unit (PPU) in the beamline that typically blocks the beam path while the X-ray FEL delivers 10 Hz pulses with all feedback running. The fast rotating disk can then select deterministically by trainID a single train or multiple trains at 10 Hz. In this scheme, the feedback remains uninterrupted, and just the X-rays are blocked at the end of the tunnel.

In order to synchronize the opening of the pulse picker with other drivers, we, together with the EEE group at EuXFEL, developed the possibility to trigger the movement of the PPU deterministic on a given trainID. This system was extended to all drivers (dDAC, laser heated DAC, ReLaX, PP laser, DiPOLE, pulsed magnetic field) and sample motors allowing to trigger all components individually on predefined trainIDs and allow complex shot sequences if required. It can also synchronize to special accelerator modes (long pulse train for HED every 100 trains) and integrate drivers running on subharmonics (e.g. DiPOLE 100X at 1 Hz).

1.1.6 Photon beamline transmission

The X-Ray Photon Diagnostics (XPD) group of EuXFEL operates two X-ray gas monitors (XGMs), which yield absolutely calibrated X-ray pulse energies [10]. Directly after the SASE 2 undulators and before the first set of attenuators, there is the first XGM (in XTD1). The HED branch has an additional XGM, which allows to directly observe the transmission after the M1–M3 mirrors and identifies potential clipping on apertures or other obstacles in the beam path (see Fig. 1.2). Typical values for the offset and distribution mirror transmission from experiments in 2022 and 2023 sorted by X-ray energy lie between 56 and 87%, with $\geq$ 80% transmission achieved for moderate photon energies of $9 - 18$ keV.

In the optics and experiment hutches, highly transmissive diamond screens can be inserted which backscatter a small fraction of the X-rays into an array of diodes called intensity pulse monitors (IPM). The IPMs backscatter X-rays into a diode array and potentially yield beam position information in addition to intensity values. In order to achieve this, the diodes are mounted in a horizontal pair and a vertical pair. These can record the relative intensity of X-ray pulses, even in a MHz train, as they are coupled to fast analogue-to-digital converters. Theoretically, a beam position being off-centre would give rise to an imbalance between opposite channels. In practice, this position-sensitivity was within the noise level. Therefore, in 2023, we redesigned a second version of the IMP1 in the optics hutch and fitted it with collimators, so that each diode is only sensitive to one quadrant of the scattering screen. The first tests indicate that now the signal is too low in general, and the acceptance of the collimators has to be increased. After we arrive at a working solution of this IPM, we

plan to apply the same upgrade to the IPM2, which is located between the CSLITs and the IC1 chamber.

Table 1.1: Transmission of HED beamline in photon tunnels.

Proposal	Photon energy	Mode	Mirror transmission
3121	7 keV	HXRSS	70%
4491	7.9 keV	SASE	76%
4493	8.2 keV	SASE	75%
3082	9 keV	SASE	84%
2806	9-10 keV	SASE	86%
2804	13 keV	SASE	87%
2758	14 keV	SASE	82%
3076	18 keV	SASE	70%
4520	18.8 keV	SASE	80%
3406	20 keV	SASE	56%
3248	24 keV	SASE	60%

Likewise, X-ray diodes with different sensitivities are installed just before the IC1 chamber as well as in the instrument beamstop (IBS, Fig. 1.8). We plan to upgrade these devices to obtain position information of the beam from the difference between pairs of diodes using collimators on the diodes. In order to cross-reference these relative diode readings to absolute values, for each beamtime and for each photon energy change, all optical elements are removed from the beam in between the absolutely calibrated XGM in the XTD6 tunnel and these diodes. The resulting conversion factors are then determined. By inserting attenuators, slits, or CRLs the effective transmission can be tracked for each X-ray train.

1.1.7 SEPS interlock and additional tunnel shutter

The powerful X-ray beam was found to be able to drill through a centimetre of steel and other materials within a few seconds if run in pulse train mode and properly focused. An analysis showed that there exist potential combinations of CRLs and photon energy that could penetrate the safety beam shutters at the end of the XTD6 tunnel (focused by CRL2 in XTD6) and the beam shutter between the HED optics and experiment hutch as well as the beamstop at the end of the HED photon beamline (focused by CRL3 in the optics hutch). Immediate measures were taken to prohibit the use of CRL2 completely, to disconnect some arms of CRL3, and to administratively restrict the number of bunches and the pulse energy to certain levels depending on the photon energy.

In 2021, a safety equipment protection system (SEPS) was installed, that recognizes the out-of-beam position of each CRL arm independently from motor positions. The signal was integrated into shutter operation. In addition, all beam shutters were retrofitted with burn-through detectors that would shut off the beam in case of a drill-through event. This allowed to release the earlier restrictions and explore the full capability of the EuXFEL. However, certain restrictions remained: it was not allowed to close the beam shutters when CRL lenses are inserted. This action is necessary to enter the hutch. In order to close the shutters, one has to first retract all the lenses. Unfortunately, the actuators on all CRL vacuum chambers (see Section 1.1.10), which position the lens cassettes into the beam, do not work reproducibly enough to re-establish the meticulously adjusted focusing conditions.

One crude solution was to switch the accelerator to *zero bunches* instead, but that means no electrons in the undulators and the feedback to maintain SASE lasing can drift, with alignment being lost after a few minutes, which reduces the pulse energy and makes re-tuning necessary. However, together with the X-Ray Optics (XRO) group of EuXFEL, we developed and installed an additional pre-absorber in 2023 installed directly after CRL2 in the XTD6 tunnel. The focal length of CRL2 is larger than the distance to this shutter, making it impossible to focus on and damage it. This pre-absorber can now be closed to safely block the beam when using CRL2. A further upgrade to the SEPS interlock allows CRL3 to remain inserted when the shutter before it (or the pre-absorber) is fully closed. The M3 mirror feedback is fed with position data from a built-in screen from this shutter. Consequently, full operation of the CRL lenses at all photon energies is now possible.

1.1.8 HIREX-II

A bent-crystal spectrometer HIREX II [11] can be inserted into the beam, upstream of the M3 mirror that is splitting the MID and HED branches (see Section1.2). At SASE 2, HIREX is mainly used for hard X-ray self-seeding (HXRSS) tuning and is operated either by EuXFEL's X-Ray Diagnostics group, the accelerator group at DESY (MXL), or the instrument. HED-HIBEF itself is equipped with two additional bent-crystal spectrometers that can be fielded behind the sample and can yield similar information but not in MHz resolved mode (for details, see Ref. [1]).

1.1.9 Si crystal monochromators

X-ray optics are essential for X-ray FEL experiments, similar to synchrotron radiation requirements, but operation of optics devices is much more challenging at the

EuXFEL. The impact of a single pulse is huge and can lead to melting or ablation of most materials. Moreover, the pulse-trains pose a special challenge for X-ray optics in terms of heat load since most X-ray induced heating processes of relevance are adiabatic or near-adiabatic over the timescale of a train (up to 600 µs). This accumulation of heat in a train is challenging, even if most cooling systems and simple heat diffusion are sufficient to restore the temperature in the 99.4 ms before the next train arrives. Many of these effects have been predicted beforehand and modelled in detail [2; 3; 12; 7], but the impact on daily operation is still problematic, for instance concerning standard cryo-cooled Si monochromators [13].

Moving to diamond-based optics is promising and there is a funded EuXFEL R&D project aiming to develop and use diamond monochromators [14] and diamond CRLs.

Many experiments at HED require reducing the intrinsic SASE bandwidth of $\sim 10^{-3}$. For this purpose, the HED layout includes two double-crystal monochromator devices using Si(111) reflections and two channel-cuts that use either Si(533) or Si(931) reflections (see Fig. 1.2). The mechanical design of the Si(111) monochromators is based on an artificial channel-cut monochromator (ACCM) concept [15; 16] with a sine-bar actuator, a design adopted from an APS synchrotron in-air design. An ACCM permits the crystal surfaces to be polished individually before mounting in a crystal cage. This leads to a better surface finish than for monolithic channel-cut crystals that are more commonly used. The MHz repetition rate of the EuXFEL poses particular challenges for Si optics that operate with tight tolerances in order to maintain the dynamical diffraction conditions. In particular, the Darwin curve degrades quickly inside a pulse train, even if cryogenic cooling to ~100 K is applied [13], reducing the monochromator's transmission. In the waiting time before the next train arrives, the crystal shape is restored and the situation is repeated with the next pulse train. Permanent damage to the crystals can be avoided, but the above-mentioned deterioration of transmission inside a train cannot, unless the beam is strongly attenuated or only a few pulses per train are used. An additional challenge is the availability of a broad photon energy range during a monochromator alignment shift: the present design requires edge scans at at least four different edges in order to characterize correctly the energy scale with respect to the ACCM movement and also iterative alignment of the crystal roll at photon energies far apart. With energy changes taking one hour of machine time, this iterative process demands significant alignment time. In addition, the required photon energies might not be reached because of restrictions imposed by the electron energy mode.

Hard X-ray self-seeding (HXRSS), which is available at SASE 2, is a mode that combines a highly monochromatic beam (bandwidth $\sim 10^{-4}$) with single pulse or MHz repetition rate and >1000 pulses/s. Nevertheless, a so-called SASE pedestal remains

in the spectrum, which can be a strongly limiting factor for IXS or resonant methods.

When the cryogenic cooling is active, we observe a strong additional beam jitter in both vertical and horizontal directions, a malfunction that does not occur with the MID and FXE monochromators, despite being almost identical in design. The EuXFEL Vacuum and XRO groups performed numerous investigations, however a final explanation or solution could not be identified yet. As time for tests is limited and user operation has priority, for now we use the Si(111) monochromators at room temperature.

The relative adjustment of the quasi channel-cut crystals in one mono stage is done with a pico motor (slip-stick, for coarse alignment) and a piezo pusher (fine alignment). There are no absolute encoders since the initial design assumed that, once aligned, these motors would be disconnected and never touched again. In reality, different heat loads on the first crystal—dependent on repetition rate and number of bunches—and potential mechanical drifts during cryogenic cooling make frequent realignment necessary, and without an encoder this is unreliable and not reproducible. The XRO group is looking into ways to replace the pico motor by a stepper motor with at least a motor-axis mounted encoder, within the framework of a monochromator upgrade project. To fit a target encoder (attached to the moving equipment rather than the motor axis) is deemed too ambitious to retrofit to the existing mechanical design and while the monochromator vessel is installed in the photon tunnel.

A design feature of the second pair of Si(111) crystal is that its relative adjustment of the Bragg angle is applied also on the first crystal, which makes subsequent adjustment of all four reflections impossible. Therefore, if no transmission of the second pair is observed, scanning the Bragg angle of the second crystal has to be done via ACCM while compensating the resulting motion of the first crystal with the pitch adjustment (pico motor and piezo, which move unreliably).

High X-ray intensity due to too small beam sizes during commissioning and troubleshooting led to heat damage (melting and crater formation) on the first crystal of the first mono stage. This crystal was replaced by a new one in the winter maintenance period 2023–2024.

1.1.10 Compound refractive Beryllium lenses

The natural divergence of SASE radiation is very low, between 0.5 mrad and 2 mrad, depending on the photon energy and linac parameters [7; 17]. However, due to the long beam transport sections of the EuXFEL (on the order of 1 km) the beam size can

exceed 1 mm at the experiment stations, which is unacceptable for many experiments at HED. Furthermore, the beam size can already be too large at the position of the M3 mirror (390 m from the source) and lead to clipping, resulting in transmission losses and diffractive artifacts. Therefore, the SASE beam needs to be collimated, which can be achieved using transmissive X-ray optics based on Be compound refractive lenses (CRLs) [18]. For this purpose, two CRL units (CRL1 and CRL2) have been installed in the tunnel. A third CRL chamber which translates along the beam axis, is installed in the HED optics hutch (CRL3). All CRL units would benefit from an upgrade in the future aiming at better alignment flexibility and reproducibility of the individual lens stacks.

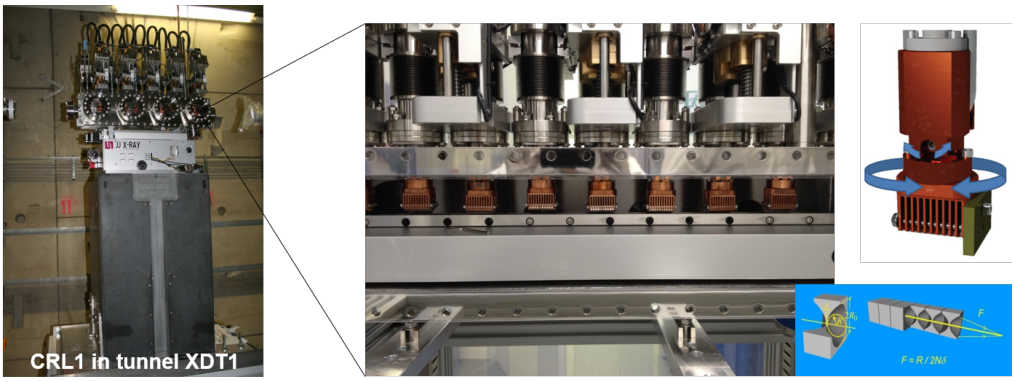

Figure 1.6: Left: The vacuum vessel containing the first CRL set right downstream of the undulators. **Centre:** View into to opened vacuum chamber, showing Cu comps holding and cooling the individual CRLs. **Right:** CAD representation of a single holder.

The lenses at HED can be used in various combinations at photon energies between 5 and 25 keV to deliver a collimated beam with ultralow nano-radian divergence and ~ 0.5 mm diameter to the instrument, or to create diffraction-limited foci of 100s of microns (CRL1), 10s of microns (CRL2), or a few microns (CRL3) at the sample position. Moreover, different lens choices can assure proper illumination of subsequent lens unit apertures. CRL1 alone can even cause an intermediate focus point in the photon transport in the tunnel. Further information about CRLs and their use at HED can be found in Ref [1].

In order to provide sub-micron beam size at the sample position, a nano-focusing CRL setup [19] has been implemented, sometimes referred to as CRL4. It uses sets of lenses a few 10s of cm before or after the sample position in the interaction chambers. More details about their application can be found in Sections 1.3.2, 3.3.5, and 3.3.6.

A *Python* GUI has been created and further developed that allows beam diameters

and foci along the HED beamline and the experiment hutch as a function of photon energy, source point, divergence, CRL lens configurations, finite bandwidth (SASE, HXRSS), and two-colour mode to be tracked. However, we discovered that, even for the same photon energy, the position of the source point within the undulators changes depending on the day-to-day performance, how X-ray lasing is set up or tuned, and how many undulators participate in the lasing process until saturation. This fact requires that, first, the position of the source point and divergence is measured. We do this by inserting a collimating lens with known refractive power right after the undulators (CRL1) and then measuring the beam size before the lens and further downstream. Once this is known, we can select an appropriate combination of lenses to achieve the desired focus at TCC.

1.1.11 X-ray focus size determination

Since 2019, we have conducted several experimental campaigns to explore and determine the most suitable method to characterize the focus of the X-ray beam.

The methods we tested included

- Edge and wire scans
- LiF imprints [20; 21] (colour centre generation)
- Ablative imprints
- Graphitization of diamond
- Hartmann wavefront sensor analysis
- X-ray imaging

The LiF and ablative imprints work on a single exposure and give a full 2D profile of each individual pulse [22]. We have published our results for µm and nm focusing [21; 20]. However, after a LiF or ablative target has been exposed to a sequence of shots, it needs to be removed from the target chamber and put under a microscope, and images need to be made and subsequently analysed using underlying models of intensity dependence. In practice, we found this method unsuitable for day-to-day operation.

Nonthermal graphitization of diamond requires a certain flux of X-rays ($\sim 2\,\mathrm{eV}$ per atom), and an X-ray diffraction detector that can tell polycrystalline diamond reflection apart from graphite [23]. It also consumes expensive diamond samples. While scanning the CRL3 lens distance with respect to the interaction point in one of the target chambers, or changing lens configurations, the diffraction signal for single exposures is observed. Once a certain intensity is reached and the phase

transition threshold surpassed, graphite diffraction will show up in a re-exposure of the irradiated spot. Now, the X-ray beam can be attenuated and focusing can be refined until graphitization is achieved again. Another drawback of this method is that the profile and size of the focus are unknown; only its peak intensity can be maximized.

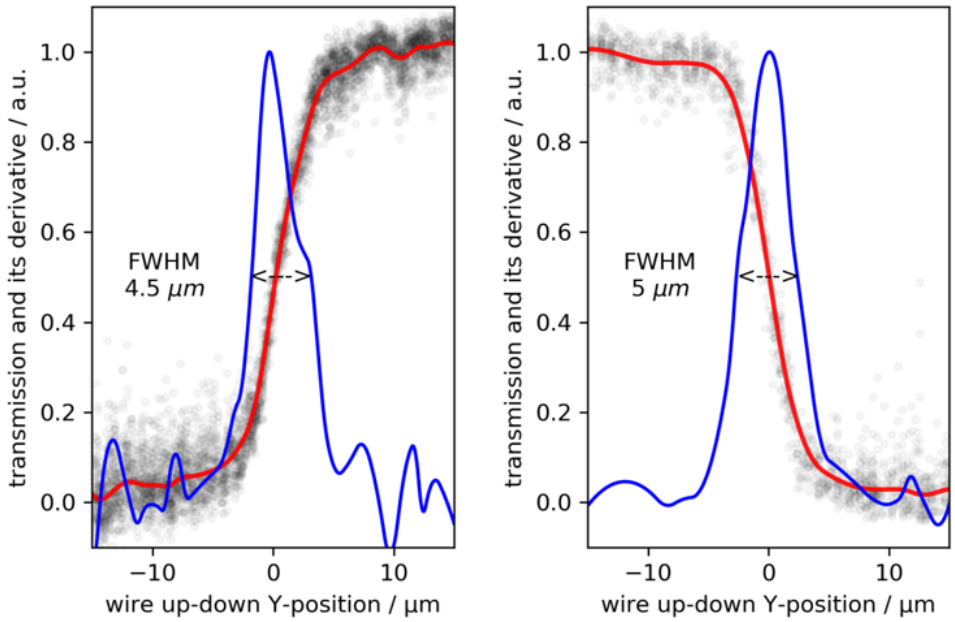

Figure 1.7: Focus measurement in IC2 at 17.8 keV photon energy by scanning with a 1 mm diameter W rod across the focus

Edge or wire scans work by scanning a straight edge (foil or wire) of an absorbing material through the X-ray beam and measuring the transmission or a sample signal (XES, elastic peak, etc). We use the diodes in the instrument beamstop for the transmission measurement (e.g. see Fig. 1.7) for IC2 experiments, but we found that the above-described Optique Peter microscope (Section 1.2.4.5), coupled to an image processor, yields a cleaner signal for IC1 experiments. Different from the above-mentioned methods, edge scans only yield a projection of the beam profile in one (the scanning) direction and this profile represents only the average beam profile since many exposures are necessary. Since the X-ray beam jitter is predominantly in the horizontal direction (left–right), we characterize our beam profiles with vertical scans only. This method is currently used at HED-HIBEF to determine and adjust the focus size *in situ* during each experiment.

A variation of the edge scan was adopted successfully for X-ray two-colour operation (see also Section 4.2.1). Here, the SASE 2 undulators are split and tuned to two different gap settings, resulting in two pulses with different photon energies. Since we focus with chromatic CRLs, the two foci will be spatially separated along the beam

axis. By scanning an edge into the beam at the target position, we can measure the increasing amount of elastically scattered X-ray by a HAPG spectrometer (Section 1.2.1.1) in a backward direction. Using the dispersion of the spectrometer, we can obtain the intensity of the scattering for the two colours independently and determine both foci simultaneously.

In collaboration with the XPD group at EuXFEL, we fielded a Hartmann wavefront sensor [24] at HED and other instruments. When this detector is placed precisely into the primary beam behind the focus, the Hartmann plate—an array of precise holes on an opaque substrate—will cast small spots on a downstream area detector. Wavefront distortions will cause these dots to change position with respect to a flat phase reference. This device should be able to give, even for a single exposure, the distance to a focus and its size. Coupled in real time to a translation of a CRL lens, alignment to a best focus and shifting of that best focus to the target position could become the gold standard. We are planning to further cooperate with the XPD group to test the Hartmann wavefront sensor further at HED in spring 2024.

Finally, we have developed the phase contrast imaging (PCI) platform (Section 1.3.2) that utilizes a nanofocusing CRL stack (Section 1.1.10) in line with the primary beam behind the target (interaction point). This lens stack is set to image the target plane onto the Optique Peter Microscope (Section 1.2.4.5) with a magnification of $M \sim 6$ and a special resolution of $\sim 500\,\mathrm{nm}$ for SASE bandwidth. We have successfully used this setup to directly image the focus of CRL3 (CRL in the optics hutch). However, this is a high-risk operation as it can lead to X-ray heating and destruction of the Beryllium lenses. Hence this method is only reasonable when following strict administrative measures.

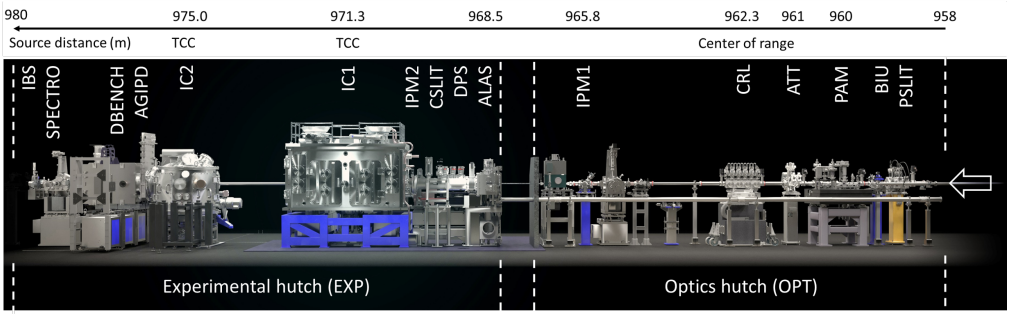

Figure 1.8: HED optics and experiment hutch layout. The X-rays enter from the right. **Optics hutch:** PSLIT – water-cooled four-blade power slits, BIU – beam imaging unit, PAM - photon arrival monitor for X-ray-optical laser timing, ATT – solid attenuator foils, CRL – compound refractive lenses made of Be (CRL3), IPM1 – intensity and position monitor. **Experiment hutch:** ALAS – incoupling for alignment laser, DPS – differential pumping, CSLIT – clean-up slits, two four-blade assemblies for soft and hard X-rays respectively, IPM2 – intensity and position monitor, IC1 and IC2 – interaction chambers, AGIPD – MHz repetition compatible X-ray detector , DBENCH - detector bench, SPECTRO – position of downstream spectrometers, IBS – instrument beamstop. The distances on the top are given from the source (centre of the last undulator, U33).

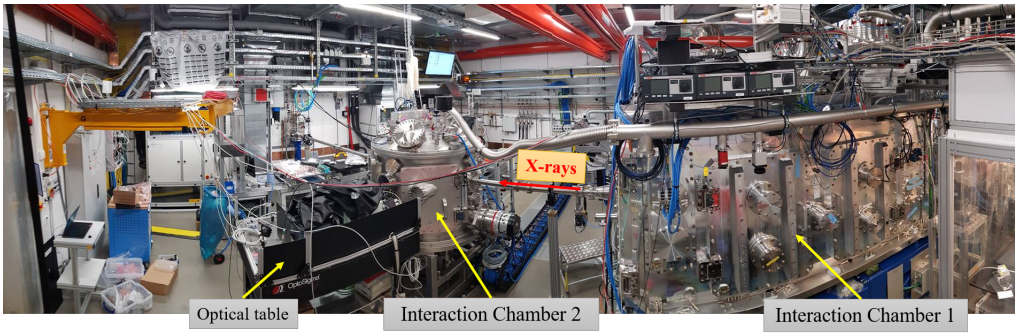

Figure 1.9: Photograph of the HED experiment hutch in 2023, with IC2 and the opical table for laser heating and SOP in place

1.2 Experiment hutch, interaction areas, drivers

This section describes the setup and instrumentation in the HED hutch. A comprehensive overview about the state of the instrument around the end of 2020 is given in Ref. [1]. Since then, we operated the instrument for an additional three years. While the gap between the initially established theoretical concept and real world user operation restrictions taught us what works and where problems lie, it also helped us to identify what needs to be modified, replaced, improved, and upgraded. Here, we focus on these recent developments and operational aspects.

1.2.1 Interaction Chamber 1

The large Interaction Chamber 1 (IC1) has been extensively used for all experiments except DAC XRD (since Oct. 2019) and shock experiments (since May 2023). All experiments that employ X-ray and particle spectrometers have been carried out in it as well as all relativistic laser-plasma experiments and all single-pulse X-ray heating experiments.

We have determined that the experiment hutch environment is too dusty and hence not compatible with the operation of the expensive large ReLaX laser optics at high fluence. Besides their cost, replacing them also consumes precious setup time and eventually compromises reliability and beam quality due to accumulated damage. We have therefore installed a **flow-box in front of the two main access doors** so that the chamber is usually opened to clean filtered air and colleagues and users working in the chamber are constantly showered by a filtered air stream from above.

In cooperation with the Sample Environment (SEC) group of EuXFEL, we have developed, commissioned, and used a so-called **fast sample exchanger**. A cassette with up to 10 sample frames sits in an air lock on top of the chamber. A frame from the sample holder in the centre of IC1 can be picked up by a motorized arm under vacuum conditions and put into this cassette, and a fresh frame can be inserted instead. The procedure needs to be supervised via view ports and cameras and takes 15–30 min. but is faster than a pumping-venting cycle. We have used this sample exchange arm in several ReLaX experiments, as the connection of the IC1 vacuum to the ReLaX compressor beamline requires a good vacuum $< 5 \cdot 10^{-5}$ mbar, and hence about an hour of pumping time before ReLaX shots can be resumed.

Initially, a fast sample scanner (FSS), an XY stage, was designed and built simultaneously to IC1 to our specifications. We requested a target stage that could position targets in a 2D plane with a few-µm precision at 10 Hz. Operational experience has shown that a 10 Hz shot rate is still futuristic because sample alignment is one of the temporal bottlenecks (see Section 4.1.3). The sample scanner was not able to meet the specifications under experimental conditions: it showed drift of the up–down direction within minutes, and its design was too bulky, not accounting for the numerous laser diagnostics that were implemented only after the device was already in place. In 2023, a second version of a fast sample scanner was built and tested for the first time at the end of Run 2023-II. It still has to be made compatible with the above-mentioned fast sample exchanger.

In IC1, mounting and dismounting X-ray detectors (Section 1.2.4) turned out to be extensively time consuming because of their electric, optic fiber cabling and

water supply lines that had to be carefully drained and vented to prevent water contamination inside the vacuum chamber. Instead, we built a few shelves inside the chamber where detectors can be left attached but stored, out of the way for other diagnostics.

1.2.1.1 X-ray spectrometers

The HED-HIBEF instrument provides X-ray spectrometers inside the IC1 chamber.

The von-Hámos spectrometers based on highly annealed pyrolytic graphite (HAPG) have proven to be a reliable, versatile, and highly demanded tool since 2019. The details of these devices, as described in Preston et al. [25], remain unchanged. In 2021, we shielded the Jungfrau detector electronics (Section 1.2.4) with high-Z metal and installed a collimating *tunnel* between the crystal and the detector to shield against stray light during high-intensity ReLaX experiments. Also, a frame to hold filter materials, such as insulators or metals (Al, PMMA), just in front of the crystal was installed. We found that the spectral resolution improves with larger bending radii (less strain). Therefore, and also to increase the target-to-spectrometer distances at lower photon energies around 4–6 keV, we have recently ordered new HAPG crystals with 120 mm bending radius (in addition to the existing 80 mm and 50 mm, for which we have ordered spare parts).

Initially designed for XES experiments from diamond anvil cells, a von-Hámos multi-crystal spectrometer with perfect Si and Ge crystals has been built, commissioned [26], and used in user experiments. The device is shown aligned in IC1 in Fig. 1.11. This goal was achieved through a BMBF-funded collaboration with the Technical University of Dortmund, which was at the same time a Ph.D. project. Details are reported in Kaa et al. [26].

Together with HIBEF members from France (CNRS), we have designed, built, and tested a bent-crystal spectrometer in the direct beam that can be used to monitor the X-ray FEL spectrum or, in combination with a second spectrometer, used for femtosecond X-ray absorption spectroscopy [27].

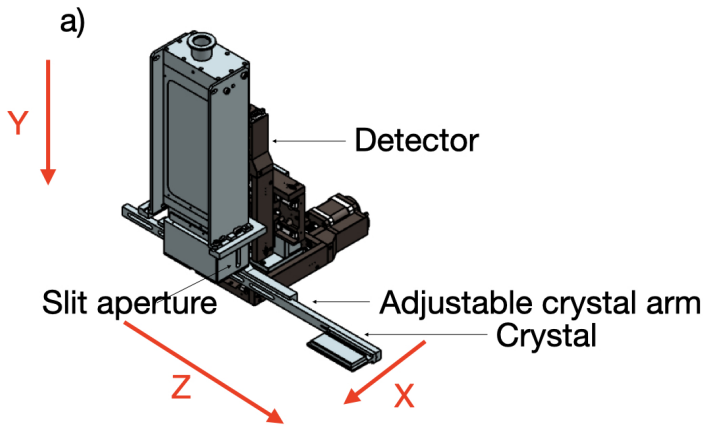

Figure 1.10: CAD representation of a typical HAPG spectrometer configuration with a Jungfrau detector

1.2.2 Interaction Area 2

Interaction Area 2 serves as a multi-purpose space. While it currently mainly accommodates Interaction Chamber 2 and the pulsed high magnetic field setup, it offers the space required for flexible setups as well as future developments.

1.2.2.1 Interaction Chamber 2

Interaction Chamber 2 is designed as a precision diffraction camera optimized for high throughput experiments exploiting the coherence, time structure, and energy range of the EuXFEL. It hosts two platforms: one for diamond anvil cell experiments and one for dynamic compression studies with the DiPOLE laser. These experiment platforms can be coupled with either of two detector systems: the HIBEF AGIPD 1M detector, designed to resolve individual pulses at the minimum bunch spacing of the EuXFEL at 220 ns, and a twin configuration of two Varex flat-panel detectors for maximum gapless coverage at 10 Hz train repetition rate in an EMP- and debris-resistant housing. A nanofocusing setup compatible with both platforms makes it possible to focus the beam to below 100 nm at X-ray energies of up to 25 keV for X-ray heating, micron-sized samples in double stage DAC experiments, and phase contrast imaging.

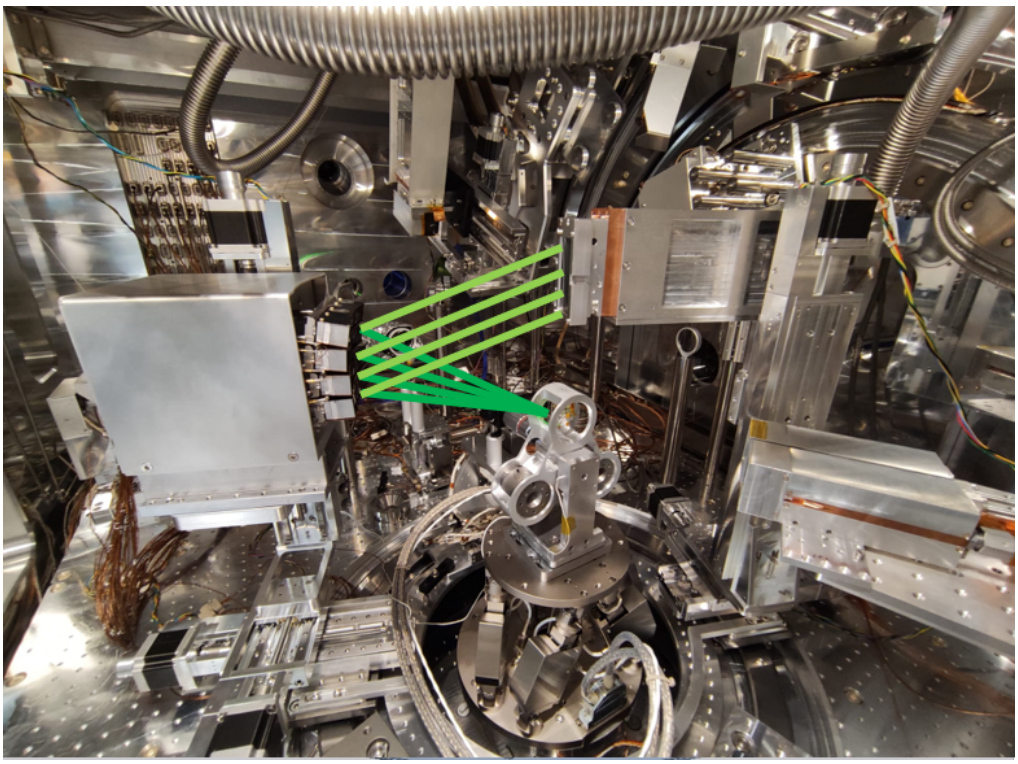

Figure 1.11: The von-Hámos spectrometer for XES from diamond anvil cells. The emission is focused by four bent crystals onto a Jungfrau detector mounted above the DAC. On the right, two ePIX modules record XRD patterns.

The chamber can be moved in and out of the beam position on a rail system.

1.2.2.2 Pulsed high magnetic field setup

The pulsed high magnetic field setup consists of a thyristor switched capacitive discharge power supply (pulser) located in a A.11, driving the coil that is integrated on a five-circle goniometer. With a stored energy of 750 kJ, the system is designed to generate the highest non-destructive fields at any X-ray source targeting 60T in a bi-conical solenoid and 40T in a future split coil with panoramic access in the equatorial plane. The goniometer is located in the beam position by kinematic mounts and can be removed on wheels.

1.2.3 Optical laser systems

1.2.3.1 EuXFEL pump–probe laser

At HED, the optical pump–probe (PP) laser is a well-established excitation source to drive samples out of equilibrium and initiate dynamics at moderate intensities or to act as a short-pulse synchronized probe beam. The three operating SASE beamlines of the EuXFEL are equipped with similar laser systems developed to match the MHz repetition rate and time structure of the SASE pulses [28; 29]. The system is contained in a separate PP laser hutch and consists of a seed laser of 800 nm wavelength (17–50 fs duration) as well as a 1030 nm pump (900 fs duration). Both wavelengths are available for the instruments with different parameters. After exiting the laser hutch, the beam is guided towards the instrument laser hutch of SASE 2, which is shared by MID and HED. Here, the intensity can be regulated between 1 % and 100 %, and the time delay between the SASE beam and the optical laser adjusted over a range of 3 ns via a mechanical delay stage. In addition, a small fraction of the laser beam is sent into a diagnostic line for further timing diagnostics. An overview of the settings and the pulse energy on sample provided by the SASE 2 PP laser system can be found in Table 1.2.

Table 1.2: Laser parameters of the PP laser system

Set point	Rep rate (MHz)	E @1030 nm (mJ)	E @ 800 nm (mJ)
1	4.5	1	0.03
2	1.13	4	0.2
3	0.188	20	1

1.2.3.2 HIBEF ReLaX laser

High-intensity lasers are essential for pushing the boundaries of science. Their development has allowed leaps forward in basic research areas, including laser—plasma interaction, high-energy density science, metrology, biology, and medical technology. The HIBEF UC contributes and operates the ReLaX laser, a short-pulse high-intensity Ti:Sa laser system. The acronym **ReLaX** stands for the *Relativistic Laser at EuXFEL*.

ReLaX is a standalone laser system based on the Pulsar 500 HR product series of Amplitude France. In maximal operation settings 400 TW can be reached on sample (10J at 25 fs). For regular user operation, nominal 200 TW (6 J at 30 fs) are offered. The laser was delivered and installed in 2018 onsite at the EuXFEL (see Fig. 1.12). The optical compressor, beam transport, and diagnostic package have been designed and manufactured as contributions to the HIBEF UC by Helmholtz-Zentrum Dresden–Rossendorf (HZDR). The commissioning and integration phase into the HED instrument was successfully finished at the end of 2019. Since then, it has been the main driver at HED-HIBEF for relativistic laser–plasma experiments, as discussed in Section 3.3.

Over the last six months, the IT infrastructure and control system (proprietary to Amplitude) was upgraded to include new features allowing a higher integration level into the EuXFEL infrastructure. For example, the EuXFEL train-ID link was incorporated and can be used with a new data logging capability. While this logging functionality, which can save all laser parameters, is still a standalone solution, several key parameters relevant for user operation and controls can be streamed and also be controlled by the Karabo framework (Section 1.5), allowing e.g. macro-automatizing of shot sequence, laser energy, etc. Furthermore, a hardware upgrade of the ReLaX internal safety rack now makes it possible to integrate additional interlocks controlled by via Karabo into the laser operation, with the interlocks defined by the used experiment procedures. Currently, as a new development, a delay-free reflective attenuator is being tested that would enable the availability of a highly attenuated full aperture beam with similar timing with respect to the X-rays as the full energy beam (the current device used to attenuate the full energy and aperture beam for focal diagnostics safe energy levels is introducing a ns delay and cannot be used for timing purposes).

So far, laser operation is limited to the 100 TW level due to the currently existing radiation safety permit of the EuXFEL for HED. While the hereby used radiation protection concept was developed early 2014 and is based on the idea of continuous operation and subsequent boundaries set by this operational mode, the reality is that

Figure 1.12: HZDR HIBEF scientists Toncian and Höppner aligning the last amplifier of the ReLaX laser system

the laser is operated as a shot-on-demand or sub-Hz-burst-mode driver. Therefore the operational setting is different than the 2014 concept and, in order to exploit the full capabilities of ReLaX, a new or extended radiation safely permit lifting existing restrictions should be requested from the authorities. This request needs to be backed up by adjusted radiation shielding calculations and adjusted operational concepts.

More information on the ReLaX laser system can be found in *Laso Garcia et al.* [30].

1.2.3.3 HIBEF DiPOLE 100-X laser

The high energy laser DiPOLE 100-X (Diode Pumped Optical Laser for Experiments) is an all diode-pumped 100 J class Ytterbium:YAG–based laser manufactured by STFC CLF (Central Laser Facility) in the UK and the University of Oxford as part of the UK's contribution to the HIBEF UC [31]. The laser system is capable of generating $<$ 100 J for a 10 ns pulse duration and 37 J for a 2 ns pulse duration at the fundamental wavelength (1030 nm). In addition, it is capable of 10 Hz operation resulting in kW output of optical light. Since the main scientific use of DiPOLE 100-X is laser-driven shock and ramp compression, the laser provides pulse shaping capabilities with a resolution of 125 ps, allowing arbitrary waveforms ranging in duration from 2 to 15 ns.

In the experiment hutch, the DiPOLE beam is frequency doubled to 515 nm using a

lithium-triborate (LBO) crystal [32] before the laser is transported via mirrors, partially in vacuum, to IC2 (see Section1.3.4). Beam transport to IC1 is currently being developed.

The laser is synchronized with the X-ray beam using the X-ray FEL timing system that has an RMS of approximately 10 ps. The total temporal jitter of the laser beam against the X-ray beam, including all components, is better than 50 ps. We have also implemented online monitoring of the arrival time of both laser and X-rays. Phase plates providing flat-top focal spot profiles ranging from 100 to 500 µm diameter are provided (Fig. 1.13).

The full capabilities of DiPOLE 100-X can be exploited in combination with the HIBEF-provided VISAR system and the high-precision XRD platform at IC2 (see Section 1.3.4).

The DiPOLE 100-X laser was commissioned in 2022 and has, at the time of writing, served as driver during four user experiments in 2023. During a large first community experiment in May 2023, $>$ 80 users from more than 20 international laboratories conducted four different science topics, including technique development for repetition-rated VISAR analysis and fast target delivery and alignment. The results are discussed in Section3.5.2.

The team shot $\sim$ 1000 samples in one week, which is a record compared to the $\sim$ 200 samples typically shot at LCLS or SACLA in the same period. The targets were still individually glued to ladder-type frames, and the system showed great scope for improvement. Later, a tape target was successfully tested at 1 Hz as well (see Section 4.1.3).

A full review paper detailing the user relevant setups and laser parameters is in preparation.

1.2.4 Detectors and data calibration

Use of pixelated 1D and 2D detectors (line and area) are necessary for nearly each experiment performed at HED. Therefore, considerable efforts have been devoted to integrate and commission various detectors at HED. To this end, an HED instrument scientist was appointed detector scientist with the Detector (DET) group for a limited number of years. The great variety of experiments conducted at HED implies challenging detector requirements, such as single photon sensitivity, low noise, small pixel sizes, high dynamic range, and MHz repetition rate. All of these requirements

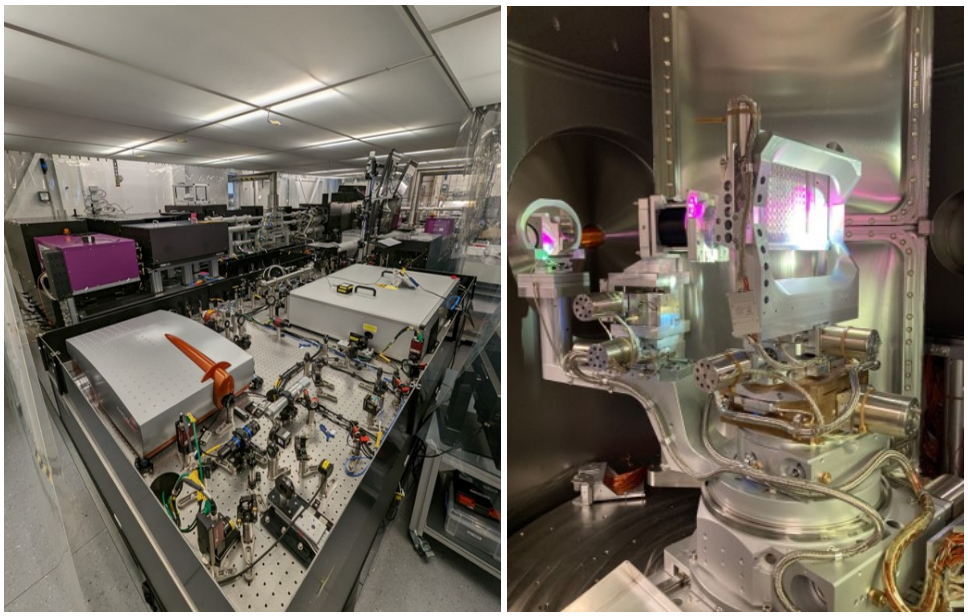

Figure 1.13: Left: View of the DiPOLE 100-X laser in the laser bay above the HED experiment hutch. **Right:** View of the shock setup in IC2.

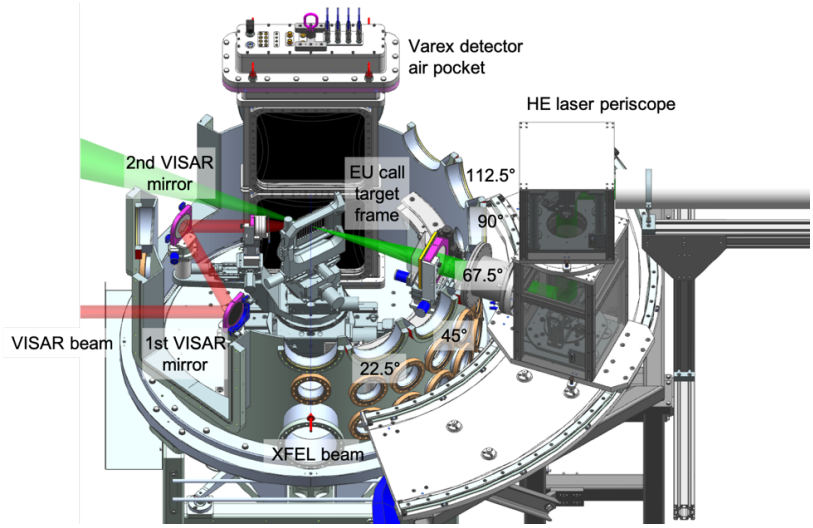

Figure 1.14: CAD representation of a possible shock configuration in IC2, combining the DiPOLE laser with the Varex flatpanel detectors and VISAR. Here, the DiPOLE laser enters at 67.5° to the X-rays and Varex are mounted symetrically around the primary beam. In the standard configuration, the X-rays enter at 45° and Varex is placed to the side (Fig. 1.22).

are not met by one detector alone, so use of different detectors is mandatory at HED.

1.2.4.1 Jungfrau detector

Five Jungfrau 500K detectors are currently being used at HED. The Si-based charge integrating hybrid pixel detector is developed at PSI (Paul Scherrer Institut, Villingen, Switzerland) [33] and features, in its standard configuration, 75 µm pixel pitch, 256×256 pixels per ASIC, and 4×2 ASICs per detector module constituting an active area of 38.4×76.2 mm^2, with sensor thickness 320 µm. The Jungfrau detector exploits dynamic gain switching technology and is optimized for operation at X-ray energies around 12 keV with a dynamic range of 10^4 photons. The detector is synchronized with the linac using a 10 Hz trigger and is usually configured to record single frames. However, recent commissioning has established the capability to record up to 16 frames per train at a maximum rate of 113 kHz, i.e. 1/40 of the 4.5 MHz maximum pulse repetition rate of EuXFEL.

As the Jungfrau detector is an in-air detector, HED has developed an inverted vacuum chamber (air pocket) that encloses the entire detector assembly except the Si chip, which is connected to the readout board via a vacuum feed-through and a heat dissipation surface (see Fig. 1.15 left). The signal and power cables, water cooling, and dry nitrogen gas purge are fed from the top of the IC1 chamber to the detector in vacuum via a KF25 vacuum bellow. This also resembles a fully shielded Faraday cage that allows this detector to function stably and reliably in the presence of strong electromagnetic pulses (EMPs), which occur during ReLaX and DiPOLE laser experiments. Four of these detectors are installed in IC1 for in-vacuum use.

The Jungfrau detector comes in different configurations: One module is reserved for in-air operation One module currently has a thicker 450 µm Si chip to boost the quantum efficiency for harder X-rays, especially suitable for X-ray diffraction (for a PDF application, see Section 3.5). We also have one so-called *Strixel* module., which has the same pixel density, but each pixel is three times narrower in the long direction of the chip and three times wider perpendicular to that. This results in pixels of 25 µm pitch along the long axis, which has been successfully deployed for spectroscopy applications (Section 1.2.1.1).

1.2.4.2 ePix detector

Two ePix100 detectors are currently in operation at HED. The ePix100 is a charge integrating hybrid pixel detector developed at SLAC National Accelerator Laboratory (Menlo Park CA, USA)[34] to resolve the 120 Hz operation of LCLS. The detector has a pixel size of 50 µm, 384×352 pixels per ASIC, an array of 2×2 ASICs per module and hence an active area of 38.4×35.2 mm^2, with sensor thickness 500 µm. The

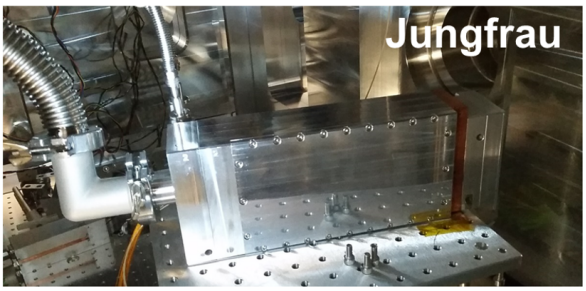

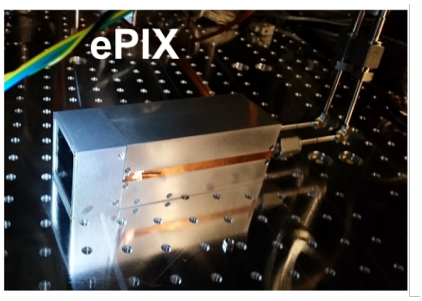

Name	Pixel size (μm)	No. of pixels (adim.)	Detection area (mm^2)	Noise (eV)	Frame rate (Hz)	Dynamic Range (photons per pixel)
ePix100	50	704×768	35×38	< 280	120	10^2 8 keV
Jungfrau	75	512×1024	38.55×77.25	< 450	2400	10^4 12 keV

Figure 1.15: Left: Jungfrau (JF) detector in the HED *air pocket* housing. **Right:** ePIX 100 detector.

detector features single photon sensitivity and a dynamic range of 10^2 photons at 8 keV. At HED, the detectors are currently operated in vacuum at 10 Hz frame rate in IC1 (see Fig. 1.15 right).

HED also possesses two ePix10k detectors from SLAC, which have larger pixels of 100 µm pitch and are gain-switching (like the Jungfrau detectors). However, at the EuXFEL we were not able to interface properly to the gain-switching functionality, and these detectors were therefore operated at fixed gain and consequently are inferior to the Jungfrau modules. The use of these modules was quickly discontinued and there was initially an agreement to replace them with ePix100 modules.

Since ePix modules have a significantly smaller chip area compared to Jungfrau modules, and EMP-proof housings have not been implemented, their use is currently restricted to *X-ray only* experiments. Because of high internal demand due to LCLS-II, we have incurred delays in repair, maintenance, and replacement requests for our ePix detectors by SLAC and have thus decided to discontinue ePix detectors in the long term in favour of expanding and upgrading our suite of Jungfrau detectors.

1.2.4.3 Varex

The Varex twin-detector system was designed to provide maximum gapless coverage and high quantum efficiency at high X-ray energies for the first DAC experiments (until arrival of the AGIPD 500K) and, primarily, for shock experiments in IC2 at the bunch-train repetition rate of 10 Hz or less (Fig. 1.16).

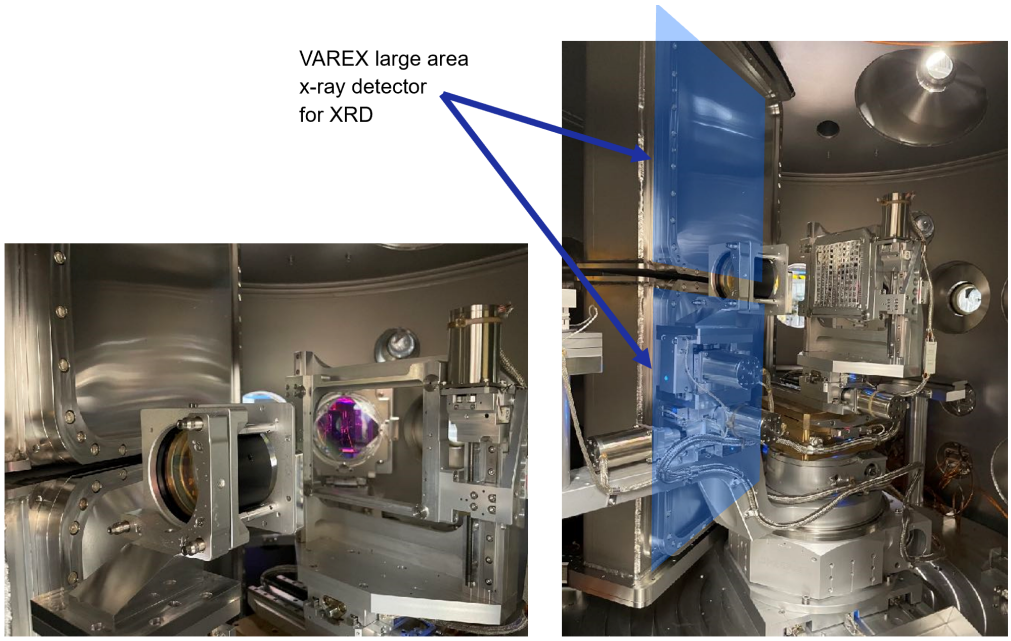

Figure 1.16: Photograph of the Varex flatpanel twin detectors in IC2 in shock standard configuration. The blue shaded area indicates the sensitive detector area.

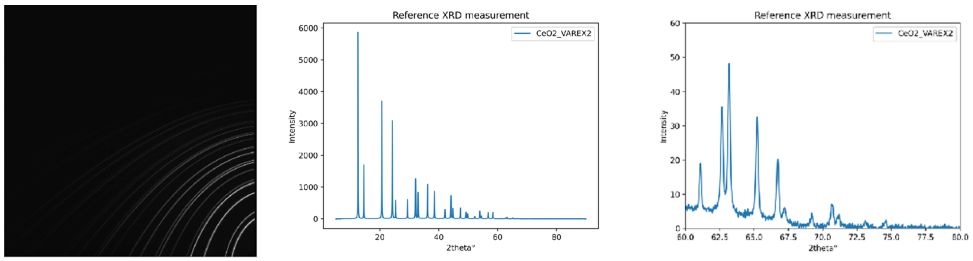

Figure 1.17: A single XRD pattern of a CeO_2 calibrant on Varex, showing the excellent gap-free data quality. The single X-ray pulse of 18 keV had a pulse energy of 400 µJ. **Left:** Raw image of upper panel. **Centre:** Radial integration (linear scale) from 0◦ to 90°. **Right:** Zoom into the range from 60° to 80°.

These specifications are matched by two Varex XRD 4343 CT flat panel detectors with scintillator panels, consisting of CsI:Tl oriented needle crystals, which are bonded to a 2880 x 2880 pixel (150 µm × 150 µm) TFT-diode array with an active surface of 432 mm × 432 mm. In order to reach 2θ angles of 64.5° in the vertical, the detectors need to be placed inside IC2 close to the sample. This is achieved by insertion of two of these detectors into an air pocket equipped with thin (400 µm) Al windows through a dedicated lid for IC2. A twin configuration with a horizontal gap in the equatorial plane was chosen in order to avoid parasitic scattering from a beamstop and provide direct access to the transmitted beam for additional downstream diagnostics (e.g. intensity monitors, SAXS, and PCI). Varex has shown excellent

low-noise, gap-free qualities and remains stable during DiPOLE operation. A single XRD calibrant exposure is shown in Fig. 1.17. In DiPOLE XRD experiments at 18 kev, we have obtained useful XRD data of melts up to q-values of 7-9Å^{-1} after absorption corrections in sample and detector filter were applied (see Section 3.5.2).

1.2.4.4 AGIPD

The Adaptive Gain Integrating Pixel Detector (AGIPD) is the only MHz-repetition-rate–capable detector at HED. A detailed description can be found in Ref. [35].

HED is due to receive an in-vacuum 1 megapixel (1M) module via the DESY part of the HIBEF UC. However, after first versions of this detector were installed at the SPB/SFX and MID instruments at the EuXFEL, internal reviews pointed to several necessary improvements on the chip layout and cooling infrastructure. The delivery of this second version AGIPD is therefore seriously delayed and currently foreseen for 2025, as a 1M version for HED-HIBEF and a 4M version for the SPB/SFX instrument.

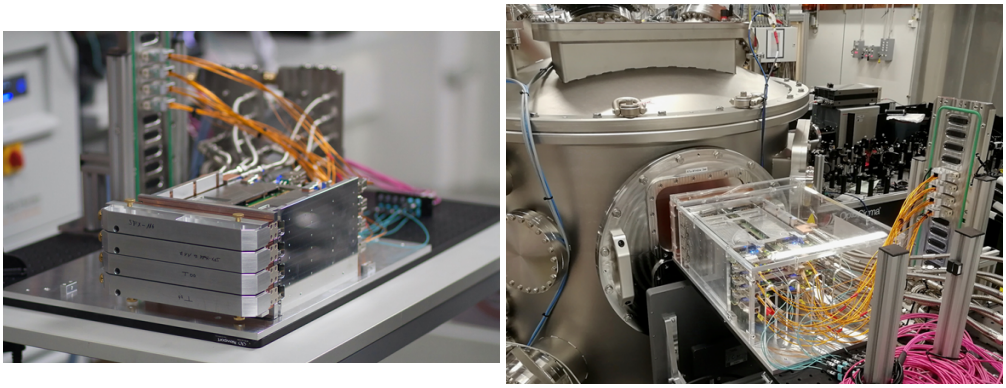

Figure 1.18: The AGIPD 500k prototype at HED-HIBEF (left), operated in air behind IC2 (right) at HED since November 2021 for DAC experiments

However, for the diamond anvil cell (DAC) programme at the HED, which saw a first user experiment already in October 2019, it is decisive to record MHz pulse-resolved X-ray diffraction patterns. Through a joint DESY–EuXFEL effort, we were able to operate a prototype AGIPD 500K-pixel module in air from November 2021 onwards, which allowed HED to boost the scientific output of the DAC programme significantly. It also helped to commission the new readout infrastructure for this second generation AGIPD, which hopefully will speed up the commissioning of the new AGIPD after their installation at the SPB/SFX and HED-HIBEF instruments in 2025.

AGIPD is mounted on the detector bench and usually sits right behind a vacuum

window of IC2 in all DAC standard configurations (Section 1.3.5) as shown in Fig. 1.18.

Small AGIPDs (sensor size 1/8 or 1/16 of the 1M AGIPD) have now become commercially available via the spin-off company XSpectrum. Such a small AGIPD module has been recently sourced by HIBEF and integrated at HED using the existing hardware for the 500K module. A full test will be performed with X-rays in February 2024 in combination with the pulsed magnetic field (PMF) platform (Section **??**). Also, the EuXFEL DET group is planning to use AGIPD hardware to develop a suite of MHz detectors for the mid-term future.

1.2.4.5 Optique Peter microscope

On the detector bench, an *Optique Peter 3* direct beam imaging system was mounted in 2021, consisting of three motorized interchangeable scintillators with microscopy objectives coupled to an Andor Zyla 5 optical camera. The 2x Objective can image a 12×12 mm field of view, and we typically use it with 250 µm thick scintillator as the depth of focus is ± 128 µm. The 7.5x objective is used with a 20–35 µm thick scintillator, and, for highest resolution, the 20x Objective is coupled with a 8 µm thick LSO:Tb scintillator supported by a 170 µm YbSO substrate.

Using this microscope we are now able to assess the quality and size of the beam when focusing with CRLs (Section 1.1.11). It is also used for transmission diagnostics, and, if coupled to the nano-focusing CRLs in IC1, it is used as an area detector for (sub-)micron X-ray imaging. For examples, see Sections 1.3.2, 3.3.5, and 3.3.6.

1.2.4.6 Gotthard-II detector

The Gotthard-II detector has been developed at PSI as a successor of the Gotthard-I line detector to allow data acquisition with a 4.5 MHz rate and with a pixel size down to 25 µm. Devices have been delivered to the EuXFEL but are not yet available at HED. Discussion about a vacuum pocket similar to the Jungfrau are under way, and this line detector is appealing to field inside IC1, coupled to a von-Hámos spectrometer, and record single-shot spectra during a MHz pulse train, such as Fe K-beta XES from DAC.

1.3 Standard configurations

The floor plan of the HED experiment hutch, split into two interaction areas with IC1, and IC2 or a secondary flexible interaction, remains unchanged to what is described in Ref. [1]. However, we have developed standard configurations of highly demanded experiment setups.

This has proven to have several benefits:

- All necessary equipment is available and fully integrated into EuXFEL control systems
- Equipment is compatible with each other
- CAD-based setup plan for positioning devices in the target chambers and in the hutch exists
- Setup time is minimized and can become routine
- Several such standard user experiments can be scheduled back-to-back because no changes in between experiments are necessary

These configurations were developed by anticipating the users needs and refined the setup together with the users in preparation of a first beamtime. Up to now, all standard platforms have been tested with users in the framework of a large community proposal before they have been offered to the general user.

We have established highly standardized configurations for the following classes of experiments:

- ReLaX experiments in IC1
- Cryogenic jet experiments in IC1
- DAC XRD experiments in IC2
- DiPOLE shock XRD experiments in IC2

Besides these, there are less strictly specified but proven experiment configurations for DAC XRD+XES in IC1, PP laser experiments in IC2, and meV experiments in IC1. We are currently working on grazing incidence setups in IC1, DiPOLE spectroscopy in IC1, PDF in IC1, and a standard setup for pulsed magnetic field experiments.

We describe the parameters of the standard configurations in the following section.

1.3.1 ReLaX laser with SAXS, PCI, and spectroscopy

The first ReLaX standard configuration is shown in Fig. 1.19

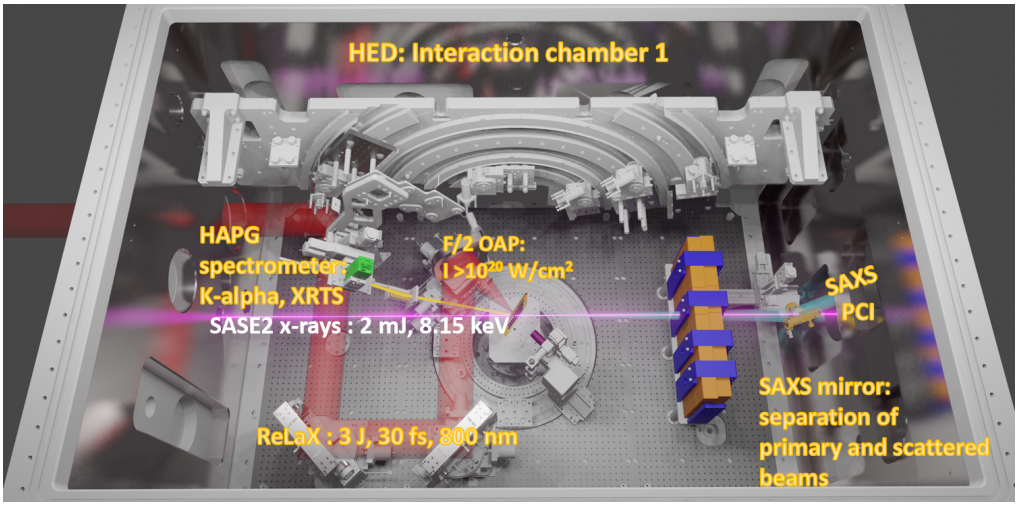

Figure 1.19: ReLaX standard configuration SAXS, PCI, and spectroscopy. The X-rays enter from the left. On the right, behind a led wall (orange–blue structure), the SAXS mirror deflects the signal on a Jungfrau detector outside the chamber (not shown).

In the IC1 chamber, the 100 TW ReLaX laser (Section 1.2.3.2) is incident on the target at an angle of 45° with respect to the X-ray FEL beam (Fig. 1.19). The target can be oriented in many angles; however, no normal incidence of ReLaX to the target is allowed.

SAXS+PCI X-ray diagnostics (Section 3.3.2) are designed for an incident X-ray FEL energy of ~ 8.15 keV SASE. This is slightly flexible; however, a minimum of 7.5 keV is required. At 8 keV, the SASE pulses have approximately 1 mJ pulse energy and a 2.25 MHz maximum repetition rate.

Both X-ray FEL and ReLaX can be focused to 5 – 50 µm spot size. Note that a > 10 µm spot by defocusing of ReLaX's off-axis parabola will produce a non-homogeneous spatial profile [30]. Phase contrast imaging will yield a moderate spatial resolution of about 1 µm and be recorded by the Optique Peter microscope (Section 1.2.4.5) a few metres downstream of the interaction.

The standard HAPG **X-ray spectrometer** (Section 1.2.1.1) is fielded in the backward direction. The second spectrometer in the forward direction can be used only with restrictions due to potential collisions with the SAXS setup. Depending on the precise X-ray photon energy ranges that are required, this has to be evaluated with beamline scientists and engineers.

Note that the spectroscopy signal may suffer from plasma background, which would require e.g. special shielding. Users are asked to discuss their anticipated setup with the instrument staff prior to submission to ensure technical feasibility of their proposal.

Laser diagnostics (upon request) can be fielded, such as EMP antennas, electron spectrometers, bremsstrahlung spectrometers, and proton diagnostics (Thomson parabola).

1.3.2 ReLaX laser with imaging and spectroscopy

The setup is identical (and derived from) the ReLaX SAXS standard configuration (Section 1.3.1), except that the X-rays can be more tightly focused to 1.5 – 50 µm. The imaging resolution is then better than 1 µm. However, this setup is not compatible with SAXS because of stronger diverging beam from the small X-ray focus. If SAXS is not fielded, neither is the lead wall (Fig. 1.19), and consequently both the forward and the backward HAPG spectrometer can be used.

High-resolution phase contrast imaging can be accomplished in two ways. First, nano-focusing lenses (Section 1.1.10) can be placed a few 10s of a cm before the target (upstream), creating a small focus before the target, and subsequently the target will be probed by a divergent beam. The magnification is determined by the distance between focus and target, and focus and Optique Peter microscope, respectively.

An alternative method, which we developed and commissioned in February 2023, is depicted in Fig. 1.20. Here, the target is illuminated by a large collimated X-ray field, and the target plane is imaged by a Beryllium lens stack downstream of the sample onto the Optique Peter microscope. This method has proved to yield superior image quality with a spatial resolution of ~ 500 nm with SASE beam, and will further improve using HXRSS due to the reduced chromatic aberration.

1.3.3 ReLaX/PP laser with cryogenic liquid jet

Liquid jets and cryogenic liquid jets have great potential to deliver replenishing targets for high repetition rate experiments without causing degeneration of laser optics by target debris [36]. Moreover, they provide solid density matter, which under ambient conditions only exists in the gas phase, and hence give experimental access to scientifically interesting samples, such as hydrogen, methane, water, and helium [37; 38]. The cryogenic jet platform implemented in IC1 issues characterized

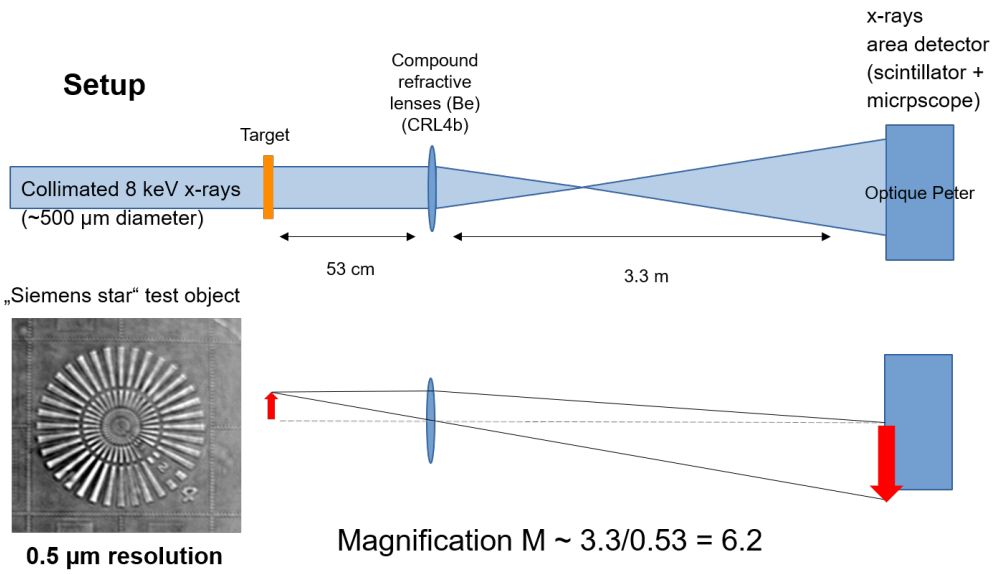

Figure 1.20: Imaging the target with a nano-focusing lens stack downstream of the sample. With SASE beam at 8 keV, we have demonstrated 500 nm spatial resolution by imaging a Siemens star.

jets of cylindrical and sheet geometries with micrometer position accuracy and $<$ 10 µm diameters (see Section 4.1.3.2). Depending on the pumping speed and the gas properties, the maximum flow is limited to rates of about 500 sccm (1 sccm= 0.016 mbar l/s), which allow target cross-sections of up to 100 µm^2 with 100 m/s flow velocities.

Larger jets with lateral dimensions exceeding 10 µm use a recently developed jet dump. For high-intensity experiments with ReLaX, a piezo-actuated blade cuts and interrupts the jet before the laser-matter interaction. This cut can be triggered on demand and prevents currents to crawl up the jet and destroy the sensitive nozzle. Since 2023, the ReLaX laser and the PP laser are offered for user experiments in combination with our cryogenic jet.

The jet flow direction is vertical (from top to bottom). Available nozzle types are round and slit-shaped, their size/shape depends on the specific gas type.

The cryogenic jet supports the following gas types: Hydrogen (tested), Methane, Argon, and others on request (not yet commissioned with the setup). The jet supports a motorized target rotation ±45 deg (z-axis).

For surveillance, a high-resolution on-shot target imaging exists in the xy-plane.

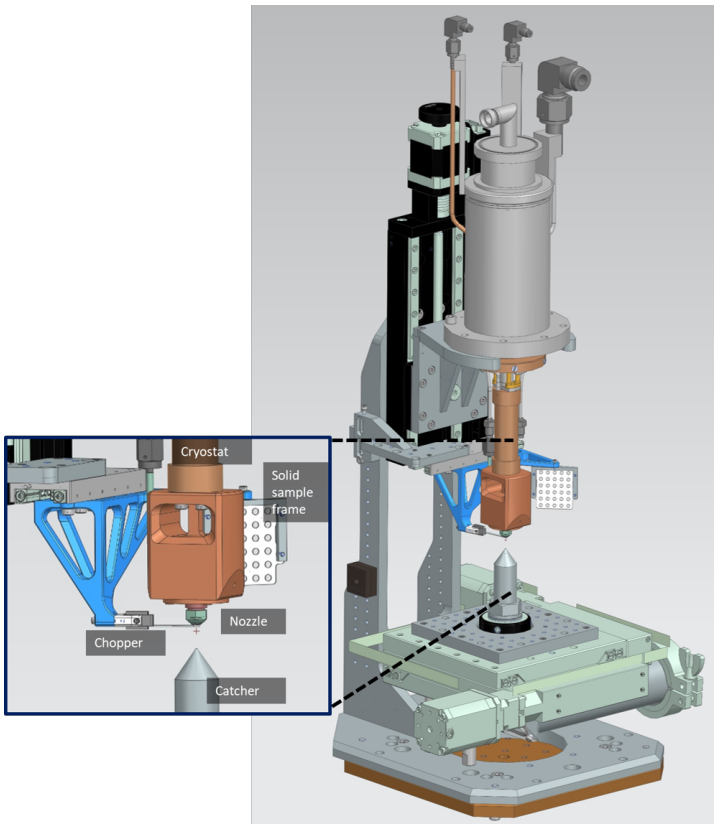

Figure 1.21: CAD representation of the cryogenic jet in IC1

Online target position recognition (see Section 1.5.2) is available.

This setup is compatible with the forward and backward HAPG spectrometers, the SAXS mirror, and XRD diagnostics, in IC1. For calibration, reference, timing, etc., a 30×30 mm target frame is provided that can be inserted into the interaction region of X-rays and laser. High repetition rate experiments with either the ReLaX or the PP laser are possible. A full CAD representation is shown in Fig. 4.1 in the *Science perspectives* part of this report.

1.3.4 DiPOLE 100X dynamic compression with XRD

Regular user proposals for DiPOLE in IC2 are focusing on X-ray diffraction via the two large Varex detectors (Section 1.2.4.3) as main diagnostics.

The photon energy has been fixed at 18 keV SASE. It can be varied within a few 100 eV, but diffraction geometry and detector response are well characterized for this photon energy.

The **geometry** is a quasi-collinear shock geometry, with 45° between the shock propagation and X-ray incidence, as shown in Fig. 1.22. The drive laser hits the sample with an angle of incidence of 22.5° to protect the VISAR system in case of a sample failure, thus the angle between Dipole and X-rays is in total 45°. However, 90° between shock direction and X-rays may be proposed, but this requires a setup change and commissioning time.

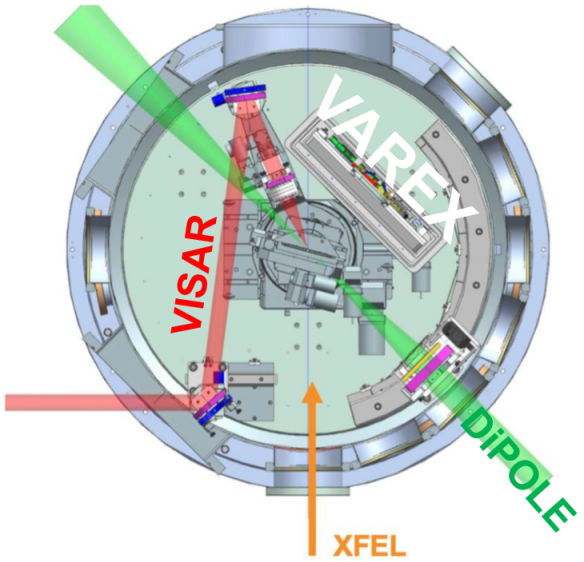

Figure 1.22: CAD representation of the standard shock configuration in IC2, combining the DiPOLE laser with the Varex flatpanel detectors and VISAR. The targets inside the central mount are oriented perpendicular to the VISAR.

The **DiPOLE 100-X laser** is 2ω frequency-doubled to the green, focused on the target, typically using a phase plate generating a flat top profile with a 100–500 µm diameter according to user request. Temporal square pulse scales as currently expected: for long pulses approximately 50 J energy in 10 ns, and for short pulses about 15 J in 2 ns. Pulse shaping (other than flattop) is on a best-effort basis, but has proven to be very stable and reproducible. For shaped pulses, the contained energy has to be evaluated case-by-case and will be lower than for a square pulse.

The target rear side is oriented perpendicular to the VISAR beam path. **VISAR** is offered as pressure diagnostic with one arm at 1064 nm and two more arms at 532 nm wavelength, plus one **Streaked Optical Pyrometry** (SOP) arm (for details, see Section 3.2.1).

A first community proposal was executed in May 2023 (Section 3.5.2), and in 2023-II three more proposals in this standard configuration were successfully completed. Currently, this is the only accepted DiPOLE configuration in IC2—more complex

proposals might be possible in future calls.

1.3.5 Diamond anvil cell (DAC) with XRD, laser heating, and SOP

The standard DAC setup in IC2, as shown in Fig. 1.23, is compatible with symmetric DACs, which the instrument can provide for users who need cells. The setup further provides an optical observation microscope and the streaked pyrometry setup. Details are adjusted depending on whether users request an X-ray heating, an IR laser heating, or a dDAC setup. The application of this setup is described in Sections 3.2.1, 3.2.2s and 3.2.3.

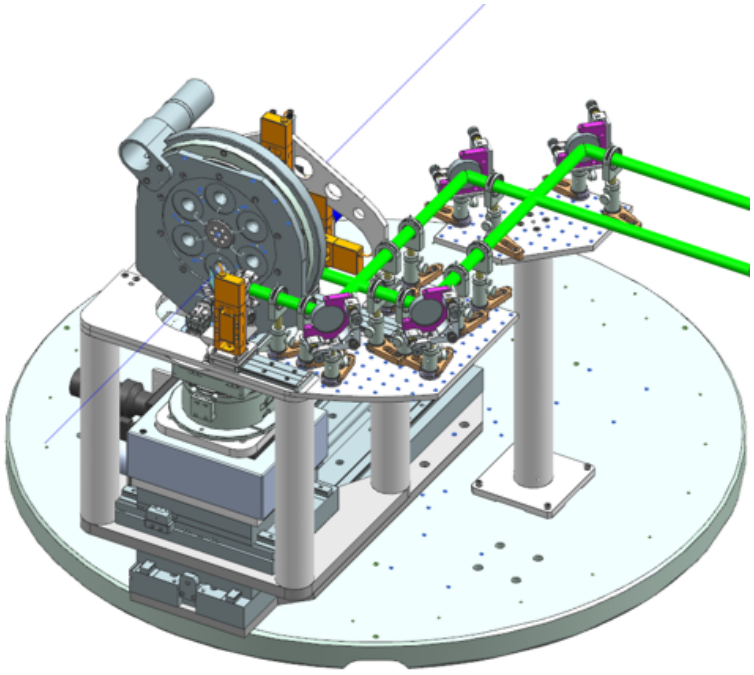

Figure 1.23: Diamond anvil cell (DAC) configuration inside IC2. The thin blue line depict the X-rays; the optical paths for NIR laser heating and temperature diagnostics are green.

The **photon energy** is fixed at 18–20 keV SASE, and the usual repetition rate is 2.2 MHz, with a maximum of 4.5 MHz (available at HED only during 1 week per run). The X-ray pulse energy is > 0.5 mJ from the undulators (not accounting for beamline transmission; see Section 1.1.6). The X-ray **focal spot size** is $5 - 15$ µm (fixed at 5 µm, but effectively larger depending on beam pointing stability). As standard **detectors**, we provide the AGIPD 500K detector (MHz-capable; see Section 1.2.4.4) and a Varex flat panel detector (10 Hz capable; see Section 1.2.4.3).

1.4 Target fabrication, characterization and alignment

1.4.1 Target fabrication laboratory

Since 2020, HED-HIBEF has built up a target fabrication laboratory that allows us to manufacture solid samples for experiments as well as to react to unforeseen or short-term requests before and even during beamtimes. A typical workflow for dynamic shock compression experiments is depicted in Fig. 1.24.

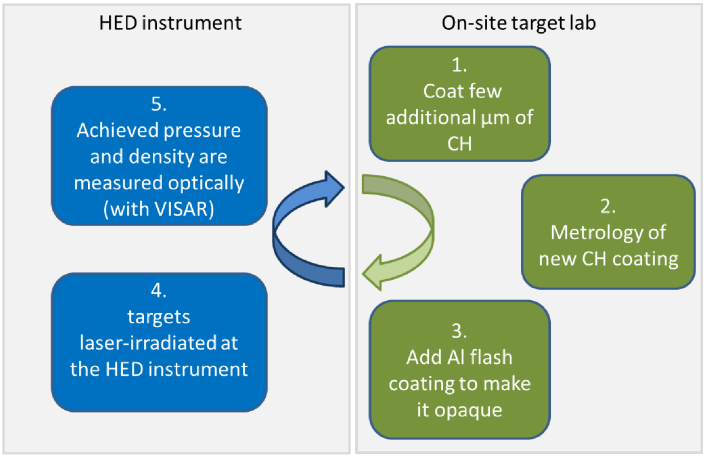

Figure 1.24: A typical work flow for dynamic compression, showing the need for an onsite target laboratory. The picture is taken from our EuXFEL Management Board proposal from 2018.

Two rooms at DESY Photon Science are equipped with the following equipment for deposition targets, slurry targets, gluing jobs, and DAC loading:

- CH coater for ablator coatings on shock targets
- Metal HEX coater for metal coatings
- Leica M165 C stereo microscope
- Micro EDM gasket drilling system for diamond anvil high-pressure experiments

Since summer 2023, an HED.owned fs laser cutter (Trumpf laser) that allows for cutting gaskets and targets is hosted at the DESY nanolaboratory. Finally, a PRL (Pressure by Ruby Luminescence), a Raman microscope, and a workbench in the EuXFEL XBI laboratory are available for users.

In addition, we have upgraded the SASE 2 target preparation lab, located right next to the HED experiment hutch, with a Keyance Digital VHX-7000 microscopy system capable of batch sample characterization of EuCall frame size frames. This system

is also equipped with a laser induced breakdown spectroscopy analysis module for elemental determination. We have organized the work area to allow fast turnover target mounting onto sample frames.

1.4.2 White light interferometry

White light interferometry (WLI) is a non-contact optical method for surface height measurement. To facilitate and improve the precision of sample alignment, we implemented the WLI for the IC2 chamber as an additional tool to determine the position of the sample surface to ensure the good overlap between the DiPOLE laser and the X-ray beam. Fig. 1.25 (top) shows a schematic of the WLI, consisting of white light source, reference and main arms, bunch of imaging optics, and cameras. The WLI optical setup is installed vertically to the 12.5° port from the X-ray entrance port, as this port corresponded to the sample surface normal. The WLI appeared a very useful tool for the quick and precise alignment of samples during the first DiPOLE beamtimes. The precision of the determination of the position appears less than $5\mu m$. We saw clear fringes from YAG crystal when aligned. But also from non-polished samples (real samples for experiments), the speckles appeared when aligned correctly (the image in the bottom-middle in Fig. 1.25) which doesn't appear when misaligned.

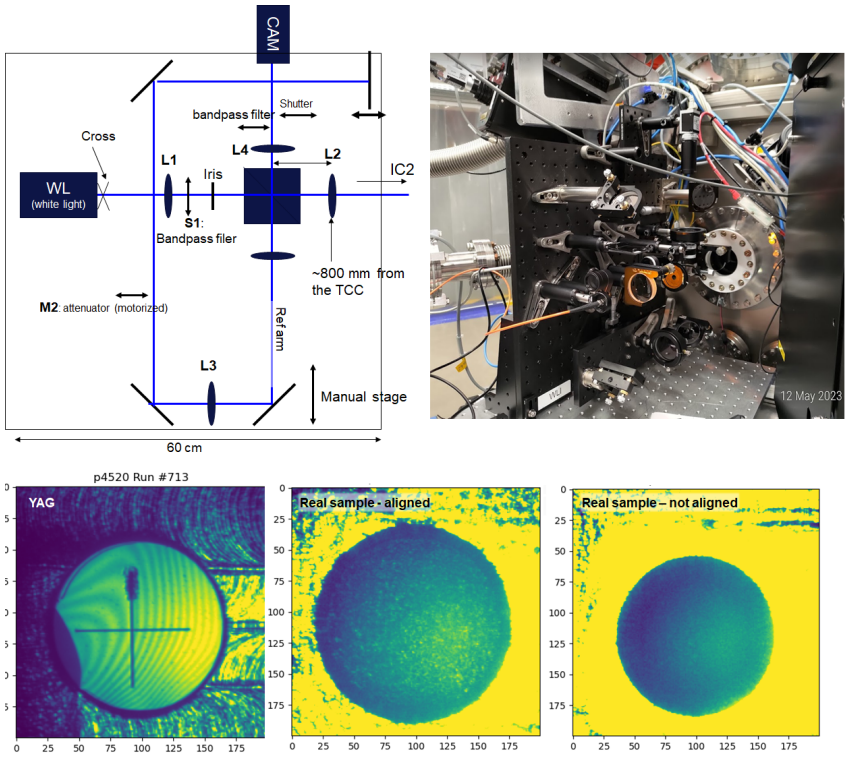

Figure 1.25: Top: WLI installed at the IC2 chamber to facilitate the sample alignment. **Bottom:** When the sample is aligned to the correct depth position, the fringes or speckles appear from polished samples or non-polished surfaces, respectively. It appeared that the WLI worked for most of the samples used for DiPOLE experiment (see Section 3.5.2).

1.5 Controls, data, and analysis

The main tool to control and monitor hardware devices is the distributed control system Karabo [39; 40]. All hardware components are represented as a device in Karabo, with specific states, properties (attributes), and functionalities. All devices and their properties are accessible via a GUI interface in which individual GUI windows (scenes) can be customized (see Section 1.5.1).

All detectors at HED exist as devices in Karabo, so that live images can be displayed and monitored. Simple data analysis tasks, e.g. mean pixel value over a region of interest (ROI) or fitting of a Gaussian function to a beam profile, can be done directly in Karabo. Often, however, the data is streamed to secondary software for more advanced and custom data analysis and data visualization (denoted online analysis). Examples of online software and applications are Extra-metro, DAMNIT (Data And Metadata iNspection Interactive Thing), and Jupyter Notebooks running on an online cluster utilizing Python packages created by the Data Department to facilitate reading of the data from the h5 files.

Data recording can be controlled via the data acquisition device (DAQ), which is a specific device in Karabo. Separate data acquisitions are organized in runs, with each start/stop action of the DAQ creating a new run. An overview of the runs recorded can be obtained from the metadata catalogue via a web interface (https://in.xfel.eu/metadata) in which run and sample types can also be specified and edited. After a run is finished, the data is available on the online cluster (computing infrastructure located at the EuXFEL), but detector data are not corrected yet unless an online calibration pipeline is set up. Otherwise, the data need to be migrated to the Maxwell computing cluster (offline cluster) at DESY. Once the data is transferred, the calibration pipeline corrects the detector data and creates next to the original data (raw) a folder containing the processed data (proc). Analysis on this data is denoted offline analysis (see Section 1.5.2).

1.5.1 User macros and scenes

Scenes in Karabo are convenient to display and group several connected devices and functionalities. Since most information and functionalities can be easily displayed and controlled via pre-defined widgets (e.g. plots, graphs, buttons, and input fields), often a specific scene is created for each higher-level device or even for every new experiment. After the initial alignment and troubleshooting phase, an experiment often consists of sequential repetitions of different measurement steps. Hence, simple ways of scripting and automatizing such procedures have been explored. The scantool provided by the Data Department at EuXFEL has improved significantly since the start of operation and is routinely used at HED.

Operations at HED have shown that, once an experiment enters the data acquisition phase, high-level automation can speed up data acquisition significantly. In addition, certain conditions, like wrong filter and laser settings, can result in damaged equipment, in particular cameras. Fur this purpose, we developed an automation framework in Karabo, which makes it possible to build complex sequences surveying machine safety and verifying automatically parameters for successful data acquisition (e.g. beam parameters).

Up-to-date sequencing includes:

- Change of laser and X-ray intensity
- Timing changes
- Sample movement
- DAQ control
- Shot-on-demand control

Figure 1.26: HZDR HIBEF instrument scientist A. Pelka operating the HED-HIBEF instrument in the instrument control room. The top screens show the solid targets arrangement. The screen in the centre shows the live view of the targets in IC1.

In addition, we developed a sample registration process to import sample information and positions of a large sample frame into Karabo.

1.5.2 Data analysis

Facility-wide, the Data Analysis group provides the means to facilitate the processing of experimental raw data. Packages such as DAMNIT and Extra-metro now display online datasets and key values in real time. In additions, we have worked with the Data Department on specific challenges for VISAR and XRD data analysis. In particular, a joint “moonshot” project in 2021 achieved the synchronization of the pulse-picker unit (PPU).

Offline, post-experiment analysis is facilitated mainly on the Maxwell computing cluster. The amount of data generated by the 10 Hz repetition rate of the machine and train-resolved diagnostics, typically including several ~MPix detectors, limits the portability of data without significant reduction. Pre- and post-facto data reduction is also a priority to limit EuXFEL’s data storage requirements, ensuring scalability and continuity for the facility. HED could notably benefit from this, as many experiment datasets are single- or few-shot, making use of the available drivers—however, it is also notably one of the least data-intensive instruments for the same reason.

In offline data analysis, we have developed advanced flatfielding of X-ray phase

contrast images. Spatial and intensity fluctuations in the illuminating X-rays affect our illumination function. Before taking imaging data from a sample, we collect on the order of 1000s of individual illuminations (a few minutes integration time) with the Optique Peter microscope, without any target (free-beam data). Simultaneously, we record the position of the X-ray beam on an upstream pointing monitor, the *HED pop-in* transmissive diamond screen at the end of the photon tunnel. This way, we build a correlation database of beam position centroids on that imager and the corresponding illumination of the target.

Another example of offline data analysis is the analysis of spectroscopy data from ReLaX high-intensity shots. We use the HAPG spectrometers to acquire e.g. emission spectra. The challenge is a strong, continuous background of $>$ MeV/pixel from bremsstrahlung and thermal plasma self-emission. On the hardware side, we developed and implemented additional spectrometer shielding, which reduces the recorded intensity by $2-3\times$. In future, magnets to deflect fast electrons are planned. However, the data can be further improved with post-processing. First, knowing the regions of interest on the 2D detector where relevant X-ray signal is present and other regions with pure background, backgrounds can be subtracted. Second, using the energy resolution of the chip via the counts a single X-ray photon in the energy range of interest creates, we can threshold the data. Using a simple upper and lower (static) threshold to flat the noise and cut all high-energy events still leaves many charge sharing events, e.g. at edges of a hard photon hit. Using dynamic *Otsu* thresholding [41] can minimize the sum of variance of datasets.

It has to be noted that other packages developed by users, such as the rosahami-processor (`https://gitlab.hzdr.de/smid55/rosahami_processor`) for flat-fielding SAXS images, VISAR-data unwarping routines, etc. are integrated and made available to the users as these are developed and tested.

As typical example of online analysis, where real-time feedback during data alignment and data acquisition is necessary, is to observe and evaluate the spatial pointing of targets, e.g. the liquid cryogenic jet. From two observation cameras, the current jet position is extracted and analysed with respect to its offset to our established target chamber centre (TCC). This builds a histogram of jet position over time, which we could use to qualify shots with *good* jet position within a run (i.e. within the Rayleigh range of both beams), counting up to qualify when sufficient statistics were obtained—as well as having someone actively steer the jet to stay in the centre.

2 Staff and operation

2.1 Joint HED and HIBEF teams

The operation of the HED-HIBEF instrument is done jointly by staff employed by EuXFEL, DESY, and HZDR (see details below). On the daily basis we work as one team with equal duties and responsibilities.

The HED group at EuXFEL currently has a base staffing of 16.5 full time equivalent (FTE) positions: a **group leader**, a 50% **assistant** (shared with MID), **10 instrument scientists** (including operation leader Konôpková and detector scientist Preston, who is seconded to DET for three years since 2021), **3 engineers**, and **3 technicians**. We are exceeding the regular 14 FTEs per instrument because (a) HED is hosting one additional engineer (Batchelor) for the integration of the split-and-delay line, (b) we have an additional instrument scientist to compensate for the secondment of Preston to the DET group, and (c) we share an assistant with MID.

Two of the engineer positions are shared with the MID instrument. This allows broadening the expertise in electrical and mechanical engineering and capitalizes on synergies with the activities at MID. These engineers are also **team leaders** and form a team with the mechanical and electrically trained technicians, respectively. The three technicians specialize in electronics/electrical work and mechanics/vacuum systems, respectively. All of the engineering and technical positions are tenured, while, among the 10 scientist positions, 5 are tenured, as illustrated in Fig. 2.1. This is in agreement with the management directive of a maximum number of permanent scientist positions in the instrument groups. The number of postdoc and Ph.D. student positions is fluctuating with time (depending on internal/external funding opportunities and success with grant applications), but currently there are **2 postdocs** (one with full external funding) and **5 Ph.D. students** (with 1 fully EuXFEL-funded, 3 fully DFG-funded, and 1 funded by a UK grant). Five previous Ph.D. students from the HED group successfully graduated between 2020 and 2023 [42; 43; 44; 45; 46] as well as two master students, who both continued their careers at HED as Ph.D. students.

Employed by the EuXFEL Laser (LAS) group, E. Brambrink serves as the laser scientist to integrate the large HIBEF-contributed laser systems into the EuXFEL infrastructure at HED.

Table 2.1: Overview of the current (Feb. 2024) staff positions and employees of the HED group. OL – operations leader, TL – team leader. TL and assistants are shared with MID. Asterisks (*) indicate limited contracts.

EuXFEL HED	HZDR HIBEF	DESY HIBEF	Other
Group heads			
U. Zastrau	T. Toncian	C. Strohm	
Administrative and scientific assistants			
C. Franke	M. Looden		
Instrument scientists			
Z. Konôpková (Operation Leader)	C. Baehtz (Coordinator)	R. Husband*	R&D postdocs*
K. Appel	A. Laso Garcia	M. X. Tang*	N. N. (hiring)
M. Andrzejewski*	H. Hoeppner		M. Banjafar
S. Goede	A. Pelka		
O. Humphries*			Ph.D. students*
M. Nakatsutsumi			D. Bespalov
T. R. Preston (DET)			K. Buakor
L. Randolph*			C. Camarda
R. S. Venkata*			M. Mishchenko
N. N. (hiring)*			C. Prestwood
E. Brambrink (LAS)			
Engineering			
A. Schmidt (TL)	J. Hauser		R&D engineer*
B. Baranasic (TL)	B. Näser		D. Loureiro
L. Batchelor	J.-P. Schwinkendorf		
	G. Shoulga		
	S. Di Dio Cafiso		
	M. Masruri		
	M. Toncian		
Technicians			
T. Feldmann		M. Röper	
E. C. Martens			
S. Wagner			

Our team is completed by **staff contributed by the HIBEF UC**. The two main institutes HZDR and DESY currently contribute 12.5 and 3 FTEs, respectively. These colleagues have full-time working places at EuXFEL and are part of the permanent operation staff for the joint HED-HIBEF instrument. HZDR, as the leading

institution of HIBEF, contributes a group leader (T.Toncian), a HIBEF coordinator (Baehtz) and a 50% assistant (Looden). HZDR furthermore puts a focus on the laser operation for the ReLaX and DiPOLE-100X lasers, which is reflected in the profile of the 4 instrument scientists and a crew of 5 laser engineers. In addition, HZDR contributes an electrical and a mechanical CAD engineer. The DESY contributions are coordinated by C. Strohm and operated together with a scientist and a laboratory technician. These include the diffraction platform IC2, detector systems (AGIPD, Varex), a nanofocus setup, and the operation of a joint HED-DESY target fabrication laboratory. Until recently, the team was complemented by a German-Chinese OCPC postdoc focusing on target fabrication and delivery which lead to a follow up Eu.XFEL R&D project for 2024-25.

Hence, currently there are a total of 40 persons working for HED-HIBEF, equivalent to 38 funded FTEs. It is estimated that this staffing and composition is just sufficient to develop, maintain, and operate the instrument and, at the same time, create a stimulating environment with resources for R&D and in-house research, in close collaboration with external partners.

2.1.1 Shift work

In *priority mode*, which is the current operation mode of SASE 2, HED receives beam every other week (typically 6 days in a row, alternating with MID) amounting to a total of about $15 \times 6 = 90$ days per year. All scientists, all laser engineers, and postdocs participate in shift work at the instrument. Additionally, Ph.D. students at HED have the opportunity to participate within a reduced frame in beamline operation duties as part of their training. The average annual shift breakdown for the post–COVID-19 pandemic years is listed in the following table.

	HED scientists	**HIBEF scientists**	**Laser staff**	**Ph.D.s / Postdocs**
2022	38	36	25	14
2023	43	48	54	10

As a reference, an average of 40 shifts per year amount to 20% of the total working time. Most of the workload is found during the preparatory and setup phase of the experiments. This includes experiment design, sourcing necessary parts and equipment, and, finally, building, alignment, calibration, and validation of the experiment setups. Due to the limited time slots available for conducting the experimental tasks, these times are regularly associated with overtime-hours accrual. Also, the more than doubling of shifts for laser engineers can be explained as DiPOLE 100-X started user operation from 2023 and also the lasers started to be offered with

onsite laser support for night shifts.

In general, shift work coverage is divided in three daily shifts of 8.5 h each, and starts every day as follows:

Day shift	07:00–15:30
Late shift	15:00–23:30
Night shift	23:00–07:30

For handover procedures from shift to shift, a 30 min overlap is built into this scheme.

Until 2023, this scheme was applied for six consecutive days, typically from Tuesday to Sunday (incl.). From 2024 onwards, it will be shifted by 1 day to Wednesday to Monday (incl.). A local contact (LC) and a deputy LC are appointed per user experiment (which often, but not always, coincides with one week) and both are responsible for organizing the shift plan, instructing and leading the shift crew, and communication with the PI/MP. There is always a minimum of two staff members on shift, but, most of the time, additional people are around to support the experiments and drivers, as necessary. We are currently performing on-call duty (OCD) for the local contacts to make them free of shift work and allow them to assign their working time flexibly and on short notice.

Shift plans are compiled by the operation leader, instructing the local contacts to choose from a pool of available operation staff and agree with them on a shift plan that covers all necessary expertise for 24 h operation. Shift plans have to be submitted no later than 6 weeks before a beamtime to Human Resources and the Works Council for review. We typically plan the shifts for a run (half-year period) in two to three blocks and submit changes accordingly.

During the days without beam, dismounting of the previous experiment takes place as well as preparations for the next experiment. This can involve a change of the setup, driver, and special preparations, all coordinated by the LC and the operation leader (OL). The team of LC and OL are also responsible for bridging knowledge gaps by requesting specialized support from EuXFEL's *expert groups*, for instance the Data Analysis group, the DET group, LAS group, Safety and Radiation Protection (SRP) group, or the Sample Environment and Characterization (SEC) group. This is essential for proper preparation of an HED experiment, which is a nexus between numerous groups with highly specialized skills and competences.

EuXFEL currently has no overarching, company-wide engineering groups that take

care of the daily operation of the instruments. Therefore, the group leaders of HED (Zastrau) and MID (Madsen) started several years ago to share engineering staff across their two SASE 2 instruments.

2.1.2 Staff profiles HED

Scientists

Ulf Zastrau – HED group leader and leading scientist at EuXFEL. At EuXFEL since 2015. Specialized in X-ray science with a focus on spectroscopy, dense plasma physics, and instrumentation.

Zuzana Konôpková – Operations leader. At EuXFEL since 2016, operation leader since 2023. Expertise in beamline operation, diamond anvil cells, high pressure physics, geophysics and planetary science, and X-ray methods.

Karen Appel – Instrument scientist. At EuXFEL since 2013. Expertise in X-ray beamline design, instrumentation and X-ray optics, and high-pressure mineralogy and geochemistry, created by DAC and shock.

Motoaki Nakatsutsumi – Instrument scientist. At EuXFEL since 2012. Expertise in ultrafast optical laser-matter interaction. Establishes femtosecond surface science using grazing-incidence X-ray geometry.

Sebastian Goede – Instrument scientist. At EuXFEL since 2015. Expertise in relativistic laser-matter interaction, and ion acceleration. He is an expert for target delivery via cryogenic jets.

Thomas Preston – HED detector scientist. At EuXFEL since 2017. Expertise in X-ray heating, ultrafast solid state physics and warm dense matter, and X-ray spectroscopy of dense plasmas.

Lisa Randolph – Instrument scientist. At EuXFEL since 2022. Expertise in ultrafast surface science and X-ray scattering.

Oliver Humphries – Instrument scientist. At EuXFEL since 2022. Expertise in X-ray heating, warm dense matter, X-ray spectroscopy, and advanced data analysis methods.

S.V. Rahul – Instrument scientist. At EuXFEL since 2021 as a research postdoc, as an instrument scientist since 2023. Expertise in femtosecond lasers and laser-excited relativistic surface effects.

Michal Andrzejewski – Instrument scientist. At EuXFEL since 2024. Expertise in diamond anvil cell research and high pressure chemistry.

NN – Instrument scientist. The position is currently being advertised with expertise in laser-shock compression.

Erik Brambrink – Laser scientist. At EuXFEL since 2018. Member of the EuXFEL LAS group for the integration an operation of the HIBEF high power lasers, expert for

radiation safety of the laser-plasma source. Expertise in laser–matter interaction.

Administration

Christiana Franke – Scientific and administrative assistant. At EuXFEL since 2021. Shared 50/50 with MID since 2023. Expertise in finance and accounting, purchasing, event management, access rights, and guest registrations.

Engineers and technicians

Andreas Schmidt – Mechanical engineer, 50/50 shared with the MID group. At EuXFEL since 2015. Responsible for instrument integration, design, and technical infrastructure of the HED instrument. Leads a team consisting of technician Feldmann and mechanic Martens.

Thomas Feldmann – Instrument technician. At EuXFEL since 2016. Works with vacuum, mechanics, and instrumentation at the HED instrument.

Eike Martens – Instrument mechanic. At EuXFEL since 2016. Works with vacuum, mechanics, and instrumentation at the HED instrument.

Bernand Baranasic – Electrical engineer, 50/50 shared with the MID group. Recently hired asa replacement for Sukharnikov (see below). Responsible for the electrical infrastructure of the HED instrument from March 2024. He leads a team consisting of technicians Wagner (HED) and Andersen (MID).

Sven Wagner – Instrument technician. At EuXFEL since 2020. Works with electrical installations and electronics at the HED instrument.

Lewis Batchelor – Mechanical engineer. At EuXFEL since 2012. Responsible for instrument integration of the split-and-delay line, a BMBF-funded project led by the University of Münster (Germany) into the HED instrument (Section 4.2.1). He also has long-term experience with diverse devices such as attenuators and the Beryllium lenses (Section 1.1.10) and associated vacuum chambers used for X-ray focusing.

Daniel Dias Loureiro – R&D engineer. At EuXFEL since 2021. Responsible for the design and implementation of the cryogenic jet setup (Section 4.1.3.2).

Postdocs

Mohammedreza Banjafar – Postdoc. At EuXFEL since 2022, was a Ph.D. student at SPB/SFX since 2017 and HED since 2019. Works with hydrodynamic and PIC codes for laser-excited ultrafast surface science.

A few members have worked in the past at HED on limited contracts and have successfully transitioned to other positions. Former instrument scientist Mikako Makita joined the EuXFEL XRO group in 2021, Valerio Cerantola was appointed a tenure-track professorship programme at the University of Milan (Italy) in 2022, Jan-Patrick Schwinkendorf joined the HIBEF laser team in 2023, and Victorien Bouffetier joined ALBA synchrotron (Barcelona, Spain) in 2023. Mechanical engineer

Ian Thorpe joined STFC CLF (UK) as a senior engineer after completion of the construction phase in 2019. Electrical engineer Konstantin Sukharnikov transitioned to EuXFEL's DET group in 2023 to join the newly established detector development programme. This illustrates that former members of the HED group are well-trained and qualified for future jobs in cutting-edge basic science.

2.1.3 Staff profiles HZDR-HIBEF

The staff permanently contributing to the operation of the HED-HIBEF infrastructure consists of personnel employed by DESY (Hamburg) and HZDR (Dresden).

Scientists

Toma Toncian – HZDR HIBEF group head. At EuXFEL since 2016. Expertise in optical high-intensity lasers, laser-plasma physics, and strong field science.
Carsten Bähtz – HIBEF coordinator. At EuXFEL since 2014. Expertise in beamline operation, X-ray optics, X-Ray diffraction, and thin film analysis
Alejandro Laso Garcia – Instrument scientist. At EuXFEL since 2020. Expertise in nuclear physics, small angle X-ray scattering, X-ray imaging, and instrumentation.
Hauke Höppner – Instrument/laser scientist. At EuXFEL since 2017. Expertise in ultrafast laser technology, laser-matter interaction, and instrumentation.
Alexander Pelka – Instrument scientist. At EuXFEL since 2013. Expertise in laser-matter interaction and small angle X-ray scattering.

Engineers and technicians

Samuele Di Dio Cafiso – Laser engineer[⋆]. At EuXFEL since 2017. Expertise in development of laser oscillators and amplifiers with Yb-doped materials.
Masruri Masruri – Laser engineer[⋆]. At EuXFEL since 2021. Expertise in high-power laser systems and post-compression techniques based on self-phase modulation of high-energy laser pulses.
Jan-Patrick Schwinkendorf – Laser engineer[⋆]. At EuXFEL since 2019. Former HED beamline scientist, since 2023 in the HIBEF laser team. Expertise in in short-pulse lasers, laser-matter interaction, particle acceleration, vacuum, and instrumentation.
Monika Toncian – Laser engineer[⋆]. At EuXFEL since 2017. Expertise in development and applications of short-pulse lasers.
Georgiy Shoulga – Laser engineer[⋆]. At EuXFEL since 2023. Expertise in extreme nonlinear optics and high harmonic generation in gases as well as optical inspection of silicon wafers in semiconductor industry.
Jens Hauser – Mechanical CAD engineer. At EuXFEL since 2019. Responsible for CAD construction of opto-mechanical, vacuum components, and mechanical integration of user-provided setups.
Björn Näser – Electrical engineer. At EuXFEL since 2022. Responsible for repairing and commissioning of high-voltage systems, commissioning and integration of stepper motors, automation systems, and cabling.

[⋆] Responsible for the maintenance and operation of the ReLaX 300 TW Ti:Sapphire and DiPOLE 100-X laser systems.

2.1.4 Staff profiles DESY-HIBEF

Scientists

Cornelius Strohm – DESY HIBEF responsible. At EuXFEL since 2017. Expertise in beamline instrumentation for time-resolved and extreme conditions science with spectroscopy and scattering, including low temperatures, pulsed high magnetic fields, and static and dynamic compression techniques. Interest in magnetism and strongly correlated systems.

Rachel Husband – Instrument scientist. At EuXFEL since 2021. Expertise in static and dynamic diamond anvil cell techniques, high-pressure science, and X-ray based techniques, including diffraction, imaging, and X-ray heating.

Postdocs

Minxue Tang - Postdoc. At EuXFEL since 2021. Expertise in dynamic compression techniques, materials science, target fabrication, high pressure science, and X-ray diffraction, working both on simulations and experiments.

Technician

Michael Röper – Laboratory technician. At EuXFEL since 2019. Training as an electrician and in communications engineering. Expertise in vacuum systems and deposition techniques for target fabrication.

2.1.5 HED-HIBEF coordination board

Strategic, operational, financial, and safety-related topics are discussed and agreed upon by the **coordination board** in regular weekly meetings between Zastrau (HED lead), Toncian (HZDR lead), Strohm (DESY lead), and Baehtz (HIBEF coordinator). A collaboration contract between HZDR and EuXFEL outlines the terms and conditions for the HIBEF UC and priority access at the EuXFEL.

2.1.6 Ph.D. student programme at HED-HIBEF

The HED group has hosted and is hosting several Ph.D. students, with positions funded by EuXFEL, HZDR, or third-party grants. As EuXFEL is not an academic institution, an academic project partner needs to be found for each student, as direct academic supervision is a prerequisite for obtaining a Ph.D. degree at a university.

Often, the students are located full time at EuXFEL, and the academic supervisor is only remotely involved. While the HZDR HIBEF group leader (Toncian) has an

Table 2.2: Recently completed Ph.D. projects as well as currently ongoing HED Ph.D. projects

Name	Topic	Supervisor/University	Deadline
Johannes Kaa	Electronic spin state studies of iron-bearing minerals contained in an x-ray heated Diamond Anvil Cell	M. Tolan, K. Appel, C. Sternemann (TU Dortmund, funded by BMBF)	8/2023 (finished)
Mohammadreza Banjafar	Dynamical evolution of a high-density plasma surface upon high-intensity laser-solid interaction	M. Nakatsutsumi, Th. Kluge (HZDR), T.E. Cowan (HZDR), A.P. Mancuso	7/2023 (finished)
Mahdi Habibi	Bremsstrahlung suppression due to high magnetic fields in relativistic laser plasmas (simulation-based study)	T. Toncian (U Düsseldorf, funded by HZDR)	10/2023 (finished)
Lennart Wollenweber	Study of matter in extreme conditions with high-resolution inelastic x-ray scattering	U. Zastrau, N. Rohringer (U Hamburg, funded by EuXFEL)	11/2023 (defense 3/2024)
Khachiwan Buakor	Dynamic compression experiments of (Mg,Fe)O solid solution at free electron lasers.	K. Appel, R. Redmer (U Rostock, funded by DFG)	8/2024
Mikhail Mishchenko	Ionization dynamics in relativistic laser plasmas studied by time-resolved resonant x-ray emission	U. Zastrau, S. Molodtsov (U. Freiberg, funded by EuXFEL)	3/2024
Anand Dwivedi	Towards higher densities of matter: ultra-high pre-compression in dynamic shock experiments (R&D Project S-278)	U. Zastrau, V. Cerantola, T. Gorkhover (U Hamburg)	8/2024
Nodoka Hara	Investigation of the spectra reconstruction requirements of high-resolution IXS using SASE	U. Zastrau, C. Milne, A. Di Cicco (funded by U Camerino, IT)	12/2024
Dmitrii Bespalov	High-resolution inelastic x-ray scattering from warm dense matter	U. Zastrau, D. Kraus (U Rostock, funded by DFG)	8/2026
Carolina Camarda	Properties of ferrous geomaterials under conditions of the core-mantle boundary	K. Appel, M. Sieber, C. Sternemann (TU Dortmund, SPP DeepDyn, funded by DFG)	1/2027
Calum Prestwood	Benchmarking collisional rates and hot electron transport in high-intensity laser-matter interaction	O. Humphries, C. Palmer (QU Belfast)	9/2027

appointment with the University of Düsseldorf and can directly supervise students, is it desirable for the group leader (Zastrau) to become a member of a university faculty in order to be able to combine the local scientific supervision and grant the academic degree within one group. The HED group runs a weekly one-hour science meeting in which the Ph.D. students are required to give group-internal updates in their Ph.D. work. With the current amount of students, each presents their progress every 4–6 weeks.

Currently (Jan. 2024), six Ph.D. students have successfully defended their theses (M. Schölmerich [42], M. Biedermann [43], M. Banjafar [45], C. Plückthun [44], J. Kaa [46], M. Habibi). The most recent Ph.D. projects as well as the currently ongoing Ph.D. projects are listed in Table 2.2.

2.1.7 Group retreats

In order to foster a good team spirit, discuss challenges, and establish trustful interpersonal relations, the joint HED and HIBEF groups and all HED students have conducted 1–3 day long group retreats. We started this activity in 2018, a few months before HED started user operation. The agenda has been organized and moderated by group leader Ulf Zastrau; however, a format with external moderators is planned for 2024. The annual rhythm was interrupted in 2021 due to the COVID-19 pandemic. In 2022, scientific director Sakura Pascarelli joined the team, and we discussed extensively with her the possibility of allowing members of the team to directly interact with management. In 2023, the entire Schenefeld-based team took a bus trip to visit the HIBEF lead institute HZDR, visited their facilities, and had discussions with their staff. This was done in order to establish more personal work relations between HED-HIBEF at EuXFEL and HZDR staff, and to inform ourselves firsthand about the laboratories and expertise at HZDR (Fig. 2.1 bottom). For June 2024, a two-day group retreat is planned in Hamburg and will include two professional business coaches.

The most prominent and recurrent topics (chosen by the staff) were lab organization and clean-up procedures, commissioning workflows, workload distribution during setup weeks, career perspectives (Section 2.1.8), documentation of the instrument and alignment procedures, reorganization of the group when new staff were to be hired, the role of the local contacts to work with staff and users to ensure a successful experiment outcome (Section 2.5), and the relationship between the instrument and the support (or expert) groups within EuXFEL when it comes to short-, mid-, and long-term planning, implementation, and troubleshooting.

Figure 2.1: Photo of the HED-HIBEF group retreat 2023

Date	Location of HED-HIBEF group retreat
27–28 November 2018	Maritim Clubhotel Timmendorfer Strand
17 June 2019	La Cocina, Hamburg
20–21 February 2020	Maritim Clubhotel Timmendorfer Strand
16–17 June 2022	Eurostrand Hotel Fintel
21-23 June 2023	Helmholtz Centre Dresden-Rossendorf

2.1.8 Career perspectives for instrument staff

As shown at the end of Section 2.1.2, HED-HIBEF is a highly attractive launchpad that has trained, educated, and developed both early and mid-career scientists and engineers who have elevated their careers after moving from EuXFEL. While these career moves can be very fruitful for the individual instrument staff members, they come with loss of continuity and accumulated knowledge required for beamline operation.

Since EuXFEL is a relatively small company, the career perspectives inside the company are limited. Within the HED group, required tasks for successful beamline operation are typically covered with topical focus by individual people. Promoting a colleague who has already gained experience and shown extraordinary performance into a more senior position is usually not possible because these positions are already

occupied and the staff quota cannot be increased. Transitions within the company are of course possible, and, frequently, well-trained internal candidates apply successfully for these job openings. A company-wide career perspective plan accounting for the individual experience track, strengths, and expertise would be very desirable, as it would also maintain the long-term knowledge needed for successful operation. As an example, currently, EuXFEL does not provide a career perspective to develop instrument scientists into more senior roles (half of whom are on limited contracts), and it lies within the initiative of each colleague to apply for other positions, within or outside of EuXFEL.

2.2 Aspects of efficient operation

At EuXFEL, each of the three undulators (SASE1–SASE3) serves two (SASE1, SASE2) or three (SASE3) scientific instruments. Until 2021-I, each instrument was receiving beam either during the day (07:00–19:00) or at night (19:00–07:00 the next day), respectively. Every other week, this pattern was swapped, and, every 4–6 weeks, an additional week for accelerator and undulator studies (without X-ray delivery to the instruments) was scheduled. Most users appreciated the distribution over several days (or nights), interrupted by 12-hour breaks, as it allowed them to analyse data, prepare new targets, and get some rest. However, the instrument operation was challenging: The photon energy needed to be changed and SASE lasing re-established at a reasonable level two times per day. As the location of the X-ray source point in the undulators could change with linac performance and the individual operators strategy, the X-ray beam transport and focusing had to be re-established at the beginning of each shift. For special modes, such as hard X-ray self seeding (HXRSS), two-colour operation, or short pulses, which require several hours of setup, this scheme was not applicable. If triggered drivers, especially the short-pulse lasers (PP laser, ReLaX) were used, the establishment of spatio-temporal overlap also took a few hours. We analysed the situation and found that, on average, between 3 and 6 hours per 12-hour shift (25–50%) were spent to bring the instrument into “data acquisition” mode. Besides the inefficiency of this process, it was not motivating for the staff to realign the beamline and instrument every 12 hours and to lose all these achievements every day. An experiment that was allocated five 12-hour shifts (60 hours) was only able to use between 30 and 45 hours.

Therefore, starting from 2021-II, we switched to weekly operation of one instrument. At SASE 2, either the HED or the MID instrument operated for a full week, and the X-ray energy, beam transport, and focusing (and potentially special modes, such as HXRSS), were set up only once (typically on Tuesdays). Also in 2021, the **Data Operation Centre (DOC)** was created, a team being physically present from 07:00 to

23:00 in a dedicated control room, solving all immediate problems at all instrument that took beam. Still being impacted by the COVID-19 pandemic, we reduced the load on the staff and minimized onsite presence, and operated only between 07:00 and 23:00. Several experiments were extended into the night until the early morning. From 2022 onwards, HED has staffed and operated all experiments around the clock with three shifts.

While the benefits of this continuous operation are evident by the arguments laid out above, we identified several challenges: Users now receive typically 48–72 hours of beamtime (2–3 days in a row), which is much more than 30–45 hours they could previously put to good use (or even the nominal 60 hours). However, now, users need to staff their experiments for 24 hours, analyse the data on the fly, and take decisions and mount targets during beamtime. Also, in case of equipment failure, repairs have to be carried out during X-ray delivery. We have nevertheless found that, with proper preparation and anticipation (e.g. ensuring data analysis tools are properly set up, users plan a shift schedule, prepare targets in advance, “plan B” in place), this scheme is still superior to the 12/12 hour switching.

We have observed in the past that setups that are built from scratch during the few days before each beam week require extensive debugging time, before and during X-ray delivery. Therefore, together with the scientific directors, we decided to schedule several experiments that require the same (or at least similar) experiment platforms in consecutive weeks, even if the PRP ranking suggests to schedule the top-ranked proposals all using different setups and/or experiment geometries. This grouping reduces setup time and improves the reliability of the setup.

Until November 2023, the group leader (Zastrau) was organizing the instrument operation by himself. Since November 2023, Zuzana Konôpková was appointed *HED operation leader* and is now overseeing the organization of these processes. The assignment of experiments to certain weeks in 2024-I and 2024-II, the assignment of local contacts to experiments, and the assignment of instrument scientist teams to experiments and shifts e.g. are already taken over by her.

2.3 Priority access, internal activities, and scheduling challenges

Since signing of the EuXFEL-HZDR collaboration contract in 2023 and the acknowledgement of the HIBEF contributions to the HED instrument by the EuXFEL Management Board (MB), the HIBEF UC is eligible for 30% of user beamtime from 2024 onward for 10 years. HIBEF member institutions will use this beamtime

for their programmatic scientific research, method development, and community building. Proposals are reviewed by a dedicated HIBEF panel and revised by the HED Proposal Review Panel (PRP) for scientific sensibility.

Typically, a run at the EuXFEL comprises 16 six-day weeks per half year, during which X-rays are delivered to the instruments around the clock (24 hours). This time is shared equally between the two instruments at the SASE 2 undulator. From the resulting eight “beam weeks” per run, the EuXFEL management suggests that two weeks are set aside for internal activities such as commissioning, developments and Ph.D. projects or internal research. The remaining six weeks are user beamtime, from which two weeks (30%) are reserved for HIBEF priority access and four weeks remain for regular user proposals.

In order to accommodate the requirements of soft and hard X-ray research, several electron energy setpoints are used for each run. Most frequently, these are 11.5 GeV, 14 GeV, and 16.3 GeV. Photon energies of $>$ 6 keV and above can be accessed with 14 GeV, and hard X-rays of $>$ 13 keV require the 16.3 GeV setpoint. The lower setpoint of 11.5 GeV (and occasionally even 10 or 8 GeV to produce soft X-rays at SASE 3) leads to poor beam intensity and quality at SASE 2, and scheduling of special modes, such as two-colour or HXRSS is not recommended. Thus, the about 2–3 weeks at 11.5 GeV cannot be used efficiently at HED, while we have a high demand for 14 GeV (HXRSS, two-colour) and 16.3 GeV (hard X-rays). Nervertheless, over the past few years, HXRSS has gained a lot of traction from the user side, and it became a highly requested operation mode. In conclusion, we would prefer HXRSS to become our regular operation mode.

The EuXFEL is currently the only X-ray FEL that can provide hard X-rays up to 25 keV with MHz burst rate. At HED, we can use the 4.5 MHz rate to X-ray heat samples and to record a time sequence in DAC and in pulsed magnetic fields studies. However, 222 ns between pulses is already slow for most HED processes, but reducing to 2.2 MHz or even less makes the pulse train unattractive to us. We cannot use it to acquire more data, as our ReLaX and DiPOLE lasers do not fire as frequently and targets (even jet targets; see Section 4.1.3) cannot be replenished fully at these rates when destroyed by the X-rays or laser driver. Special delivery schemes, such as long-pulse trains or 4.5 MHz, both essential for DAC research and a unique feature of the EuXFEL, can be scheduled for selected weeks only, as they often impact the operation of the other instruments negatively.

2.4 Choice of proposals by scientific topics

The suite of methods and drivers at HED-HIBEF enables not only HED science but also experiments in other scientific fields (*off-topic* experiments). Concrete examples that were carried out at HED-HIBEF are Axion search (Section 3.6.1), pair distribution function analysis of chemical reaction in solutions (Section 3.5), and non-linear X-ray science, such as frequency mixing.

However, during the preparation and execution, it becomes obvious that the lack of experience with non-established methods and setups is reducing the performance, and potential technical deficiencies are not always identified. This comes with its own challenges, as the overlap with the onsite scientific and technical expertise does not exist for these non-standard methods. Instrument scientists cannot discuss in depth the expected science case and subsequent technical and methodological requirements with users, which often is a prerequisite to a successful experiment. One relies in these cases heavily on the expertise level of the users providing equipment, which bears operational risks.

The *off-topic* experiments are also exclusively non-standard setups, which implies that more setup time is required, which directly translates into a higher workload for staff, less commissioned equipment, and non-optimized diagnostics. The opposite to this approach would be a community proposal using a fully established standard setup.

Looking at the over-subscription rate, the question arises whether we should limit our programme to the very core of HED science, using our drivers optimally and but also the expertise and scientific involvement of the HED-HIBEF staff as collaborators rather than operators. If the HED-HIBEF instrument aims to excel in a few scientific areas, then we should predominantly focus on those. Off-topic experiments should be either refused or accepted only on a case-by-case basis after discussion with the management.

2.5 Workflow from proposal to publication

In 2023, the HED-HIBEF team as well as EuXFEL started an effort to standardize and streamline, thereby improving the process of user beamtimes. This process should ensure quality control and communicate clear deadlines to the users to enforce proper preparations. The following guidelines were developed by HED (status: Sep. 2023) and will be followed by the local contacts in their communication with the users right after the acknowledgement of the allocated beamtime.

European XFEL – HED-HIBEF instrument (v.1, 9/2023)
EXPERIMENTAL READINESS SHEET FOR MP/PI

The local contact (LC) and a deputy are assigned by the facility to the user, represented by the main proposer (MP) and principal investigator (PI). The LC will communicate these preparation guidelines to the user. They ensure quality control of the user experiment.

T-6 months: Readiness review (~ 1 hr duration)

- PI/MP goes over rough experiment plan:
  - Experiment background/overview
  - X-ray/laser requirements
  - Planned diagnostics/detectors
  - Potential safety concerns:
    - Eye, radiation, particulates, cryogens, fall, etc.
- Start thinking about:
  - Equipment needed from EuXFEL. LC will inform corresponding person responsible that their equipment is requested.
  - Assistance needed from EuXFEL personnel.
  - List of visiting team members, rough breakdown of roles.
- What information or help does this experiment require from the EuXFEL team now to make it successful?

T-3 months: Readiness review (~ 1 hr duration)

- Estimated list of visiting team members with expected breakdown of roles.
- Safety concerns:
  - Dealt with satisfactorily?
  - Will we need to implement any unusual safety procedures? Transport activated material? Additional shielding?
- PI/MP goes over more detailed experiment plan:
  - Experiment background/overview
  - X-ray/laser requirements
  - Planned diagnostics/detectors (especially if user-provided)
  - Potential safety concerns
- Equipment needed from EuXFEL.
- Assistance expected from EuXFEL personnel
- What information or help does this experiment require from the EuXFEL team now for success (long lead time activities or items, shipment through customs)?

- Go over housing possibilities (guest house, reimbursement rules, arrival time before experiment is limited).
- Go over packing and shipping:
  - Shipping methods to get components to the EuXFEL (and how to ship it back afterward)
  - Users need to budget time for packing and shipping at the end of their experiment
- Rough shot plan, focusing on EuXFEL internal planning (night activities, roles covered 24 h, expected parameters changes of drivers and X-rays, venting/pumping cycles, etc.)

T-2 months: Ask MP/PI for the following information from their team

- MP/PI are reminded of their responsibility to follow up on the submission of arrival form (A-form) one month later (four weeks prior to the experiment).
  This requires:
  - All participants have UPEX registration.
  - All expected arrival and departure dates for the team, especially in the case of required visas.
  - Necessary safety training completed before arrival.
  - Are any targets planned that are not part of the original proposal? If yes, the "additional sample request" process has to be initiated with the User Office.
  - When in doubt, users should contact the User Office (useroffice@xfel.eu).
- Did the EuXFEL X-ray energy change from what was requested in the proposal? If yes, the "X-ray operations" group (xo@xfel.eu) has to be informed by the LC.
- If applicable, UPEX registration for long-term or earlier stay (laser-only shots, preparations, etc.).
- If applicable, MP/PI needs to send a radiation production summary/analysis for the final experimental safety review:
  - Types, quantities, energies, and spatial distribution of ionizing radiation generated by the experiment (e.g. protons, 10^6 per shot, 2.45 MeV, 4π)
- Shipping plan to the EuXFEL:
  - What?
  - When?
  - Who will receive it and how? (Usually LC – coordinate with, involve assistant)

T-1.5 months: Final readiness review

- Attendees of meeting:
  - PI/MP and all team members

  - LC and deputy
  - Relevant beamline scientists or required EuXFEL experts
- Receiving of shipments, storage considerations
- List of EuXFEL equipment required:
  - Make sure component responsible has confirmed availability (of themselves and their components)
  - Gather other equipment, perform maintenance and repairs as necessary, etc.
- From EuXFEL:
  - Who will pack up? When?
  - How will things be shipped back? Where?
  - Procurement: Any materials expected to be procured during the experiment? Consumables like gases, LN2, etc.
  - Setup plan, especially for user-provided equipment:
    * Walk us through the experiment setup.
    * Who does what?
    * How long does it take?
    * What components might you need from us?
    * Do you have spares of things that might break?
    * Rough risk analysis: most likely problems, possible solutions.
    * Review shot plan.

T-1.0 month

- Latest date to submit A-form
- Instruct PI/MP how to check whether their team has completed their safety training and submit their training certificates

Documentation submission prior to the experiment

A summary of links can be found at:

https://www.xfel.eu/users/quick_links/

- A-form and PAF:
  - Must be submitted no later than four weeks before the start of the experiment.
  - Lists all the experiment team (onsite and remote).
  - Used to generate the elog/ZULIP and data access rights, therefore try to fill in all people expected to take part in the experiment as well as data analysis.
  - Designates the travel-funded people and the targets to be used in the experiment.

- Safety assessment:
  - To be filled in by the MP/PI and sent no later than one week before the experiment begins.
  - It is always better to submit the paperwork in a timely fashion!
- Beamtime preparation document exchange:
  - An online shareable folder will be created in our “Sync & Share” system by the LC.
- When the experiment is finished:
  - An experiment report must be submitted between three and six months after the experiment.
- Publication policy:
  - A link to EuXFEL publication policy can be found here: https://www.xfel.eu/users/user_guide/publications
  - Explicitly,
    * Make sure to agree with the LC (and the HED group leader) on an author list that includes instrument team members that contributed to the work (shift work, setup, data analysis, etc.).
    * A DOI of the experiment dataset should be requested via the User Office and cited in your paper.
    * There are two mandatory sentences for the “Acknowledgements” section of each publication:
      · We acknowledge the European XFEL in Schenefeld, Germany, for provision of X-ray free-electron laser beam time at the Scientific Instrument HED (High Energy Density Science) under proposal number <Proposal Number> and would like to thank the staff for their assistance.
      · The authors are indebted to the HIBEF User Consortium for the provision of instrumentation and staff that enabled this experiment.
    * Approx. six weeks before the anticipated submission, an early draft has to be sent to the HED group leader (ulf.zastrau@xfel.eu) with the request to pass it on to the department heads of the support groups (in case their staff contributed significantly and deserve authorship, or their equipment was used and should be cited).
    * Approx. two weeks before submission, a close-to-final draft has to be sent to the responsible scientific director (sakura.pascarelli@xfel.eu).

3 Science highlights

At the time of writing the instrument review article [1] in 2021, a few early science publications had been published and were included. Here, we would like to give an overview of the current status, 4.5 years after the start of user operation.

As the HED-HIBEF group makes an effort to be not only technically but also scientifically involved in user experiments, we aim to have instrument scientists as active co-proposers on all of our proposals. We likewise often invite external users to our internal beamtimes. It would therefore be artificial to separate this chapter into in-house activities and external user science. Therefore, the structure of this part of the report is organized by scientific areas.

At the time of writing, the EuXFEL publication database registers about 100 scientific publications, based either on data acquired at the HED instrument or measured during external collaborations. Other than at the EuXFEL, the HED-HIBEF scientists also work on their individual scientific agendas and lead or join experiments at other FELs (SACLA [47; 48; 49], LCLS [47; 50; 51; 52; 53; 49; 54], PAL-XFEL [55] FERMI, SwissFEL, and FLASH [56]), synchrotrons (APS [57], PETRAIII [58; 59; 60; 57; 61; 62], and ESRF [58; 59; 63; 64; 53; 65]), and large laser facilities (DRACO [66; 67; 68], TexasPW, OMEGA [69], MTW [70], NIF, LULI, and LMJ), or computational studies [71; 72; 73; 74; 75; 76]. This enables us to compare the performance of the HED-HIBEF instrument to competitive facilities worldwide, learn quickly about new developments, and keep an active links to the international scientific community in our field. However, this important part of our work is not described in more detail by this instrument review.

In 2021, a team of high-pressure scientists from EuXFEL and ESRF published a paper entitled “New frontiers in extreme conditions science at synchrotrons and free electron lasers” (Cerantola et al.) [77] in which the two major European-funded laboratories, ESRF and EuXFEL, showcase similarities and differences between storage rings and X-ray FELs when it comes to extreme conditions research.

Synchrotrons and FELs are unique facilities to probe the atomic structure and electronic properties of matter at extreme thermodynamical conditions. In this context, “matter at extreme pressures and temperatures” was one of the science drivers for the construction of low emittance 4th generation synchrotron sources, such as the Extremely Brilliant Source of ESRF, and hard X-ray FELS, such as the EuXFEL. These new user facilities combine static high pressure and dynamic

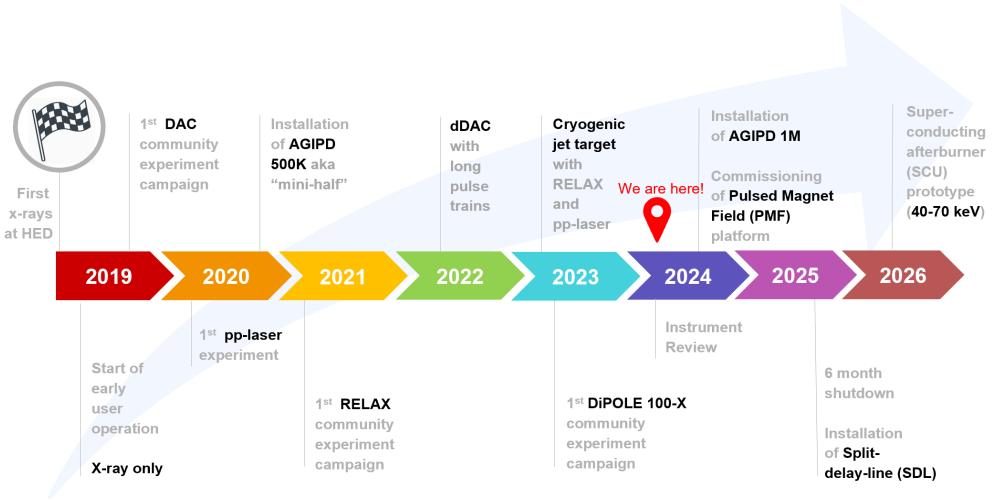

Figure 3.1: Development of the HED-HIBEF instrument in the last five years

shock compression experiments with high brilliance and sub-micron beams. This combination not only increases the data quality but also enlarges tremendously the accessible pressure, temperature, and density space. At the same time, the large spectrum of available complementary X-ray diagnostics for static and shock compression studies opens unprecedented insights into the state of matter at extremes.

A major strength of X-ray FELs is the ultrafast time resolution of < 100 fs, while synchrotrons operate well in the picosecond domain. Any X-ray science that requires this ultimate resolution can be done only with laser-based sources (betatron) or at X-ray FELs. Also, the single pulse intensity at the EuXFEL is so high that a full diffraction pattern or spectrum can be generated in a single shot. These two characteristics together also enable pulsed X-ray heating, a field which only X-ray FELs or otherwise very strong laser-driven backlighters (NIF) offer.

Synchrotrons provide higher photon energies for large q-coverage and deep sample penetration. In the coming decade, X-ray FELs equipped with superconducting undulators (SCUs) may match these hardest photon energies. Also, X-ray absorption spectroscopy (XANES, EXAFS) is currently better done at synchrotrons, unless < 100 ps time resolution is necessary. Synchrotrons also have a better stability, more reliable beam delivery, and are more economic by sharing the electron beam across many 10s of dedicated instruments.

3.1 Warm dense matter by intense X-ray excitation

The scientific field of isochoric heating (ultrafast at constant density) of matter by SASE FELs was first motivated by Lee et al. in their classic publication, “Finite temperature dense matter studies on next-generation light sources”, in 2003. At the first SASE FEL FLASH at DESY, an FEL-generated aluminium plasma was characterized by emission spectroscopy in 2008 [78] and saturable absorption in 2009 [79]. When LCLS came online, soft X-ray heating studies [80] from 2012 launched years of further detailed research on ionization potential depression and collision rates. The field has extended its method into X-ray diffraction and inelastic X-ray scattering, both non-resonant and resonant (RIXS). At HED-HIBEF, the creation and diagnosis of warm dense matter by intense X-ray FEL pulses is equally important as it is on other X-ray FEL facilities.

In 2021, users led by Voigt and Kraus (HZDR/U Dresden and U Rostock) demonstrated X-ray Raman spectroscopy at HED, in particular to study warm dense carbon in the future [81]. The setup of this experiment, benchmarking the X-ray Raman scattering spectra of ambient diamond and graphite, is well-suited for future warm dense matter (WDM) experiments. Using our HED HAPG spectrometers, this inelastic X-ray scattering of bound-free states probes the ionization edges in the 1 – 10s eV range (see Fig. 3.4 for carbon in the diamond phase) with 2.7 eV spectral resolution (Fig. 3.2) using a volumetrically penetrating multi-keV probe.

The setup allows for a straightforward combination with multiple additional diagnostics, such as XRD, X-ray Thomson scattering, and SAXS, which have been routinely fielded for WDM experiments, and can be adapted to perform experiments with different low-Z material samples besides carbon. The exceptionally high brightness of the EuXFEL, together with the high-resolution HAPG spectrometer, made it possible to record full-range spectra within one X-ray pulse, which is essential when investigating transient warm dense material states.

However, an accumulation of multiple spectra is necessary to study substructures in the XRS signal due to the exceedingly small cross section of the X-ray Raman scattering process. The users have presented DFT-MD calculations in combination with XRS simulations that corroborate the great potential of the demonstrated setup observing samples at pressure and temperature conditions in the WDM regime.

Samples that are pumped to WDM conditions will be irreversibly damaged in each shot. Thus, very often, single-shot measurements are required, which can be

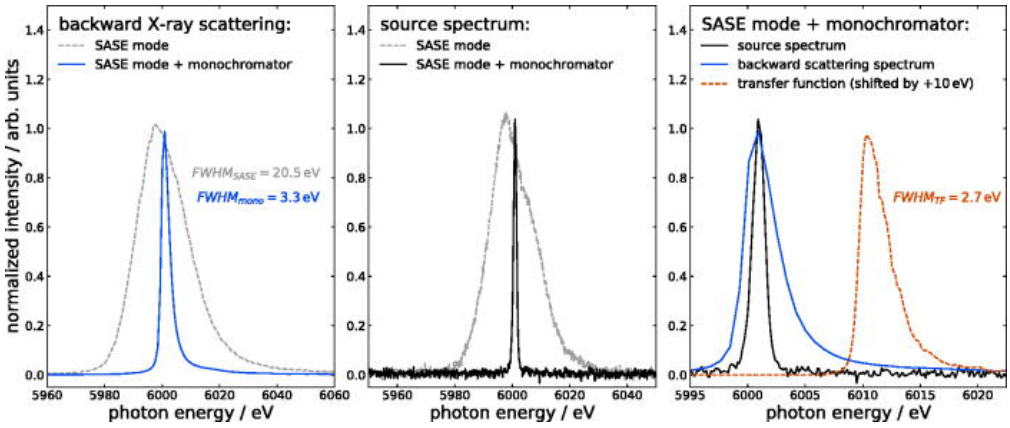

Figure 3.2: Determination of the transfer function between the backward spectrometer and the source monitor by deconvolution of the source spectrum from the elastic scattering signal from a metallic glass sample. **Left**: Elastic scattering signal in SASE mode (dashed gray) and with monochromatic X-rays (blue). **Middle**: Source spectra in SASE mode (dashed gray) and with monochromatic X-rays (black). **Right**: Transfer function (dashed orange, shifted by +10 eV relative to the elastic scattering peak) obtained by deconvolving the source spectrum (black) from the backward scattering spectrum (blue) both in the SASE mode with the monochromator. From Voigt et al. [81]

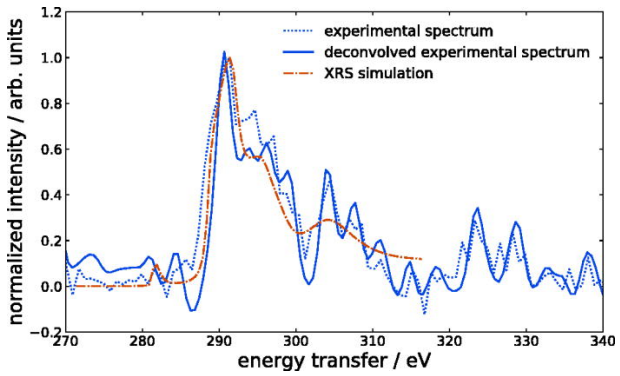

Figure 3.3: Measured X-ray Raman spectrum pre- (dotted blue) and post- (continuous blue) deconvolution procedure compared with the calculated X-ray Raman spectrum (dashed orange) of a diamond sample in the backward (Compton, non-collective) regime. From Voigt et al. [81]

provided at HED in the shot-on-demand mode using a pulse picker. Alternatively, depending on the degree of damage, rapid raster scans are a great option to accumulate a large number of data shots.

At the time of the experiment, HXRSS was not yet available, and the users employed the SASE beam with subsequent monochromatization by our Si (111) monochromator. The accumulation of ~ 10 000 shots per XRS spectrum was required, due to the limited X-ray flux after insertion of the monochromator. Using seeded X-ray (HXRSS)

beam will give approximately 50 times more X-ray photons hitting the sample, assuming pulse energies of ~ 1 mJ, based on the best performance of the two-chicane seeding design of the EuXFEL at a repetition rate of 10 Hz at 7.5 keV. This means only 200 shots would be required instead of 10 000, which is within the capacity of a single target frame.

3.1.1 C–H demixing and hydrogen metallization

In 2023, a team led by Ranjan and Kraus (HZDR, U Rostock) [82] used collective (forward) X-ray Thomson scattering to study C–H demixing and hydrogen metallization in warm dense matter conditions.

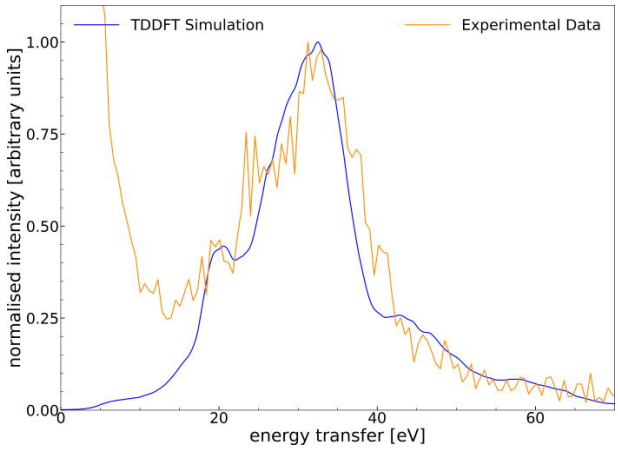

Figure 3.4: Measured plasmon feature (orange) from diamond. Spectra were obtained by averaging over 18 000 shots using the X-ray beam in the SASE configuration along with a monochromator. Shown in comparison with the calculated plasmon feature (blue) after convolution with the instrument function. From Rajan et al. [82].

They could shown that collective X-ray Thomson scattering from plasmon oscillations is applicable to characterize liquid metallic hydrogen in the bulk of the sample, which is advantageous over the reflectivity measurements that can only probe the surface (which may be in a non-equilibrium state, e.g. a shock front). Ranjan et al. presented how the exemplar scattering spectrum from ambient diamond recorded at the HED instrument agrees well with time-dependent DFT simulations. The existing resolution is capable of distinguishing the expected metallic hydrogen feature after demixing.

In their demonstration experiment, ~ 18 000 shots were accumulated with SASE and the monochromator. The samples applied in their demonstration experiment were notably thinner than those in typical shock-compression experiments at X-ray FEL sources (10 µm vs 50 – 100 µm). Therefore, it can be expected that an accumulation of

approximately 1000 shots or even less is required to obtain the data quality presented here. While high repetition rates place high demands on target design and the target delivery system, the corresponding developments are under way at the HED instrument, e.g. by making it possible to replace targets without the need to break the vacuum in the interaction chamber. Furthermore, plastics as a base target material allow for using tape samples that enable such rep-rated experiments with several 1000s of shots before targets have to be swapped (and less with excellent seeding performance). Novel diagnostic tools combined with the new DiPOLE high-energy laser system will enable bulk-sensitive measurements of planetary core conditions.

3.1.2 Re-binding of valence states in isochorically heated zinc

A team lead by Humphries (EuXFEL) and Smid (HZDR) are working on RIXS data that describes re-binding of valence states in zinc.

In this single-pulse X-ray experiment, we have observed the evolution of the vacant electronic DOS of solid-density Zn at temperatures up to 65 eV via RIXS. Good agreement is seen in the behaviour of states that rebind to the atomic centres as extracted from data when compared to DFT calculations. The ability to extract well-defined bound states without relying on forward modelling shows the great promise of this technique for *in situ* temperature and ionization measurements.

The ability to accurately resolve states and populations close to the chemical potential of transient warm dense systems, which dominate the electronic properties of a material, promises to greatly enhance our understanding of atomic interactions in this regime. This could also improve our ability to diagnose chemical processes that are known or postulated to occur in these energetic states, requiring pump–probe experiments to allow for the timescales of atomic motion.

3.1.3 MHz X-ray FEL heating of Ti

Under submission is a work entitled “Measurement bias in self-heating X-ray free electron laser experiments from diffraction studies of phase transformation in titanium” by a team of users and HED-HIBEF scientists led by O. Ball and S. McWilliams (University of Edinburgh). X-ray heating by the MHz pulse train and its effect on the simultaneously measured X-ray diffraction were investigated, providing a unique extension to single-pulse X-ray heating into the nano- and microsecond domain.

Diagnosis of heating and induced changes in samples is performed using the X-ray

beam itself using X-ray diffraction. Here, the relationship between conditions created by and inferred from X-ray irradiation is unclear and may be highly dependent on the material system under consideration. We report on a simple case study of a titanium foil irradiated, heated, and probed by a MHz X-ray FEL pulse train at 18.1 keV, using measured MHz X-ray diffraction (from AGIPD) to determine temperature and finite element analysis to interpret the experiment data.

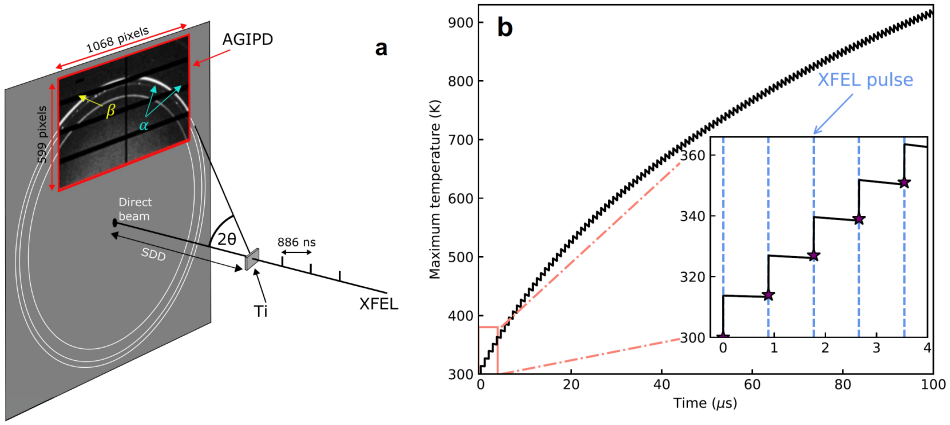

Figure 3.5: Experiment setup and predicted temperature of Ti foil. (a) Experiment setup. The full detection area of the AGIPD is shown with a representative pattern, with the Debye-Scherrer rings of the α and β phases labeled. (b) FEA modeled peak sample temperature of Ti foil under irradiation by 112 X-ray FEL pulses at 1.1 MHz assuming a constant energy of 1 μJ per pulse on target. The inset shows the temperature response for the first five pulses. The vertical dashed lines indicate the timings of the X-ray FEL pulses with the peak temperature in the sample probed by the X-ray FEL pulses indicated with stars.

We have examined how, under irradiation by a MHz train of X-ray FEL pulses, a titanium sample undergoes serial volumetric heating to hundreds or thousands of degrees Kelvin. The apparent temperature evolution of the sample—based on X-ray diffraction measurements from this same pulse train—is compared to numerical models, giving insight into the temperature dynamics within the sample and effects of large temperature gradients.

This study uses a material experiencing a temperature-induced phase transition. We observe in Ti the emergence of the high-temperature β phase at a completely different apparent temperature to the initial α phase. The prominent radial temperature gradient within the foil gives rise to the large apparent temperature difference between the two phases, which is present in both XRD-determined and FEA-predicted temperature evolution. We hence observe a first-order temperature-driven phase transition in a sample containing a continuous temperature distribution that exhibits discontinuous behaviour in apparent temperatures, with limiting temperatures of the low-temperature phase well below the known transition

temperature. This is even the case after heat conduction has reduced temperature gradients in the probed region to relatively small values. Treating observed conditions as simple averages over irradiated samples is not effective where rapid changes in state such as phase transformations occur, as these need to be accounted for explicitly in averaging schemes along with the impact on specific measurements. Our findings support future experiment measurements for more complex and unknown systems, particularly where accurate temperature assessment is critical to establishing the conditions explored using X-ray FEL irradiation.

The results have implications for studies employing X-ray probing of systems with large temperature gradients, particularly where these gradients are produced by the beam itself. Finally, this study shows the potential complexity of studying sample behaviour such as phase transformations where biasing effects of temperature gradients can become paramount, precluding clear observation of actual phase transformation conditions.

3.2 High-pressure research in diamond anvil cells

Worldwide unique science in diamond anvil cells (DAC) can be performed at the EuXFEL due to its availability to deliver hard X-rays $>$ 10 keV at MHz repetition rates. This allows for single-shot diffraction patterns, detected individually by the AGIPD detector. Fig. 3.6 shows the three sub-classes of science in DAC where the HED-HIBEF instrument excels: this is the materials response upon IR laser heating, upon dDAC compression via a fast piezo, and upon X-ray heating.

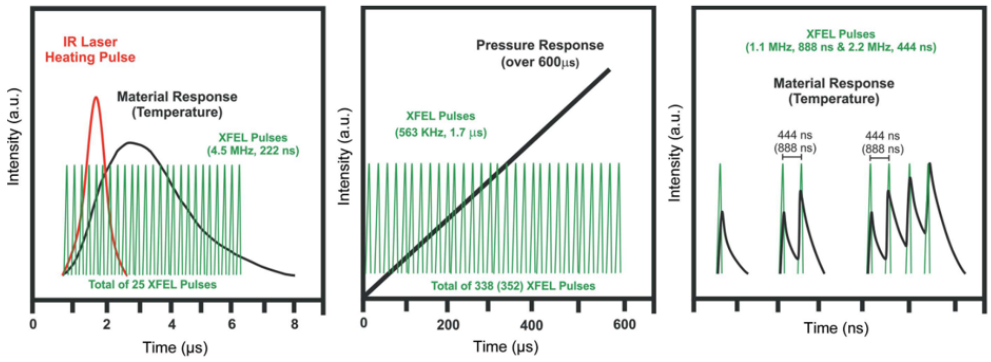

Figure 3.6: The three unique MHz DAC experiments at HED-HIBEF: pulsed IR laser heating (left), piezo-dynamic DAC (centre) and X-ray heating (right). The green lines represent the MHz X-ray pulse train, the black curves the material response.

3.2.1 Dynamic optical spectroscopy and pyrometry under optical and X-ray laser heating

A team of instrument scientists and international experts, led by O. Ball (Edinburgh) and Z. Konôpková (EuXFEL), published an extensive paper in 2023 on dynamic optical spectroscopy and pyrometry of static targets under optical and X-ray laser heating [83] in our DAC standard configuration.

Spectrally and time-resolved optical emission is measured using a spectrometer mounted on a streak camera, coupled with an optical microscope equipped with a confocal spatial filter, to isolate a 50 µm diameter area on target and exclude signal away from the focal plane. X-ray FEL irradiation comprised of 17.8 keV, 20-fs X-ray FEL pulses in single-shot or 2.2 MHz pulse trains (443 ns repetition rate), while the optical laser was NIR (1070 nm) with a pulse length of 250 ns. These are focused to spots of 10 µm diameter on targets. The time-dependent thermal emission spectra are least squares fitted to the Planck function, with the time integration bins, the temporal point spread function, and selected streak window affecting the time resolution of the temperature measurement.

We study a suite of representative targets including freestanding foils and multi-layer targets in a DAC to contain heated samples and apply high pressures (GPa) prior to irradiation. Measured temperature is dominated by the peak temperature in the field of view, whereas emission intensity has a more complex development accurately predicted by numerical modeling of dynamic temperature gradients. When DACs are irradiated by the X-ray FEL, background emission due to sample fluorescence is often detected. Thermal and fluorescent signals have distinct spectral–temporal appearance, and, when similar in amplitude, fluorescence can perturb temperature measurements. Fluorescence appears at lower powers than required to produce a detectable thermal signal, such that data where only fluorescence is recorded can be used to interpret and model fluorescence behaviour for a particular target and extract the thermal component of emission before the sample temperature is analysed. Fluorescence contributions are mitigated through spatial filtering and use of low fluorescence materials (e.g., type II rather than type I diamond). For optical laser heating, results broadly follow previous work using streak optical pyrometry methods.

The streaked optical pyrometry (SOP) in the current standard configuration is compatible with a range of X-ray and optical laser experiments. Modification of the sample imaging optics (e.g. for different targets, environments, and measurements) can allow compatibility with a wider range of experiments. For example, SOP is well demonstrated in conjunction with shock wave compression, and the streak camera range (0.5 ns to 1 ms) covers what is typically required for laser-shock techniques.

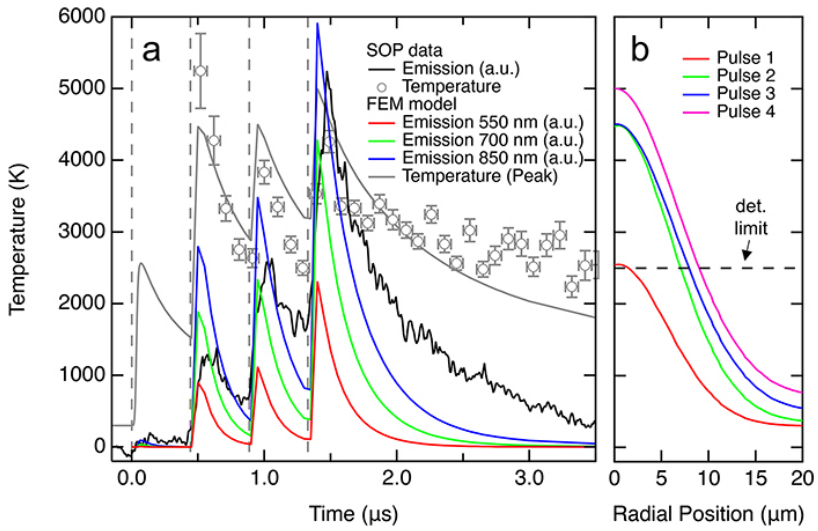

Figure 3.7: Emission intensity behaviour of 5 µm Tantalum foil at 12 GPa together with finite element model results. (a) Experiment data compared to finite element model, with emission intensity in arbitrary units. Observed emission intensity is averaged over the wavelength range 575—775 nm. Predicted intensities in FEM are the total intensity at 550, 700, and 850 nm, integrated over the metal foil surface. (b) Radial temperature gradient on the observed (upstream) metal foil surface just after each X-ray pulse. Dashed line shows approximate detection limit. Emission intensity is calculated in the FEM model by integrating the Planck function over this surface. From Ball et al. [83].

The spectral SOP is particularly useful for lower temperature ranges (< 10 000 K) where the emission wavelength dependence varies strongly with temperature.

3.2.2 MHz X-ray diffraction of pulsed laser heating

A team of instrument scientists and international experts, led by N. Jaisle and G. Morard (U Grenoble Alps), worked on pulsed laser heating and measurement of cooling effects by MHz diffraction [84] in 2023, using our DAC standard configuration.

This is a new approach in which crystallization sequences upon cooling from a homogeneous liquid state with limited chemical migration due to heating are reproduced. Diffraction data collected during several heating cycles (Fig. 3.8), combined with chemical analysis, confirmed the reduced amount of chemical migration induced by short laser heating pulses. This enabled, in some cases, to observe the successive phase appearance of SiO_2 and FeSi-fcc phase.

Even though the AGIPD 500K does not provide full angular and wide q-space

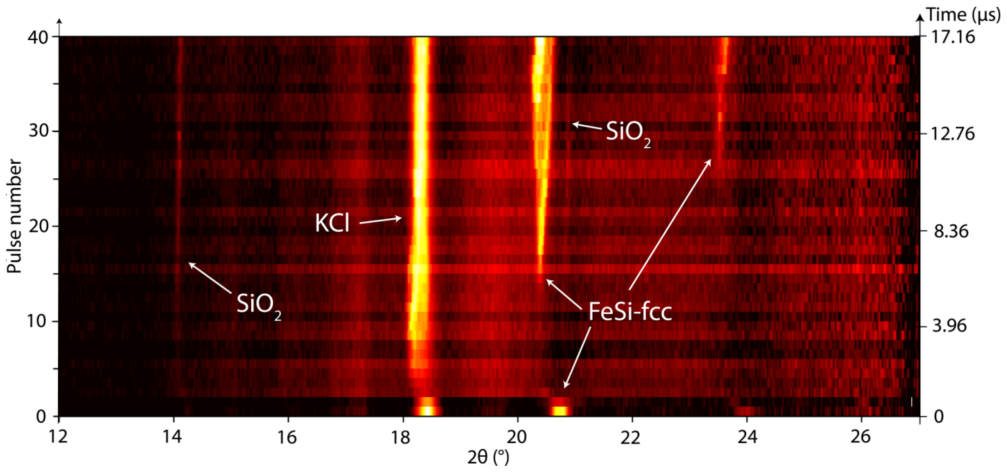

Figure 3.8: 2.2 MHz pulse train diffraction series (time span of 17 µs for 40 pulses). The moments in which phases are first observed (spawn times) can be constrained by seeking the line apparition and checking for spots on the image plate. Observable phases are highlighted and designated. The KCl peak partly fades over the first pulses where the maximum fiber laser intensity is delivered to the sample, meaning that it is likely almost entirely molten inside the X-ray sampling zone. The first sample phase to crystallize upon cooling is SiO_2. It is observed for the first time on the diffraction spectra at 2.2 µs (time zero corresponding to the first X-ray pulse). The FeSi-fcc peaks entirely disappear within the first three pulses before re-appearing at 5.72 µs for the left peak. Note that the second and fainter higher angle peaks of FeSi-fcc and SiO_2 appear later in time, likely due to signal degradation at higher angles and large crystal size. From Jaisle et al. [84].

coverage, we can still measure a liquidous temperature with the SiO_2 recrystallization from the liquid.

This opens up a new pathway for future *chemical-migration limited* experiments, giving access to phase diagrams and melting curves of previously never explored phases and alloys. In that framework, numerical simulations are required to solve for temperature gradients, particularly strong during the first microseconds of the heating phase, as well as to provide accurate global temperature evolution and constrain the amount of thermal pressure. Model and experiment data are complementary for X-ray diffraction data interpretation.

3.2.3 MHz X-ray diffraction from dDAC with long pulse trains

The HED-HIBEF team has worked with the X-Ray Operations (XO) and the XFEL Accelerator Coordination (MXL) divisions to establish a special mode of X-ray delivery

in 2022. Usually, the available train length per instrument at the EuXFEL is $\leq 200\,\mu s$. However, dDAC benefits from a maximum time window. A special mode (called full bunch trains) delivers 1–2 pulses at 10 Hz at SASE 2 and the remainder goes to SASE 1 and SASE3. Every 10 s, however, SASE 1 and SASE3 do not receive anything, and the entire train goes to SASE 2 at a repetition rate of 0.5 MHz. This corresponds to one X-ray pulse every 1.77 µs, and 352 events can be recorded by AGIPD over 625 µs. At 1.1 MHz, dDAC compression can be recorded over a time span of 312 µs. Typical compression timescales of 100s of µs are perfectly suited to the practically available pulse train length (200 – 550 µs) at the EuXFEL, where AGIPD provides the essential pulse-resolved XRD data.

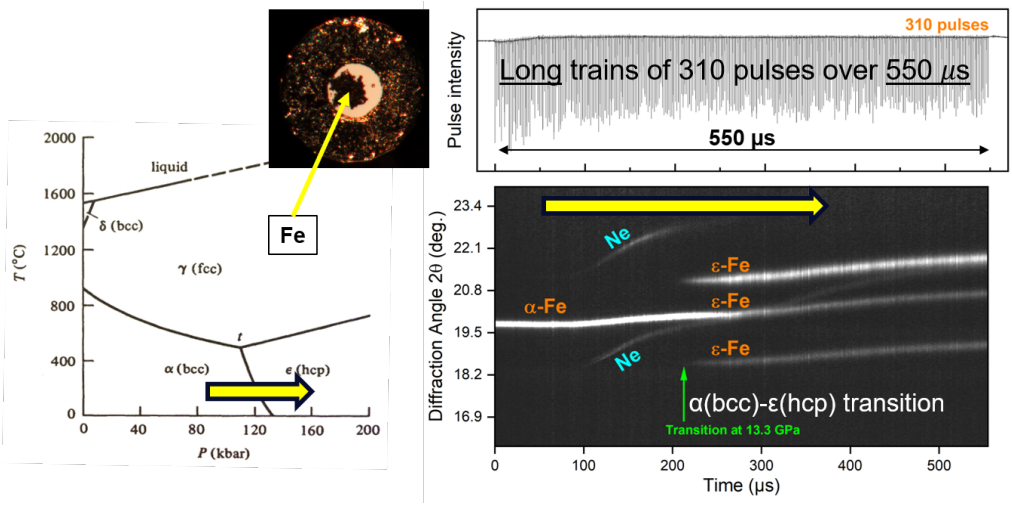

Figure 3.9: The maximum length of a bunch train at the EuXFEL, 550 µs at 0.5 MHz repetition rate, was used to collect 310 XRD patterns of iron undergoing the *alpha*-to-ϵ phase transition around 13 GPa.

During internal commissioning time in May 2022, we benchmarked the dDAC platform by dynamically compressing an iron sample. As shown in Fig. 3.9, the well-known *alpha* (bcc) ϵ (hcp) phase transition happens around 10 – 13 GPa pressure, depending on the exact temperature. By exploiting the maximum length of a bunch train at the EuXFEL, 550 µs at 0.5 MHz repetition rate, we were able to collect 310 XRD patterns (close to the maximum of 352 that AGIPD can acquire) and beautifully resolve the phase transition at $\sim 220\,\mu s$ after start of the exposure.

A team of instrument scientists and international experts, led by R. Husband (HIBEF/DESY) and H. P. Liermann (DESY PETRAIII) published the details of the MHz X-ray diffraction setup [85] in 2023. They focus on our capability to collect pulse-resolved XRD data from samples as they are dynamically compressed using piezo- driven diamond anvil cells.

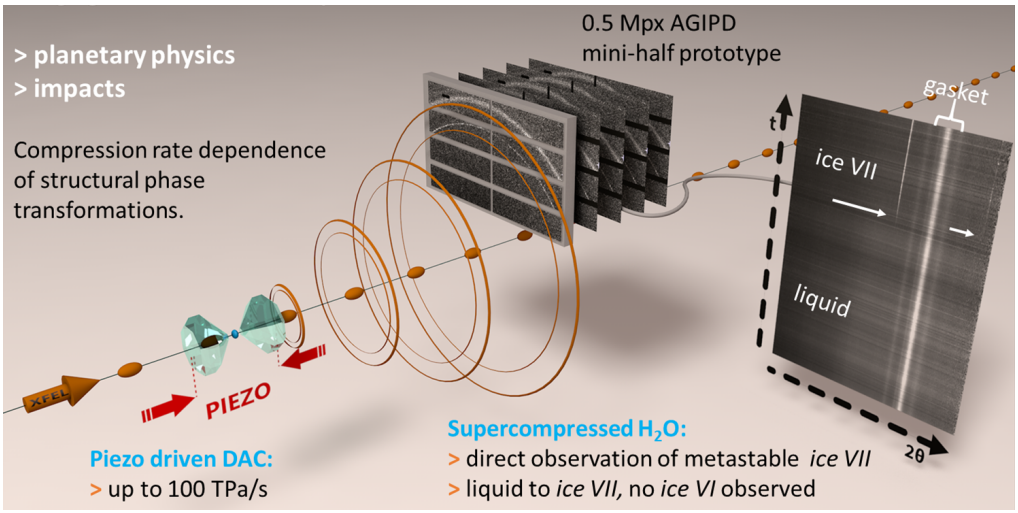

Figure 3.10: Dynamic compression of H_2O. The panels show integrated XRD data as a function of time, indicating the growth of the ice-VII reflection during compression. Also visible are reflections from the gasket. The EuXFEL was delivering a full train at 1.1 MHz repetition rate.

The capabilities of this platform are demonstrated by results from experiments on a range of different material systems with different X-ray absorption lengths (for water, see Fig. 3.10). A maximum compression rate of $\sim 87\,\mathrm{TPa\,s^{-1}}$ was achieved during the fast compression of Au, and a maximum strain rate of $\sim 1100\,\mathrm{s^{-1}}$ was achieved during the compression of N_2 at $18\,\mathrm{TPa\,s^{-1}}$.

Varying the X-ray fluence and using a relatively large focal spot size limited X-ray heating even in the high-Z systems, demonstrating that this platform is suitable for kinetic studies in which the P–T path must be well constrained.

3.2.4 X-ray FEL–induced synthesis of ϵ-Iron Nitride

Already in 2021, H. Hwang at al. [86] from Yonsei University in South Korea reported about their observation of X-ray FEL–induced ϵ-Iron Nitride at high pressures. This was one of the first X-ray heating experiments at HED-HIBEF. It was done before the train-resolved AGIPD detector was available; Varex was used instead to record train-integrated data.

The ultrafast synthesis of ϵ-Fe_3N_{1+x} in a DAC from Fe and N_2 under pressure was observed while irradiating it with a pulse train of 1.1 MHz (spacing of 443 ns), as shown in Fig. 3.11. The estimated sample temperature at the delay time was above 1400 K, confirmed by *in situ* transformation of α- to γ-iron (fcc). Ultimately, the Fe and

N_2 reacted uniformly throughout the beam path to form $Fe_3N_{1.33}$, as deduced from its established equation of state.

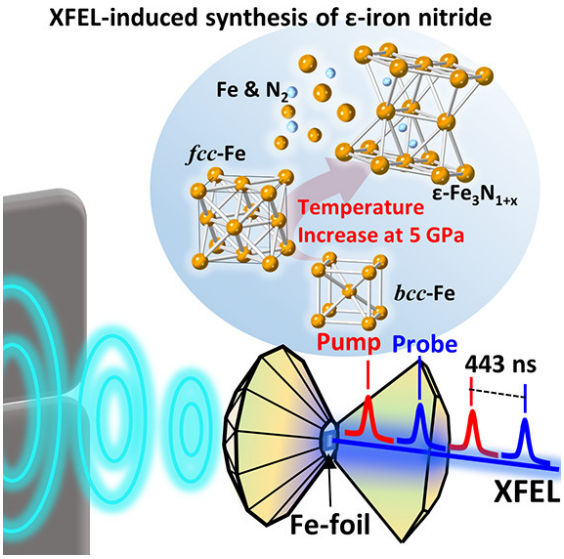

Figure 3.11: Setup for observing the X-ray FEL–induced synthesis of ϵ-$Fe_3N_{1.33}$ from Fe and N_2 at 5 GPa. From Hwang et al. [86].

They could thus demonstrate that the required activation energy for chemical reactions controlled by the X-ray FEL radiation is an important experiment parameter. The observed kinetics of the X-ray FEL–induced synthesis of ϵ-$Fe_3N_{1.33}$ are noteworthy and unprecedented: Hwang et al. found a remarkably homogeneous reaction product after the ultrafast reaction. Their study concludes that following chemical reactions between gas and solid at high pressures and temperatures in a DAC using a tailored pump-–probe setup at an X-ray FEL opens up a new parameter space for the exploration of new materials forming on fast timescales at high pressure.

3.2.5 X-ray heating of low-Z samples in DAC

During a DAC community proposal in 2021, we investigated advanced methods of X-ray heating. The challenge is that direct heating of low-Z planetary ices (e.g. H_2O, NH_3, CH_4) is not very efficient. The concept was brought forward to use a high-Z coupler inside the DAC that is in thermal conductive contact with a low-Z sample. The X-rays get absorbed by the coupler, and its heat is transferred to the low-Z material, which subsequently is probed by XRD (Fig. 3.12).

As can be seen from the pulse-resolved diffraction data in Fig. 3.13, we could determine the thermal expansion of the sample during irradiation. Furthermore, we see evidence of bcc and fcc superionic ice, where protons are free to move within the

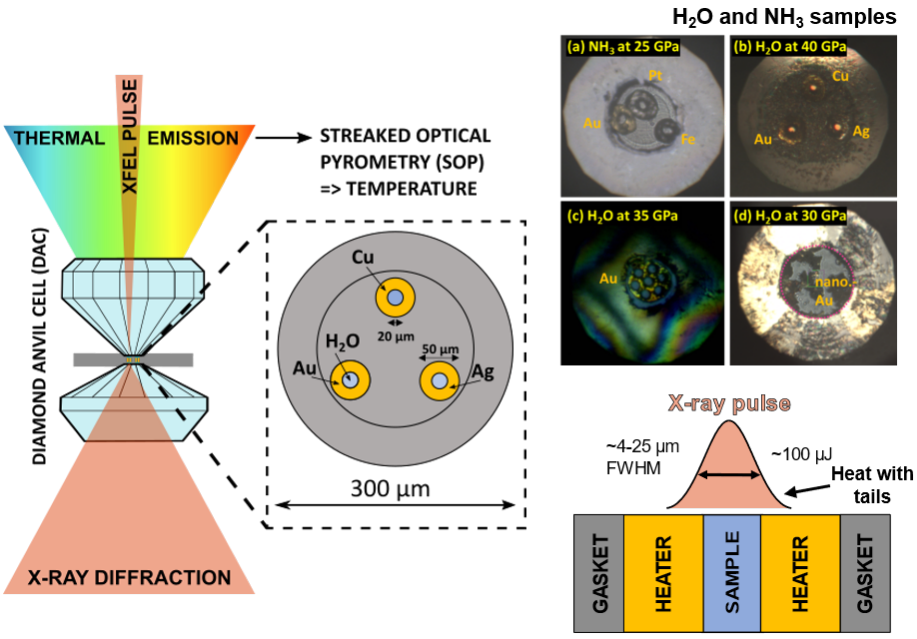

Figure 3.12: Concept to use a high-Z coupler to X-ray heat a low-Z ice. Here, Au, Ag, and Cu couplers are used inside the DAC to heat H_2O and NH_3 samples.

oxygen lattice.

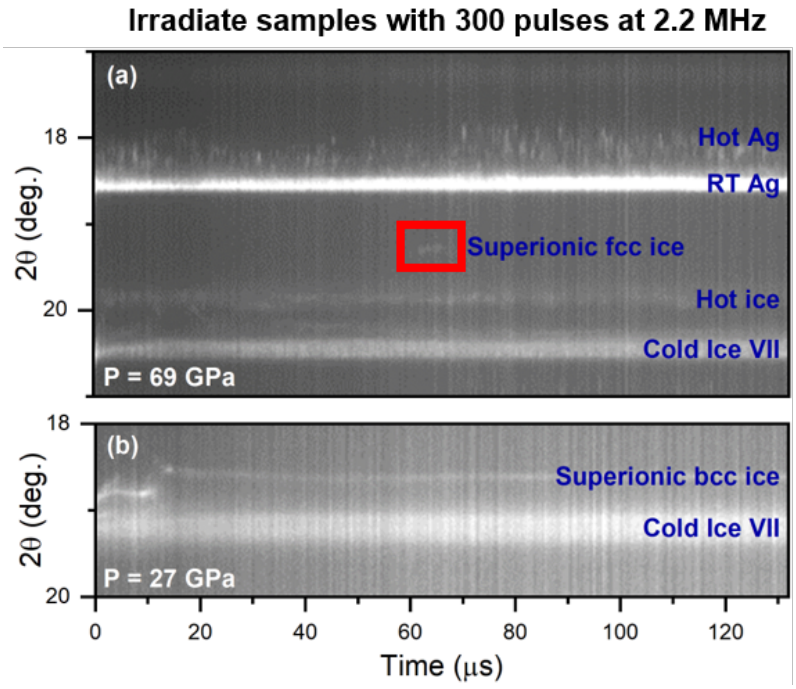

Figure 3.13: Pulse-resolved X-ray diffraction data collected using the AGIPD 500K, showing evidence of bcc and fcc superionic ice

3.2.6 Diamond precipitation dynamics from hydrocarbons at icy planet interior conditions

Researchers around by M. Frost and S.H. Glenzer (SLAC) published in *Nature Astronomy* about the growth rates of diamond from CH at the conditions found in icy planets [87]. The setup made use of the DAC standard configuration in a week with X-ray delivery at our maximum repetition rate of 4.5 MHz.

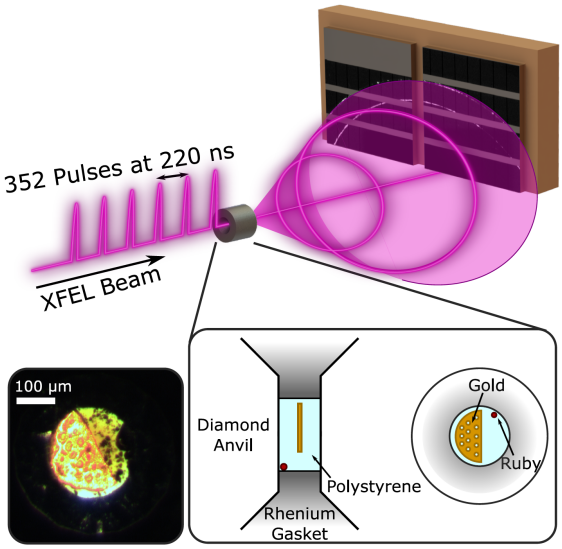

Figure 3.14: Experiment setup showing the 4.5 MHz X-ray pulse train acting as pump and probe on the sample compressed in a DAC with diffracted X-rays incident on the AGIPD 500K module. Enlargement shows the DAC loading configuration with the perforated gold coupler embedded in polystyrene. The inset shows a micrograph of the sample prior to the experiment.

The conditions at which precipitation of diamond occurs from hydrocarbon mixtures are important for modeling the interior dynamics of icy planets. Despite this, there is disagreement in the literature over the conditions at which this reaction occurs, particularly between static and shock compression experiments. The users report the time-resolved observation of diamond formation from statically compressed polystyrene, $(C_8H_8)_n$, heated using 4.5 MHz X-ray pulse trains.

Diamond formation is observed by X-ray diffraction above 2500 K from 19 to 27 GPa, conditions representative of Uranus and Neptune's shallow interiors, on 30 to 40 µs timescales, revealing the origin of the discrepancy between static and shock studies to be reaction kinetics. If these results can be generalized to the CH compounds expected to exist in planetary bodies, the reduced pressure and temperature conditions of diamond formation have implications for icy planetary interiors, where diamond subduction plumes provide a source of internal energy and could drive convection in the conductive ice layer which is proposed to give rise to their complex

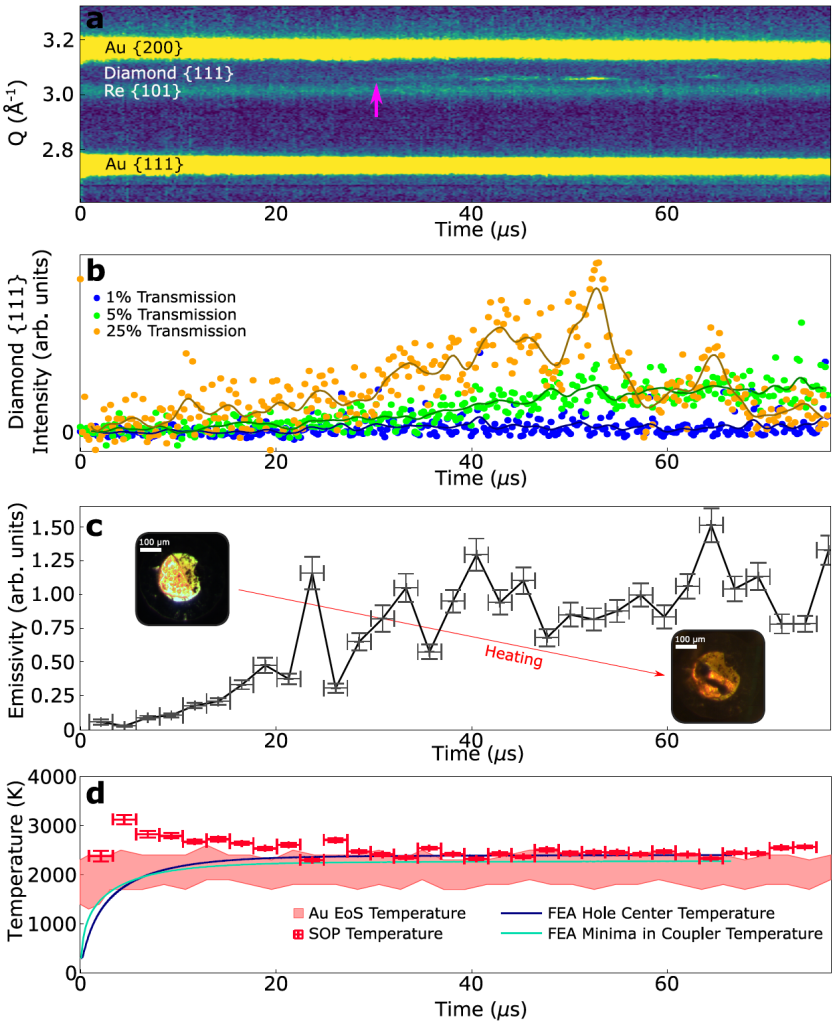

Figure 3.15: Time-resolved data from a run starting at ~20 GPa with average pulse energy of ~71 µJ. The initial X-ray FEL pulse occurs at time 0. (a) Integrated diffraction patterns from the AGPID detector as a function of time in region of interest, background subtracted and normalized to the beam intensity monitoring diode. Yellow shades correspond to higher intensity. The pink arrow indicates the onset of observable diamond signal. (b) Intensity of the diamond peak as a function of time for different X-ray absorber transmissions. 25% transmission is the same run as the other panels in this figure. Lines are smoothed by a 15 pulse wide Hamming window. (c) Emissivity increases during the run. Inset photos show the sample before and after heating. (d) Temperature as a function of time. Bars show fitted temperatures from SOP with a 2.4 µs bin width; the error shown is the fitting error; in addition to this, there is ±200 K from thermal gradients. The red region is temperature from the equation of state of the gold coupler; blue and teal lines are temperatures modeled using finite element analysis. [87]

magnetic fields.

3.2.7 Structural and electron spin state changes in an X-ray FEL–heated iron carbonate

Through a BMBF instrumentation proposal (Federal Ministry of Education and Research of Germany, Project 05K19PE2), the HED group and U Dortmund (C. Sternemann) collaborated over several years to established emission spectroscopy from sample inside a DAC at the HED-HIBEF instrument. This project also funded the Ph.D. of J. Kaa, a student supervised by Sternemann in Dortmund but working full time at EuXFEL.

First, we successfully commissioned a von-Hámos spectrometer that provides a setup to measure spectra in the hard X-ray regime from various samples contained in a DAC [26]. The setup was tested in an energy range between 6400 and 11200 eV using Si(111) and Si(531) crystal cuts. It provides a sub-eV energy resolution with an energy window between 100 and 150 eV. The setup shows a sufficiently high efficiency for single-pulse XES measurements that ultimately enables MHz-resolved and pump—probe experiments from pre-compressed samples contained in a DAC.

This spectrometer, together with XRD, was then successfully used to study structural and electron spin state changes in an X-ray heated iron carbonate system at the Earth's lower mantle pressures [88]. It must be noted that no MHz-capable detector is yet available for spectroscopy applications in IC1. Such a detector, either a vacuum-compatible AGIPD single module or a vacuum-compatible Gotthard strip detector, would allow for pulsed-resolved measurements.

Even though the X-ray detector was train-integrating, we were able to monitor the spin state and structure during decomposition of $FeCO_3$ at extreme pressures, while generating high temperatures through X-ray heating. The sample reached melting temperatures during pumping and probing at 2.2 MHz at a fraction of the available EuXFEL pulse energy. The simultaneously measured XRD expanded the information about the spin state of $FeCO_3$ by adding valuable data on the structural state and phase composition. At a repetition rate of 455 kHz 78.4 J was sufficient to cause a temperature-induced spin change at roughly 600 K. At 2.2 MHz, the same heating-induced spin state change occurred at 18.1 J, while at 51.8 J our sample started to melt, suggesting temperatures above 3000 K (see Fig. 3.16).

The average spin state of Fe in all decomposition phases combined is above $S = 1$ and persists after quenching. Moreover, the data suggest the presence of Fe in high

spin in a FeCO melt at 51 GPa.

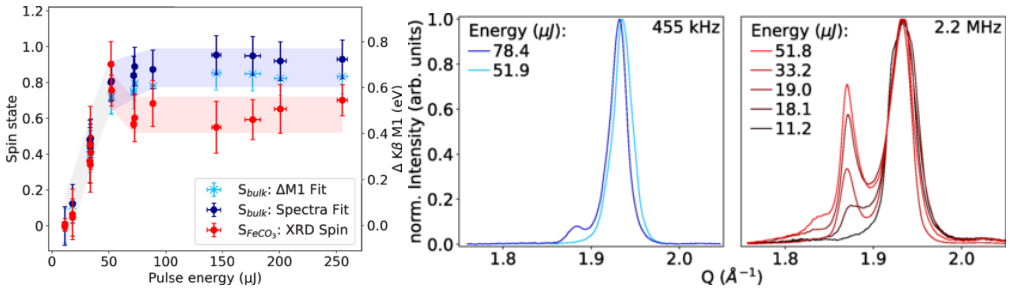

Figure 3.16: Left: The dependence of Fe spin state on the X-ray FEL pulse energy obtained by three methods (see inset). The $FeCO_3$ diffraction peak intensity ratio (red) estimates the spin state of $FeCO_3$. **Right:** $FeCO_3$ (012) diffraction peak measured for 455kHz (blue). At 51.9 J, a single low-spin (LS) peak is visible. At 78.4 J, two peaks are observed which can be attributed to low- and high-spin. Red lines: $FeCO_3$ (012) diffraction peaks measured for 2.2 MHz. In the XRD data at 11.2 J, we see only the low-spin phase. Afterward, the peak splits into a LS/HS set with increasing HS portion. From Kaa et al. [88].

The energy threshold for non-thermal damage for diamonds was not reached during the experiment; however, a slight graphitization was observed. Nevertheless, this experiment clearly shows the compatibility of using a DAC in combination with a highly focused and intense X-ray FEL beam as a probe over tens of minutes.

This successful proof-of-principle experiment allows us now to further improve our approach and the experiment setup for future measurements. It also marks a step toward microsecond time-resolved XES measurements from X-ray heated samples contained in a DAC and provides a probing scheme of the structure and spin state of melts at extreme static pressures by the combination of XES and XRD measurements. Such measurements permit the collection of highly relevant information for our understanding of the interior of planets in our solar system and beyond and will explore phase spaces on short timescales in future experiments at X-ray FELs.

3.3 Relativistic laser plasma science

The coupling of a shortpulse laser capable of generating ultrarelativistic 10^{21} W/cm^2 intensities to an X-ray FEL brings together two light sources that match perfectly in their pulse duration of a few tens of femtoseconds. These are excellent specifications compared to other X-ray FEL facilities—at MEC (LCLS), the laser energy is limited to 1 J on target and standard focusing achieved ~ 10^{19} W/cm^2, and the 500 TW laser at SACLA has not been used successfully for user experiments at highest intensities. Using optical locking, we were able to synchronize the lasers to a residual of 20–30 fs.

A timing tool [1] can be used to measure the arrival time between optical and X-ray laser pulses for each individual event.

Scientific applications enabled by relativistic laser include studying properties of highly excited solids, ionization dynamics at high intensities, relativistic laser plasma interaction, high energy density states of matter, energetic particle propagation in matter, investigation of microscopic dynamics details of laser-driven radiations and acceleration of particles(mostly in solid density systems), development of X-ray FEL probing techniques for high-intensity laser matter interactions (e.g., X-ray Thomson scattering, small angle X-ray scattering, coherent X-ray Diffraction Imaging, X-ray Faraday rotation, X-ray diffraction, X-ray absorption spectroscopies, etc.), and probing QED effects.

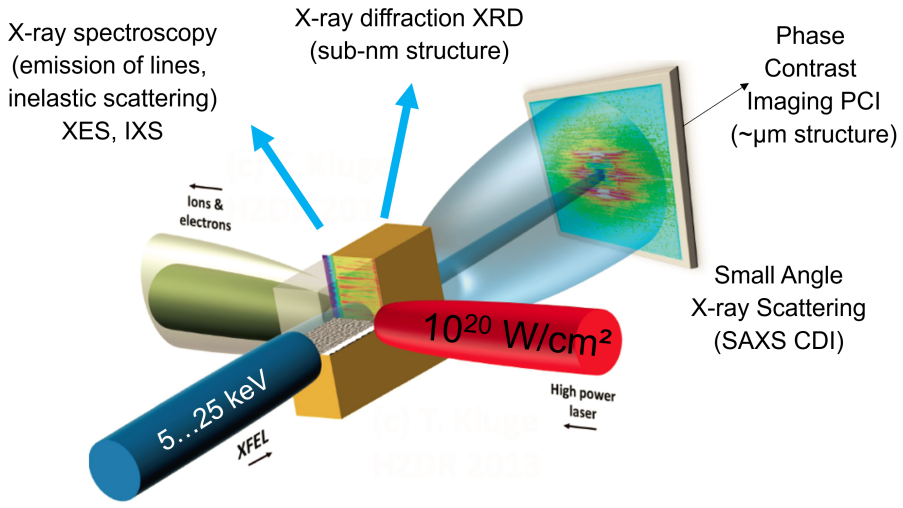

Figure 3.17: Schematics of X-ray diagnostics for relativistic laser plasmas. Adopted after Phys. Plasmas **21**, 033110 (2014).

Over the past year, we have developed and commissioned, as summarized by Fig. 3.17, a variety of X-ray probes that can be employed by users to study the ultrafast physics of relativistic laser plasmas, namely

- X-ray line and bremsstrahlung emission spectroscopy
- Inelastic X-ray scattering
- X-ray diffraction (sub-nm structure information)
- Small angle X-ray scattering (SAXS) (nm-scale information)
- Phase contrast imaging (PCI) (> 200 nm structure)

Since all these are complex and difficult to set up, and users can be easily overwhelmed in choosing a meaningful combination, we have derived two standard

configurations from the most frequent and scientifically outstanding user requests. We have worked on EMP-hard detectors, improved shielding of spectrometers, and developed in-vacuum target and focus microscopes. The ReLaX SAXS standard configuration was inaugurated in a first community experiment in May 2021 and has since (together with a PCI variation) been used by several user groups.

3.3.1 ReLaX community-assisted commissioning experiment

The main goal of the first ReLaX community-assisted experiment was to validate several X-ray diagnostic methods, such as small angle X-ray scattering, phase contrast imaging, and X-ray emission spectroscopy in relativistic laser–plasma interactions. The experiment studied a variety of scenarios of interest to the community, such as hole boring, relativistic transparency, fast electron transport along extended target, isochoric heating of buried targets, EOS determination by shocked targets, and plasma instabilities in relativistic intensity regime. This community-assisted commissioning proposal was dedicated to study, for the first time, the effect of a heavy noise environment (EMP, bremsstrahlung background, salt and pepper noise by direct hot electron hits) as generated by a highly relativistic laser–plasma interaction on XFEL X-ray diagnostics. The experiment was very successful and paved the way for multiple follow-up submissions using the knowledge and experience gained from this experiment. In particular, improvements of shielding improving signal/noise ration have been developed for SAXS and X-ray spectrometers that have allowed to use in subsequent beamtimes the full capabilities of these diagnostics. Targets that have been investigated ranged from thin foams with densities as low as 6x critical density, to solid foils of CH-compounds or metals. Also, more complex targets as buried wire or coated blocks have been investigated. While K-alpha spectroscopy was deemed to be feasible for the full range of explored laser intensities of target covering 10^{18} W/cm^2 to 10^{20} W/cm^2, XRTS was found to be of limited use above 10^{18} W/cm^2. PCI in a diffracting regime has be applied simultaneously with SAXS and has proved to be feasible for all intensity ranges. SAXS has shown a limited S/N ratio but has been improved in follow-up beamtimes by adding more shielding and usage of anti-scattering slits to clean up the beam. More details on the SAXS developments are given in the next section.

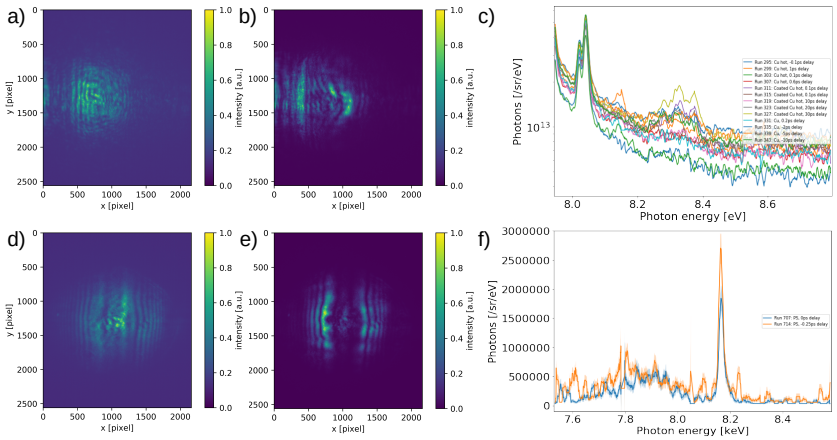

Figure 3.18: Exemplary results obtained during the user-assisted commissioning of the ReLaX platform: Panels (a) and (b) show the case of a CH block with an aluminium ablator (dark vertical line on the left). Panel (a) depicts the cold target, (b) shows the shock generated after ReLaX irradiation probed 350 ps after laser arrival. The case of a buried tungsten wire inside a CH block is shown in panels (d) and (e). Panel (d) presents the cold target; panel (e) shows the wire expanding due to the hot electrons generated when the laser hits the CH surface. The case of X-ray emission from copper foils irradiated by ReLaX is seen in panel (c) for a series of time delays. XRTS on polystyrene is presented in panel (f) for two delays.

3.3.2 Mirror to measure small angle X-ray scattering signal

Small angle X-ray scattering (SAXS) is a diagnostic technique where the X-ray beam is scattered to small angles of the order of 10 – 100 mrad. It is used to measure electron spatial distribution structures in the order of 10–100 nm. It is a well established technique at synchrotrons and X-ray FELs recently, where it has been used to study high intensity laser–plasma interactions. In this case, the scattering target is directly heated by a high-intensity optical laser, and therefore, a significant amount of radiation and high-energy particles are produced. This broadband divergent radiation increases the background (noise) level on the SAXS detector. The electromagnetic pulse (EMP) can also create issues with the electronics of the detector. Therefore, with the increasing performance of available lasers, the usage of such diagnostics with a direct line of sight to the target might suffer from low signal/noise ratios.

Together with HIBEF colleagues at HZDR, we have designed, fabricated, and commissioned the SAXS mirror [89], a novel tool to measure the small angle X-ray scattering (SAXS) signal in harsh laser—plasma interaction experiments. The schematics are shown in Fig. 3.19. This instrument was commissioned in an experiment at the HED instrument in 2020 and is since available there for further

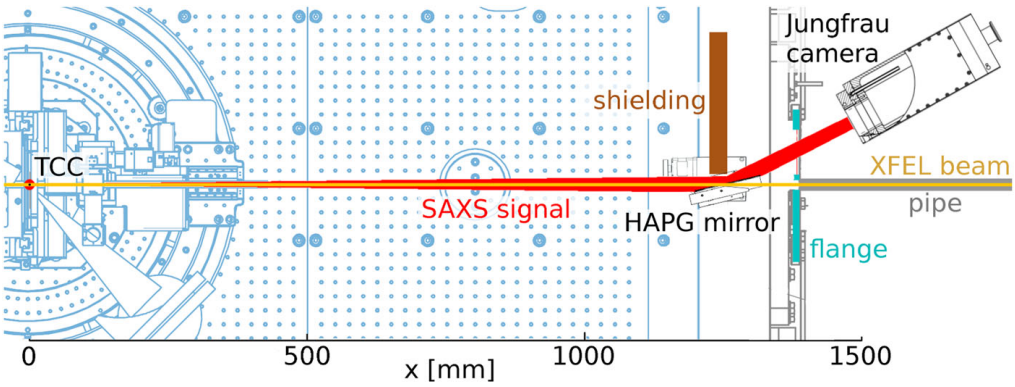

Figure 3.19: Schematics of the SAXS mirror instrument located in the IC1 chamber of the EuXFEL. The light blue background represents an optical table and a target tower in the chamber. The X-ray FEL beam (orange) is being scattered on a target at TCC, and the scattering signal (red) is propagating downstream toward the rear part of the chamber, where it is reflected to the detector by the HAPG mirror. The detector is located outside of the chamber behind a Kapton window. The X-ray FEL beam propagates through a gap between the two parts of the crystal further downstream, where it might be used for further diagnostics before reaching the beam dump.

use. With the current curvature of the HAPG mirror, it can be used to measure scattering at energies between roughly 7500 and 9000 eV. In the basic setup, the mirror provides a bandwidth of roughly 30 eV and an angular resolution of 0.2 mrad and works at scattering angles from 2 to 30 mrad, providing a q-range of roughly 0.06 nm^1–1 nm^1.The lower range is limited by the positional stability of the X-ray beam, the higher by the size and vertical position of the mirror.

In general, the principles of this instrument can be used to measure SAXS in various configurations and facilities. The instrument is used in combination with an optical-laser irradiated target and is part of a ReLaX standard configuration.

3.3.3 Visualizing plasmons and ultrafast kinetic instabilities

A study led by P. Ordyna and T. Kluge (HZDR), titled “Visualizing Plasmons and Ultrafast Kinetic Instabilities in Laser-Driven Solids using X-ray Scattering”, using the ReLaX standard configuration for SAXS, is under review.

Combining experiment results, simulations, and analytic estimates, the users can draw a complete picture of the dominant plasma dynamics in the current experiment: As the relativistic laser accelerated forward electron current streams through the bulk, return current transverse filaments are growing rapidly during the laser irradiation, and

at the same time longitudinal plasmons are driven. Both filaments and plasmons add up to generate a mesh-like electron density pattern that is responsible for the measured cross-like scattering pattern.

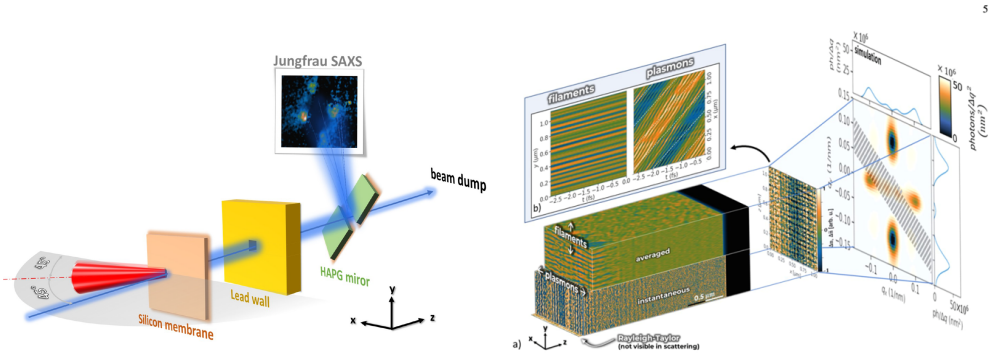

Figure 3.20: Left: Experiment setup of Ordyna et al., not to scale. The ReLaX UHI laser (red) is focused onto the silicon membrane target under 45° in p-polarization, and the X-ray FEL (blue) is probing the plasma density under target normal direction. The Jungfrau CCD detector records the SAXS image reflected from the HAPG chromatic mirror. **Right:** illustration the SAXS contributions from plasmons and filamentations.

This is the first ultrafast dynamic signal visualized by SAXS from UHI laser-driven solids, highlighting the great potential of this novel method. More comprehensive measurements of the growth rates and spatial scales will make it possible to refine and benchmark our simulations and overall knowledge of important key topics in relativistic plasma physics, including laser absorption, return current generation, instability growth and thermal stabilization, and the plasmon dispersion relation.

This topic was also selected as a talk during the HED-HIBEF satellite meeting of the Users' Meeting in January 2024.

3.3.4 Ultrafast foam dynamics

A team led by Nagler (SLAC) and Toncian (HDRZ) has applied the SAXS method to investigate the structural changes and homogenization during the irradiation of a low-density foam with a laser at relativistic intensities. Near critical plasmas are considered as a promising environment for the efficient coupling of laser energy and acceleration of electrons and ions to high energies. However, critical density for optical lasers corresponds to the mass density of about 10 mg/cc, which can be only achieved with porous materials (foams). Interaction of high-intensity lasers with foams is a subject of ongoing research. It is known that the foam response is very different from that of a homogeneous material of the same average density. Typical foam

consists of solid elements of characteristic size of 10–100 nm separated by m-sized pores. The process of foam homogenization takes place in tens of picoseconds, and a detailed understanding of this process requires experiments with a sub-ps and less than 10 nm resolution that can only be achieved on the X-ray FEL coupled to a high-intensity laser. The knowledge of the processes leading to the homogenization are paramount to predictive understanding of all associated processes, such as direct laser light absorption and subsequent ionization wave, non-local electron heating and ionization, and Coulomb and hydro expansion of the foam substructure. The foams used in this experiments had a density of 30 mg/cc, and the cold structure has been pre-characterized by SEM imaging Figure 3.21(a). The foam structure is made by filaments of 20 nm in diameter, separated by a few hundred nanometers from each other. Figure 3.21(b) summarizes the dataset; each delay shown corresponds to a single X-ray pulse irradiation.

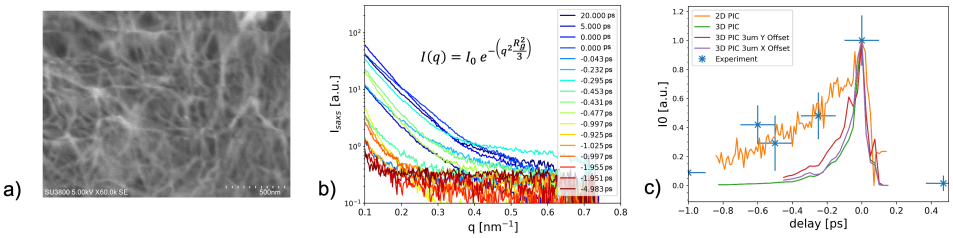

Figure 3.21: (a) SEM image of the foam. (b) Structural changes of foam structure probed by SAXS as function of the probe delay (fit function shown on plot). (c) Comparison with PIC simuation.

While final analysis in combination with particle in cell simulations of the data is ongoing, several features can be extracted by performing a Guinier analysis. Before the main laser interaction, preheating of the foam can be observed starting 20 ps before the main laser pulse, leading to a decrease of overall signal strength. This can be explained by ionization and subsequent heating and loss of electrons from the foam filaments that do not contribute to SAXS signal intensity anymore. Unexpectedly, the bulk of the foam structure remains constant. This changes at the time of main laser pulse irradiation. The SAXS signal shape changes dramatically, explained by the bulk heating and expansion of the filament structure, thus the foam homogenization observed on 500 fs timescale.

3.3.5 Cylindrical compression of thin wires

An internal team of HED-HIBEF scientists under the lead of A. Laso Garcia and T. Toncian (HZDR) have submitted a paper entitled “Cylindrical compression of thin wires by irradiation of a Joule class short pulse laser”. This work makes use of the ReLaX standard configuration optimized for phase contrast imaging (PCI), with data taken in spring 2023.

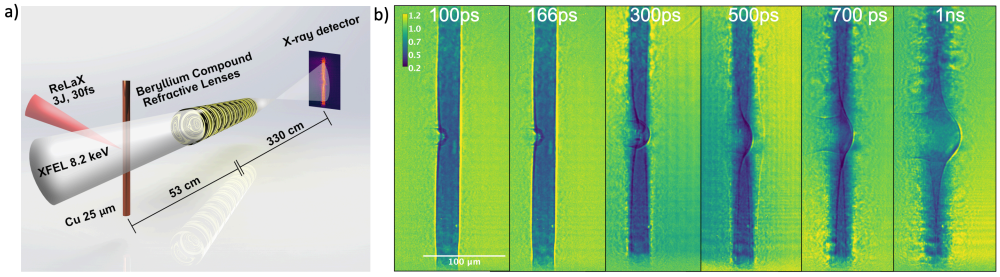

Figure 3.22: (a) Experiment setup of the PCI configuration used for imaging the compressed wire. The whole setup until the last 50 cm before of the detector is placed in vacuum conditions, minimizing air scattering. A slit system (not shown) is used to limit the X-ray illumination to a field of view at the sample position to 250 × 250 µm and minimize fringe scattering by the CRLs (300 µm^2 diameter). (b) X-ray PCI data measured at delays from 100 to 1000 ps after the irradiation of a 25 µm Cu wire by a 3 J, 30 fs laser pulse. The colour-scale gives the change in transmission compared to free beam propagation.

In this work, it is demonstrated that a Joule-class laser (ReLaX) irradiating thin wire targets is sufficient to generate extreme pressure states relevant to astrophysical studies. These states have been characterized via imaging techniques exploiting the ultrashort duration and high brilliance of the X-ray FEL beam. In particular, converging cylindrical shocks in copper with pressures up to 8.9 Mbar have been measured, with simulations predicting pressures of to 830 Mbar at convergence, supported by the excellent quantitative agreement between experiment and forward calculated data (Fig. 3.22). The generation of the radial compression wave is attributed to an ablative shock created by transient resistive heating of a thin surface layer of the wire. Hydrodynamic simulations recover the experimentally measured compression wave evolution. As an outlook, the potential of this compression scheme for different materials relevant in astrophysical context is investigated, showing that Jovian and white dwarf conditions could be reached, enabling complementary studies to those performed at kJ-class facilities.

This novel method of shock-generation discovered at HED-HIBEF paves the way to performing astrophysical experiments in the laboratory providing large statistics thanks to the high repetition rate of the lasers (shot per minute) and involving simple

and ubiquitous targets.

3.3.6 Resonant probing of ionization states

The idea of exploiting the unique capability of an X-ray FEL source to be tuned to any X-ray photon energy to study plasmas is not new. In particular, transition energies between atomic shells are changing with ionization state, predominantly due to the modified Coulomb shielding of the core.

A team of international researchers and HED-HIBEF colleagues, led by U. Zastrau, and Ph.D. student M. Mishchenko and Zastrau (both EuXFEL) have successfully conducted two experiments in 2022 and 2023 in which ReLaX was used in imaging standard configuration. Also in 2022, a team led by Huang/Kluge (HZDR) applied the spectroscopic method simultaneously with SAXS/PCI with the aim of investigating return current physics on wires in the context of high-intensity laser–matter interaction. The results on resonant absorption throughout the three beamtimes are consistent and complement each other while validating the technique as diagnostics of the ionization/relaxation dynamic.

Exemplarily, we show the results of Cu foil irradiation by ReLaX at 10^{21} W/cm^2. The laser–matter interaction creates a relativistic solid density plasma with strong radial gradients. We probed the plasma with X-ray pulses tuned to the K-L transition of Cu 21^+, which has vacancies in the L-shell. When and where this ionic state exists in the plasma, the X-ray probe will experience enhanced absorption, which leads to an increase in opacity for transmissive imaging. The electron that was promoted to the L-shell vacancy will decay within a femtosecond and cause additional isotropic X-ray emission at this particular wavelength.

Fig. 3.23 (top) shows the opacity increase as a result of ReLaX–foil interaction. Estimated temperatures are of the order 300 eV to 1 keV on a region that corresponds to the ReLaX laser focus of ~ 3 µm FWHM. This data was obtained using the ReLaX imaging standard configuration. Fig. 3.23 (bottom) shows the corresponding X-ray emission spectroscopy, recorded with the backward HAPG spectrometer. The blue shaded area corresponds to the X-ray FEL photon energy, and the additional emission of the Cu 21^+ K-L transition is clearly visible.

With this new method, we determined, for the first time, the ionization and recombination rates of ultrarelativistic laser plasmas with 100-fs precision.

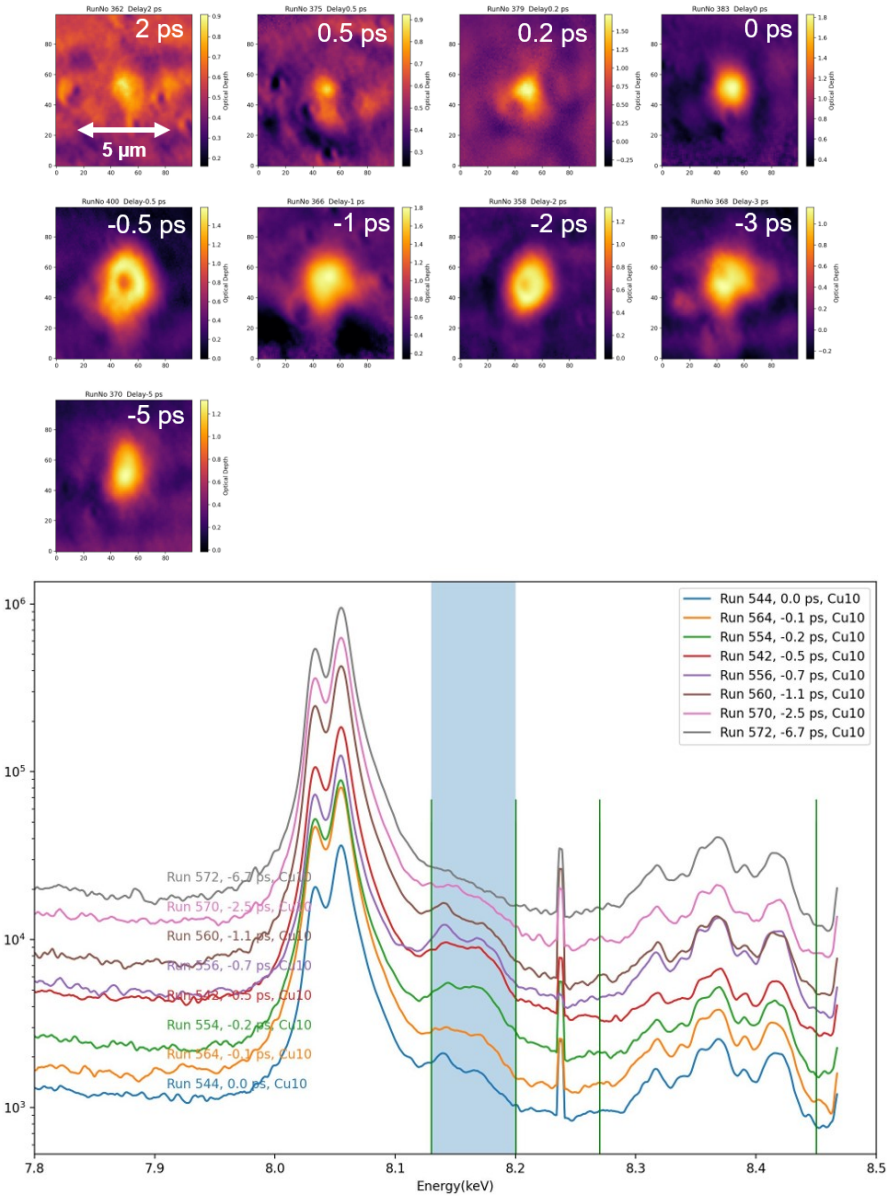

Figure 3.23: Top: Transmissive imaging with 0.5 µm resolution, showing an opacity increase as a result of ReLaX-foil interaction. **Bottom:** Corresponding X-ray emission on logarithmic scale. The dominant feature is the Cu Kα doublet. The blue shaded area corresponds to the X-ray FEL photon energy, and the additional emission of the Cu 21^+ K-L transition is clearly visible.

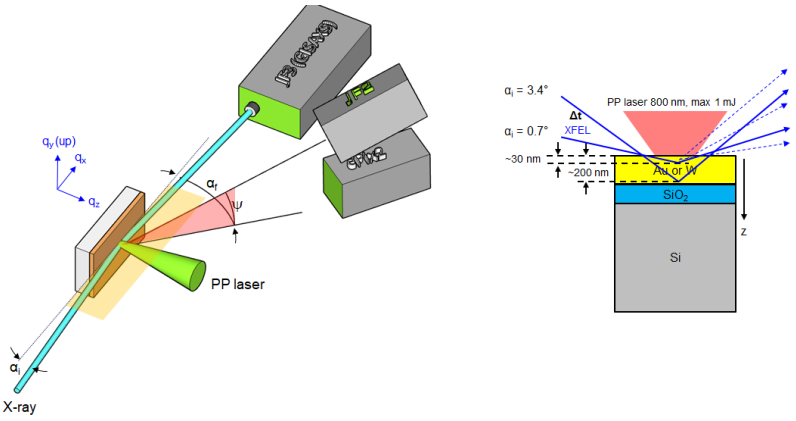

Figure 3.24: Left: Schematics of a grazing-incidence X-ray experiment performed at HED in the IC1 chamber. The X-ray pulses with 9 keV photon energy are irradiated on sample with grazing incidence angle α_i slightly above the critical angle of total external reflection. The sample surface is set to be perpendicular to the ground. **Right:** The sample consists of Gold (Au) or Tungsten (W) of 50, 100, or 200 nm thickness deposited on the thick (~ 700 μm) silicon substrate.

3.4 Surface nano-dynamics upon femtosecond laser–solid interaction

3.4.1 Grazing-incidence X-ray scattering (GIXS) for surface and subsurface dynamics

The interaction between high-power, sub-ps lasers with metals or high-density plasmas occurs within the skin depth of the overcritical plasma, where the laser wave is evanescent. The laser–plasma coupling therefore relies on the details of the surface nano-structure within the skin layer, which amounts to a few tens of nm for solids. For a clear understanding of the complex physics involved in laser–matter coupling and subsequent energy transport, phase transition, ablation, and surface nano-processing, it is crucial to visualize the surface and sub-surface with (sub-)ps resolution in nano- to atomic-resolution. X-rays can be surface-sensitive in a grazing incidence geometry, i.e. close to the critical angle for external total reflection, which is typically below 1° for solids in the hard X-ray regime. Grazing-incidence small-angle X-ray scattering (GISAXS), or grazing-incidence diffraction (GID), is a powerful tool to determine the surface nano-morphology as well as sub-surface atomic structure within ~ 100 nm depth. This technique is routinely used at various synchrotron facilities to determine, e.g. spray coating dynamics on timescales below a millisecond [90]. The first grazing-incidence X-ray scattering of a femtosecond X-ray FEL beam combined with a high-intensity femtosecond laser has been successfully

demonstrated at the SACLA X-ray FEL in Japan [48] and recently at the HED instrument using the PP laser and the ReLaX laser. These experiments are led by in-house HED scientists in collaboration with various external groups, in particular the group of Prof. Christian Gutt of University of Siegen.

Figure 3.25 shows the schematics of how a grazing-incidence experiment could be performed at the HED instrument at the IC1 chamber (proposal 3082 in October 2022, led by J. Schwinkendorf and M. Nakatsutsumi). The sample consists of Gold (Au) or Tungsten (W) of 50, 100, or 200 nm thickness deposited on the thick ($\sim$ 700 μm) silicon substrate. The X-ray pulses with 9 keV photon energy, about 500 μJ are irradiated on sample with grazing incidence angle (below 1°) slightly above the critical angle of total external reflection. One Jungfrau detector is put close to the specular reflection (blocked) for GISAXS, and an additional three GID detectors (Jungfrau and ePix100) are placed at different athomtal (α_f) and polar (ψ) angles to measure the diffraction from particular planes. The PP laser at 800 nm wavelength, 50 fs duration, $\sim$ 0.8 mJ was irradiated on metallic samples of 50—200 nm thickness deposited on the thick ($\sim$ 700 μm) silicon substrate. Single-shot GISAXS and GID data were successfully obtained simultaneously. The GISAXS signal indicates the increase in roughness RMS after laser irradiation, change in the surface nano-structure, and the increase of roughness correlation length on the surface plane. The GID signal from the surface region of 30—200 nm (by changing the incidence angle) shows the change in the diffraction Bragg peak Q position indicating compression. However, we could not observe the appearance of the broad liquid peak. The demonstrated new method is expected to provide an important insight into e.g. the physics of laser-induced surface nano-structuring and benchmark complex models [91], which allows tailoring optical, mechanical, and chemical surface properties for various applications in the field of optics, fluidics, medicine, and tribology [92]. The data is under analysis for publication.

We also tested the feasibility of GISAXS under harsh plasma conditions using the ReLaX laser to study the ultrafast change in surface structure initiated by the neutralized surface current flow or by exciting the surface plasmon (proposal 3449, led by in-house postdoc team members R.V. Rahul and M. Banjafar). As the GISAXS detector is imposed by the strong self-emission from laser-excited plasma on surface, to mitigate the strong plasma self-emission, which would overwhelm the signal, the detector is placed at the end of the hutch about 6 m from the sample. The GISAXS signal was obtained successfully in this configuration.

As one of the challenges, due to the grazing-incidence geometry, the tiny shift of the sample in position Z (=depth) shifts the X-ray footprint on the sample significantly. At α_i = 0.75° incident angle, 2 μm of Z offset corresponds to a 150 μm offset on

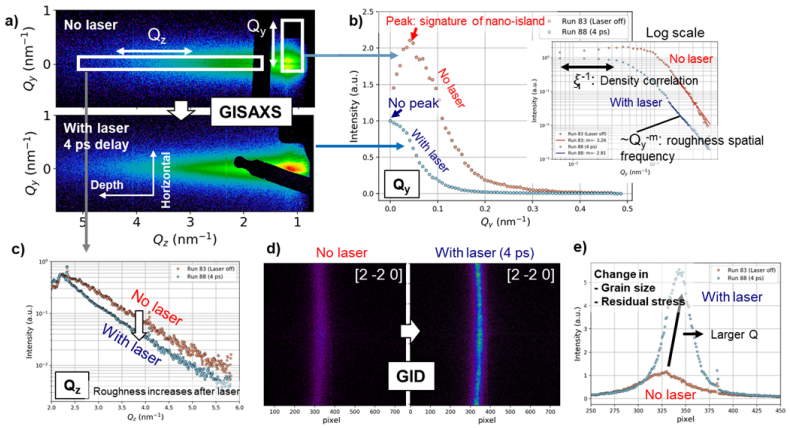

Figure 3.25: First simultaneous measurement of GISAXS and GID using X-ray FEL (beamtime p2716). (a) Single pulse GISAXS patterns before (top) and after laser excitation (bottom). (b) Lineout in Q_y direction displaying a peak at Q_y=0.05 nm^{-1} indicating the presence of nano-islands on the gold film sample that vanishes after laser excitation. **Inset:** log-log-plot, which indicates an increase in correlation length ξ and spatial frequency of roughness. (c) Signal in Q_z direction associated with the electron density profiles showing a larger roughness after laser excitation. (d) GID images from the [2 -2 0] peak without and with laser excitation. (e) Horizontal lineout of the GID image showing a shift of the peak position and increase in intensity.

sample, which leads to the loss of overlap between the X-ray and the laser. The sample alignment procedure was successfully established by using the specularly reflected X-ray beam in attenuated mode, allowing about 1 μm alignment precision, and good overlap was proven by the post-analysis investigating the damage pattern with a microscope. However, even if the sample is aligned correctly, the X-ray pointing jitter may cause the loss of the spatial overlap. To mitigate this, we used the nano-focusing CRL setup about 30 cm before the sample. This mitigates the beam-pointing fluctuation sufficiently on sample.

To conclude, this new geometry has been successfully demonstrated, which potentially opens a new opportunity to study ultrafast surface dynamics upon intense laser irradiation.

3.5 X-ray precision diffraction and shocks

3.5.1 Total scattering / pair distribution function techniques

Total scattering (TS) with its Fourier transform, the pair distribution function (PDF), is the benchmark method for determining local structure in disordered crystals, amorphous materials, and liquids. Over the past 30 years, the TS/PDF community has grown considerably, as has the range of science being tackled. However, its implementation at X-ray FELs has been patchy, as their relatively low X-ray energies gives limited real-space resolution. Now that XFEL photon energies are increasing and large-area fast detectors are available, it is timely to develop XFEL ultrafast TS/PDF techniques fully.

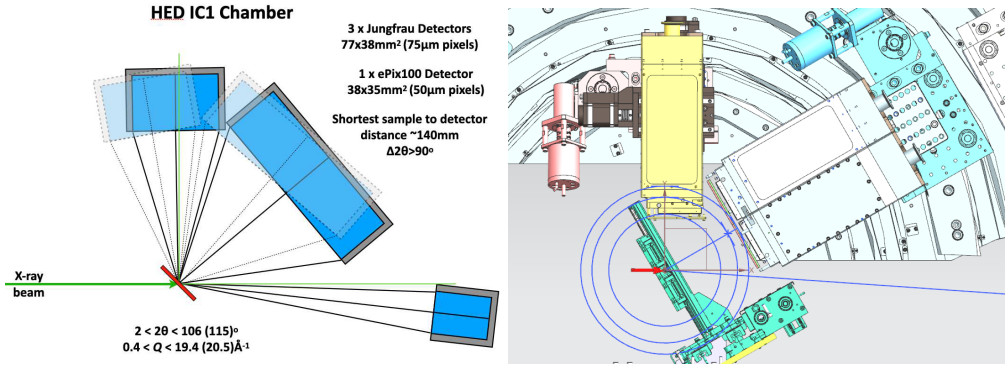

Figure 3.26: Arrangement for ultrafast TS/PDF measurements in HED IC1. **Left:** Proposed plan. **Right;** CAD design as implemented in HED IC1. The Jungfrau detectors are mounted within existing housings onto a single wagon on the inner vertical arc and can rotate to different scattering angles. The ePix100 detector is placed below the X-ray beam to collect the lowest-Q data. Further details, including Q-ranges (for 24 keV X-rays), are given within the figure.

A large collaboration led by D. Keen (U Oxford) has received beamtime for a long-term proposal across several runs and several instruments at EuXFEL. It will establish the protocols for high-quality, quantitative µf-TS/PDF measurements on HED and MID that exploit the unique time characteristics of the EuXFEL and will use them to address key science questions across several disciplines. We will provide the large TS/PDF community with a new X-ray FEL–based technique, looking towards plans at the EuXFEL for producing still higher X-ray energies.

A first beamtime at HED was conducted in November 2023 at 24 keV X-ray energy. It aimed at commissioning the arrangement sketched in Fig. 3.26, using a series of calibration samples to establish the idea detector positions and calibration, data normalization, and analysis protocols for ultrafast TS/PDF (e.g. Ni and LaB_6

powders, silica glass). Keen et al. also ran a number of experimentally straightforward measurements using samples in flat plate or (horizontal) capillary geometry, including laser-induced Pt nanoparticle formation from solution, laser excitation of thin coatings of $FAPbBr_3$ and $CsPbBr_3$ nanoparticles, laser interactions with CDW in VO_2, and ultrafast thermal heating studies of negative thermal expansion material ZrW_2O_8.

Preliminary analysis of the novel detector setup in IC1 in combination with 24 keV photon energy shows that q-values as high as 19 $Å^{-1}$ could be achieved. A second beamtime is scheduled for 2024-II.

3.5.2 First DiPOLE shock experiments

With the DiPOLE-100X laser coming online, we followed our tradition and organized a large community proposal to inaugurate the IC2 shock setup. The PI and Main Proposer were M. McMahon (U Edinburgh) and K. Appel (HED, EuXFEL), respectively. This user proposal received three full days (72 hrs) of beamtime in May 2023, preceded by 1.5 weeks of X-ray setup time and commissioning by in-house scientists. As can be seen from the respective standard configuration, XRD with the large Varex detectors at 18 keV and a three-arm VISAR are the main diagnostics. Several scientific topics were addressed during this proposal, of which a few are summarized below. The users reported their astonishment about the very high stability and excellent reproducibility of the DiPOLE laser parameters, pulse shaping, and timing.

Liquid carbon is predicted to be a tetrahedrally bonded liquid, highly structured with $\sim$ 4 nearest neighbors [93]. No diffraction from liquid carbon is published so far; the structure factor was tested from spectroscopy data only, and this yielded very few data points [94].

At HED-HIBEF, this goal was now achieved. An amorphous carbon sample without an ablator and without a VISAR window was driven by DiPOLE. The users observed nucleation of diamond at pressures of 60–90 GPa. Temperatures were hot enough for melting around 100 GPa, and liquid diffraction data was acquired for pressures up to 160 GPa. The pressures were derived from the shock transit time and the XRD-density. Each of five pressure set point that were studied consist of a minimum five shots to improve statistics. The liquid density is $\sim 3.7\, g/cc$, whereas the diamond density is $\sim$ 3.92 g/cc, which corresponds to a 5% volume change. The liquid temperature is 6500–7000 K, well within the DFT-MD simulation predictions.

Technically, the usable detector range for XRD had to be limited to 1–7 $Å^{-1}$ because

higher diffraction angles require complex filtering corrections due to strongly oblique incidence of X-rays though a 400 µm Al filter. However this is still larger than typical data obtained at other X-ray FEL facilities.

For **liquid Sn**, diffraction patterns from HED-HIBEF compare nicely to experiment data from DCS (Argonne National laboratory) and MEC (LCLS) after several corrections have been applied (detector, filter, sample re-absorption) out to as high as 9 $Å^{-1}$. In comparison, the MEC data had a limited q-range, while the DCS synchrotron data had artifacts due to asymmetric X-ray spectrum. Note that this spectral broadening is now overcome with the narrow beam at the ESRF-EBS; however, ESRF currently offers no XRD-shock beamline.

Copper undergoes a fcc-bcc transition at about 180 GPa [95]. At HED-HIBEF, **stacking faults in Cu** were measured under shock loading. These faults form due to stress release and lead to slight shifts in the diffraction peak positions. Previous studies were limited using only Bragg peak shifts in only lower-order (111) and (200) Debye rings. Using our large q-coverage, the users could cover the (400), (311), and (420) peaks in addition, which improved the data analysis. Preliminary analysis shows the observation of the bcc phase at lower pressures than expected. However, pre-heating of the sample using parylene-N ablators could play a role here. In general, the acquired data agrees with previously published data, but the EuXFEL generated more data with larger q-coverage and better signal-to-noise.

The α-to-ϵ transition in iron occurs around 10–13 GPa, and using DiPOLE, orientation relationships for a textured sample were studied during shock loading. The users obtained maximum pressures of up to 100 GPa in a total of 64 shots. Using strongly textured Fe foils, they observed a strong localization of driven bcc and hcp peaks.

Three more user experiments on low-Z and liquid materials were successfully conducted in October 2023. Also, for 2024-II, we received a number of DiPOLE proposals, including a follow-up XRD community proposal, and a community proposal to implement X-ray spectroscopy of shocked samples in IC1. These topics were selected for talks during the HED-HIBEF satellite meeting and the plenary session of the EuXFEL Users' Meeting in January 2024.

3.5.3 High repetition rate targets

During the community experiment in May 2023, it was also demonstrated that subsequent shots on a long strip of Fe foil can be done with few Hz repetition rate and data collected.

After the user run in summer 2023. we fielded a tape target by STFC (UK) and successfully shot it with the DiPOLE laser, while acquiring the shock breakout time with VISAR. Three metres of aluminized Kapton tape were moved at a speed of 15 mm/s, and DiPOLE fired a pulse every second (1 Hz) at full power, ~ 37 J in green (2ω). VISAR diagnostics was running at 0.5 Hz, and the breakout time reproducibility was excellent. Using white light interferometry, we were able to show focus reproducibility within 5 µm. In total, 600 shots were executed in 10 minutes. This development will be offered to upcoming user proposals.

3.6 Strong field science

3.6.1 Axion search

Researchers from the University of Oxford, lead by G. Gregori, have a manuscript under review entitled “Search for heavy axions with an X-Ray free electron laser”.

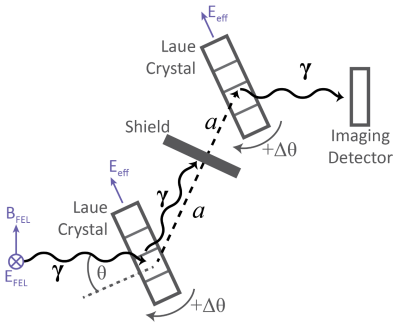

Figure 3.27: Diagram showing the setup employed in the Axion experiment. The X-ray beam propagates from left to right. Axion production and photon regeneration are expected to take place via the effective electric field within a pair of monolithic crystals (Germanium 220, Laue geometry) with dimensions: 10 mm × 10 mm × 0.5 mm. A pair of piezoelectric rotation stages were used to orient the germanium crystals. The radiation shield is a 1 mm thick titanium sheet.

The setup to convert photons into axions and back into photons is shown in Fig. 3.27. The axion generation is assisted by the strong Coulomb fields during Bragg diffraction in the Ge crystals. This measurement at HED did not show any axion signal. Therefore, the users claim to have extended the results from a 2018 study at the SPring-8 synchrotron by T. Yamaji et al. [96] at several discrete axion masses and also to have probed at an axion mass of 2.4 keV, which is a point in parameter space that was previously unexplored in terrestrial laboratory searches. In the mass range > 1 eV, they were able to surpass the sensitivity of bounds from all of the previous searches for laboratory-generated axions that we are aware of. The relevant previous searches are from NOMAD, PVALS, and ALPS.

3.6.2 Vacuum fluctuations and birefringence

Vacuum in the presence of a strong electromagnetic field contains pairs of short-lived quantum particles that can act as an electric dipole, which may, in turn, change properties of the background field, a process called vacuum polarization [97]. To detect vacuum polarization effects, the probing light, in this case the X-ray FEL beam, has to be linearly polarized with a high degree of purity [98]. Detecting this faint signal is one of the high-risk endeavors of the HIBEF UC. If successful, confirmation and quantification of vacuum birefringence would be a major scientific breakthrough.

In 2022, a team of HIBEF scientists and crystal optics experts led by K.S. Schulze and G.G. Paulus (U and HI Jena) [99] reported about their path towards perfectly linearly polarized X-rays.

Fig. 3.28 shows a sketch of the experiment setup. The X-ray FEL was operated in SASE mode at 10 Hz and a mean pulse energy of about 1.4 mJ. The X-ray beam was collimated to a high degree by a Beryllium lens (CRL1) located 229 m behind the source. The measured divergence has a root-mean-square divergence of 273 nrad in the horizontal and a negligible divergence in the vertical direction, which, in turn, is suitable to achieve a theoretical limit for the polarization purity of 7×10^{14}. The beam is further monochromatized.

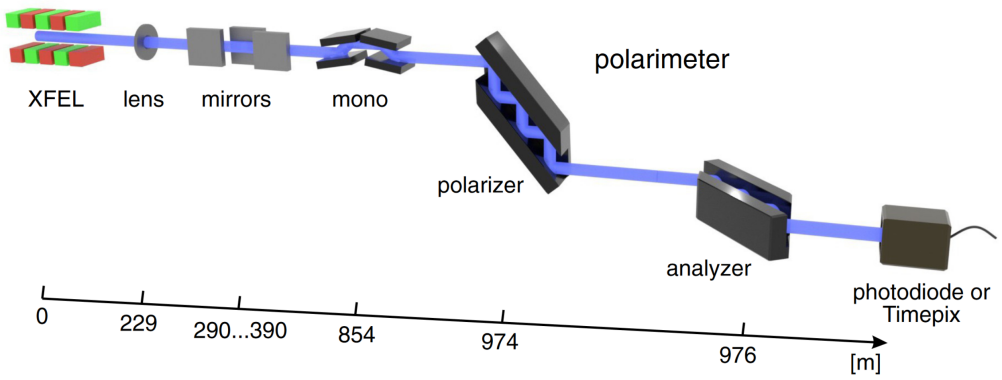

Figure 3.28: Experiment scheme used to create perfect linear polarization. The X-ray FEL radiation with a photon energy of 6.457 keV was collimated to a high degree by a Beryllium lens, followed by mirrors, which guided the beam to the experiment. A high-heat load monochromator (mono) selected and stabilized the photon energy and reduced the heat load on the polarizer. The polarimeter consisted of two so-called “channel-cut crystals” made from silicon. Each of the crystals supported six consecutive reflections with a scattering angle of 90°. The analyser crystal could be rotated around the beam to analyse the created polarization state. From Schulze et al. [99].

Using channel-cut crystals made from silicon, Schulze et al. demonstrated an unprecedented experimental polarization purity of better than 8×10^{11} at the HED-HIBEF instrument. Since a single X-ray pulse consists of the order 10^{12} photons, this amounts to a suppression of the entire photon flux of our highly brilliant source to the noise level.

Such polarization purity is unprecedented for X-ray sources and opens up new opportunities for quantum optics and polarimetric experiments at X-ray FELs. However, the higher the polarization degree, the lower the throughput. Ultimately, these experiments are limited by the available flux, and a very large number of shots would be necessary to identify VB events, making this detection scheme experimentally and time-wise very demanding. Nevertheless, the shown results are an important achievement for future polarimetric experiments at X-ray FELs. On the one hand, the high sensitivity achieved is pivotal for testing fundamental physical phenomena, such as vacuum birefringence. On the other hand, the realized purity corresponds to a well-defined quantum state of the X-ray photons, which will open new opportunities for quantum optics at X-ray FELs.

In 2015, Karbstein et al. [100] suggested an alternative approach to vacuum birefringence, using the *angular refraction* of the light-by-light scattering in the strong optical laser field to spatially separate the nonlinear vacuum signal induced by the quasi-elastic scattering of X-ray probe photons at the intensity profile of the strong optical pump from the large background of the X-ray beam. Using this dark-field-like configuration, this approach obviates the need for precision Bragg polarimetry and makes it possible to measure simultaneously the direct and the birefringent intensities, with an overall gain of about two orders of magnitude.

This approach is now pursued by the HIBEF UC using part of their priority access (one week each in 2024-I and 2024-II). They plan to design and test this X-ray setup to demonstrate its feasibility (March 2024) for further experiments with the addition of the ReLaX laser in the near future.

4 Future perspectives and plans

Looking back on almost five years of operation, the HED-HIBEF instrument has successfully implemented, fulfilled, and expanded the original objectives that were set when the instrument was designed. All drivers and the associated methods now shape the respective scientific fields. The last HIBEF-contributed driver, the pulsed magnetic field setup, will see first users in 2024-II. The next two sections on instrumentation developments and science perspectives describe the short- and mid-term plans that we have to further optimize the scientific output of the beamline. The emphasis is not on the addition of new drivers but on instrumentation and method developments that will allow us to expand the user science cases covered by the existing drivers. At the end of the chapter, we present long-term plans and the science case for the addition of a kJ-laser that would serve to expand both the dynamic compression and high-field science community.

4.1 Instrumentation developments

4.1.1 SASE 2 performance, drift, and stability

Comparing the performance of the SASE 1 and SASE 2 undulators, the latter showed systematically lower pulse energy and worse pointing stability. This is unfortunate because the experiments at SASE 2 are more demanding with respect to X-ray delivery (hard X-ray energies, high single-shot pulse energy, µm pointing requirements, HXRSS). However, since autumn 2023 significant improvements have been achieved after the implementation of a combination of electron- and photon-beam-based alignment.

Regarding the pointing jitter, the root causes are not known, despite facility-wide efforts and the establishment of a “stability task force”. It seems that the distribution mirrors are at least a part of the problem, and a design revision would be welcome.

4.1.2 Improvements for self-seeding

Commissioning of hard X-ray self-seeding (HXRSS) at SASE 2 has shown a great potential for this technique [101] and also triggered a strong interest by users. One or two diamond seeding crystals are used inside the undulator to achieve self-seeded beams with a record gain in spectral brightness (factor of 8–10) compared to SASE.

Until end of 2023, HXRSS was challenging to tune up, and the final performance is closely linked to the setup of the linac and to the phase-space and emittance of the electron beam. In this respect, SASE 2 is a difficult beamline due to the kick the electrons experience to enter the XTD1 tunnel. With the new electron- and photon-beam-based alignment, we have experienced significant improvements of the HXRSS performance in 2024.

HXRSS sometimes suffers from a SASE background (a broader spectral pedestal) that needs to be filtered away to obtain a narrow spectrum.

HXRSS is often used at HED-HIBEF and is a game changer for the most demanding experiments in terms of spectral brightness, for instance inelastic X-ray scattering. But imaging applications with chromatic CRLs also benefit largely from the narrow bandwidth. It remains to be seen, however, whether HXRSS can fully replace the need for traditional monochromators. Currently, HXRSS is considered a special mode, it is established by an expert group that is not available around the clock, and it is offered only on a best effort basis. Tuning of HXRSS usually has to be scheduled during user delivery time.

4.1.3 High repetition rate target delivery

One bottleneck on the quest towards high repetition rate HED experiments is the supply and alignment of targets as well as the management of resulting debris. Here, two strategies are discussed, both funded with internal R&D funds of European XFEL.

4.1.3.1 Solid targets

HED uses two high repetition rate (< 10 Hz) laser systems as drivers to generate extreme states of matter. Under the name *high repetition rate target delivery (HRRTD)*, the HED group is currently starting a research and development (R&D) project for two years. It is aimed at making more efficient use of these drivers and beamtime, and to enable new science.

While experiments at other facilities are limited by drive laser repetition rate, at HED, we are currently limited through the shot workflow, which includes target registration and tracking, target delivery, target alignment, shot diagnostics, near online analysis tools, and debris management. At present, this negatively affects the lifetime of the lasers operated at high base-rates and limits the effective use of beamtime. At the same time, high repetition rate target delivery is a prerequisite for photon counting

experiments, such as inelastic X-ray spectroscopy on shock compressed matter. This project aims to implement and extend work performed by SEC in close collaboration and to add hardware specific to HED in order to evolve from minutes per shot via shots per minute to 10 Hz operation.

The main project goals address:

- Target registration in a lab with respect to target frame reference marks
- Target alignment at instrument, including white-light interferometry
- Target interlock (shoot only when target present)
- High repetition rate scanning by XYZ sample scanner
- Tape target
- Debris management
- Data workflow
- Automatic workflow, shot procedures, shot strategy

Many of these topics are already partially addressed or plans exist. We hope to practically apply them during user experiments in the next two years. Currently, we are hiring an R&D postdoc for this project.

4.1.3.2 Cryogenic jets

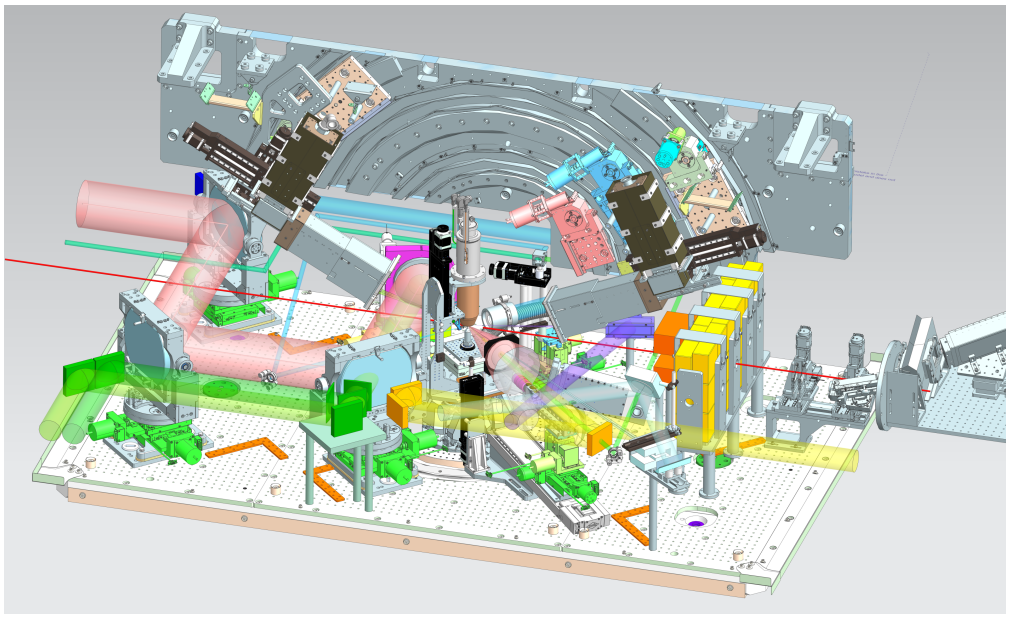

Figure 4.1: CAD representation of a ReLaX experiment in IC1 with the cryogenic jet as high repetition rate replenishing target

An R&D project titled “Instrument completion for high rep rate, debris free sample delivery”, led by instrument scientist Goede, will come to an end in 2024. As the title suggests, a cryogenic jet was identified already in the technical design of the HED instrument [3] as a strong candidate for high repetition rate target supply at close to solid density, which can cover many astrophysically relevant materials (H, He, methane, etc.) and is debris-free. This device exists in general and is used internationally for HED-class experiments. Instrument scientist Göde is an expert in this field [36; 38]. The operation, together with high-intensity lasers, needs a chopper to physically detach the jet from the sensitive nozzle and a catcher to manage a high vacuum even with high throughput jets of significant cross section.

Since 2021, this R&D project allowed us to bring the HED cryogenic jet target supply to a state of full operation during a user experiment in September 2023 and also established a test infrastructure with vacuum chamber and high throughput vacuum pumps in a Sample Environment and Characterization (SEC) group laboratory. This lab will allow jet developments and improvements outside the busy HED-HIBEF target chamber. For the duration of three years, a research engineer (Loureiro) joined us and designed and implemented a catcher and a chopper device, among other improvements.

Fig. 4.1 shows a CAD vacuum chamber setup in IC1 together with the full ReLaX standard configuration, as it will be used in the future. Fig. 4.2 gives an impression of the test chamber, which allows for further improvements and preparations, and two closeups of the jet in the IC1 chamber.

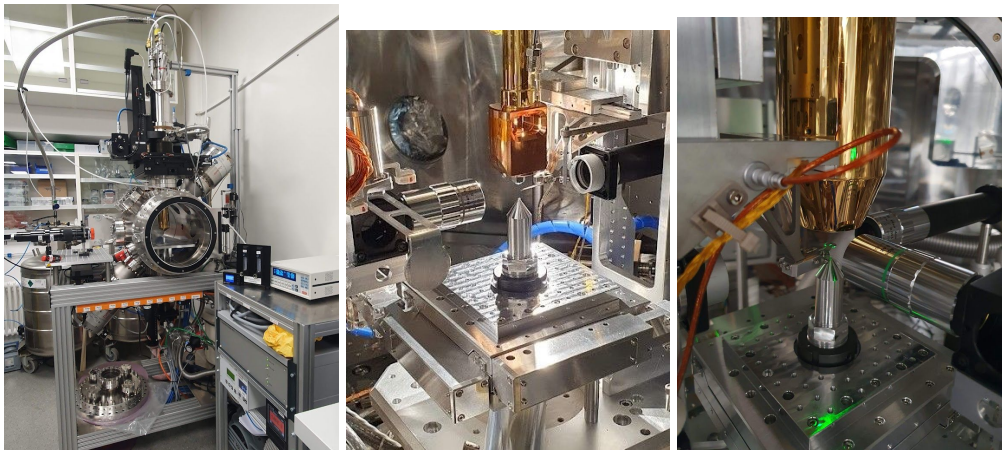

Figure 4.2: Left: Cryojet test chamber in a SEC laboratory. **Centre:**: Copper nozzle without heat shield from top, catcher (silver cone) below. **Right:** Heat shield installed.

4.1.4 Towards harder X-rays

A subset of experiments at European XFEL would benefit from the availability of higher photon energy as detailed in a workshop in January 2023 (https://indico.desy.de/event/33463/). This is also true for a subset of HED experiments, for instance in the categories of imaging and scattering. Potentially, harmonic lasing could, in the future, extend the current SASE 2 limit of ~25 keV to reach higher photon energies. A project is under way at EuXFEL to fabricate a prototype of a planned superconducting undulator (SCU) to be installed after the SASE 2 undulator as an afterburner [9]. Hence, HED and MID could benefit from an intense and hard X-ray beam in the future, potentially 10^9–10^{10} photons/pulse at 40–70 keV if the project is successful. Most diamond anvil cell (DAC) experiments at HED have been performed at 18 keV, which is a good compromise between penetration through the diamond cell and X-ray heating of high-Z matter inside the cell. To obtain sufficient transmission through thicker or denser samples, however, it is necessary to go beyond the current limitation of 25 keV. Working with a flat Ewald sphere and a compressed reciprocal space can also be advantageous for some diffraction experiments, and, in pair distribution function (PDF) analysis, it is essential to reach sufficiently high q for a proper reconstruction, down to inter-atomic distances. This is all facilitated by operating at higher photon energies. In a recent PDF experiment at HED, 24 keV was successfully used to reach a maximum q of 19 $Å^{-1}$. This was only possible by a special detector arrangement. However, 83% of the 24 keV photons are not stopped in the 320 µm thick Si sensor of the Jungfrau detector and potentially leads to radiation damage of the detector electronics. This necessitates the development of detector with a high-Z sensor if experiments at 25 keV and beyond are to take place.

It should be noted that X-ray heating experiments, or ReLaX experiments that use SAXS or collective (Plasmon) scattering, or work with high-purity polarization, still require photon energies between 6 and 9 keV.

4.1.5 Need for secondary target areas

The cutting-edge scientific infrastructure at the HED-HIBEF instrument is superior to most university labs, even without the combination with the X-ray FEL beam. If these devices can be only used during X-ray beamtimes, it makes very little use of their capabilities and they remain in storage of switched off most time of the year.

Since we schedule DAC research only in the first semester of each calendar year, high-end equipment stays unused for more than six months per year. We have

recently been able to move our mechanical setup workshop from a lab in the headquarters building (XHQ) to a shaft building on the campus and have started to convert it into a laboratory for laser-heated DAC research. Streaked optical pyrometry, Raman spectroscopy, and IR laser-heating DAC research can soon be done there at times when the DAC infrastructure is not used in the experiment hutch.

The situation is more complicated for the two large optical lasers, ReLaX and DiPOLE. Even though these lasers are among the best in Germany and Europe, they cannot be used for experiment campaigns in weeks between X-ray beamtimes, as in this time hutch access is necessary for setup changes. Working with the lasers during maintenance periods (currently one month in summer and two months in winter) is practically impossible because of equipment maintenance, water and electricity, interlock systems, IT infrastructure, etc. interferes with laser operation. It would therefore be beneficial to be able to route these lasers into an additional laser-only hutch to make more use of these expensive machines and to prepare for X-ray beamtimes.

With the future planning of additional drivers, such as a kJ laser, this problem becomes even more evident. Any additional driver needs to share the available beamtime with the existing drivers (lasers, DAC, pulsed magnetic field, X-ray only experiments). If a (multi-)kJ-class laser would be installed at the EuXFEL, it would be the only one in Germany and would be economically reasonable only if it got its own dedicated hutch. There, laser-only experiments with VISAR and SOP could be carried out, target design, pulse shaping, and timing could be optimized, and eventually the experiment could culminate in a well-prepared X-ray beamtime for a few days per semester. This could either be realized by a second, *laser-only* target area in the laser building (easier to find the floor space, but necessity to duplicate beam transport, target chamber, and all diagnostics) or by building an additional, dedicated X-ray hutch with a new target chamber where single hard X-ray FEL pulses could be brought in certain weeks by fast beam switching, but which would be accessible for kJ-experiments for the entire remainder of the year. It could be cast into a separate user facility and incorporated into networks, such as LaserLab Europe.

4.1.6 Third hard X-ray port at SASE 2

Similar to what was done at SASE 3, a third instrument will be fitted to the SASE 2 undulator. A distribution mirror, similar to M3, will deflect the X-ray beam to the north. This strategic decision has been taken by the EuXFEL management and is executed by the DO division. In the scheduled half-year maintenance period in the second half of 2025, a third port (beam transport and experiment hutch) will be constructed. A

newly designed mirror chamber, aiming to reduce beam vibrations and allow fast switching, will be installed only in 2026.

Initially, this hutch will be used for developments, under the administration of the EuXFEL DO division (staffing and operation). In a later second phase (to still be approved and timeline unknown), the hutch will be used for science. Given the huge investment made on the instrumentation, the increasing demand from the user community and complexity in operation to accommodate a large number of experiment setups, we have started an internal analysis to identify successful HED and MID science applications with their associated setups that could be proposed for the third port.

A suitable HED science case is a dedicated DAC experiment station. Such a station could reduce the workload during the change between DiPOLE and DAC setups in a limited time window and subsequently the required realignment of the X-ray path. Scientifically, we would use a pulse train of 352 SASE pulses at 2.2 MHz (or even 4.5 MHz) to obtain MHz X-ray diffraction patterns with an AGIPD detector on timescales of nanoseconds to microseconds. X-rays could be used as a pump (MHz X-ray heating) or just as a probe with IR laser-heating. At harder X-ray energies of $15 - 25\,\mathrm{keV}$, this setup does not require a vacuum chamber for X-ray or IR laser heating. As a permanent installation, an in-air AGIPD 500 k-like detector seems feasible.

For MID, speckle-based experiments are ruled out because they need a large propagation distance, and the hutch will be rather small. However, X-ray diffraction experiments with a femtosecond $> kHz$ laser on liquid jets in a small vacuum chamber or solids seem possible.

4.2 Scientific perspectives

This section describes our future plans for in-house research, completion of the HIBEF scientific pillars, and our response to emerging novel research directions.

4.2.1 Creation of warm dense matter by intense X-ray heating

Striving towards smaller focused beam spots is essential for X-ray heating to create volumetric warm dense matter. They are also essential in our scientific ambitions to acquire fs-resolved sub-µm phase contrast images of laser-matter interaction and hot electron dynamics.

The nanofocus CRLs (Section 1.1.10) makes it possible to achieve beam sizes down to ~250 nm but only by applying proper aberration corrections[19]. Moreover, the lens aperture, limited to about 300 µm, requires pre-focusing of the beam to achieve high transmission and flux density. This sets a limit on the maximum pulse energy and power because of the limited yield strength and the safety risk associated with damaging and oxidation of Be.

Potentially, a Kirkpatrick-Baez (KB) mirror system could solve these problems and, in addition, provide non-chromatic focusing. The drawbacks are that a KB system is more complex to use than refractive lenses, there could be vibration issues, and it will require much more space to be implemented than Be lenses. However, the overall experience with KB mirrors at FELs seems to be good, for instance at SACLA and LCLS, and a system is also in use at SPB/SFX. Focusing by KBs is definitely worthwhile to consider for a future upgrade of the HED instrument, maybe as an installation in IC1 to focus into IC2. Scientists at SACLA have utilized 2D-Wolter mirrors to obtain sub-10 nm focus, but this type of optics might not be compatible with MHz hard X-ray operation. Multilayer Laue lenses (MLLs) have been tested at MID [102] and spot sizes down to 12 nm observed, but, in the current implementation this type of optics, they are not MHz compatible due to heat load effects.

Although we have already published results from single pulse X-ray heating, the EuXFEL offers excellent capabilities to extend this field to X-ray pump–probe.

In 2022, we performed first two-colour two-pulse experiments, where the undulators were split into two sections with different gaps resulting in two ~ 100 eV separated X-ray pulses. The seeding chicane can be used to introduce delays of up to 400 fs. During this first experiment, we were able to co-locate ~ 10 µm foci using lenses upstream of the target chamber. Focusing schemes and characterization methods

making use of the nanofocus lenses are planned to achieve ~ 1 µm and ~ 5 µm spots on target, allowing for more intense X-ray pump–probe studies. X-ray diffraction from the pump and the probe pulse has also used to differentiate the two diffraction patterns from predicted ultrafast non-thermal phase transitions. However, the results are so far unsatisfactory because of the limited power in this mode, usually only around 100 µJ in each colour. If the overall performance of SASE 2 would be increased, this class of experiment would gain.

In order to extend the range of X-ray pump–probe delays into the picosecond range, the University of Münster (Germany) has built a split-and-delay unit (SDU) [103]. This project was supported by the German Federal Ministry of Education and Research (BMBF) via grants 05K10PM2, 05K13PM1, and 05K16PM.

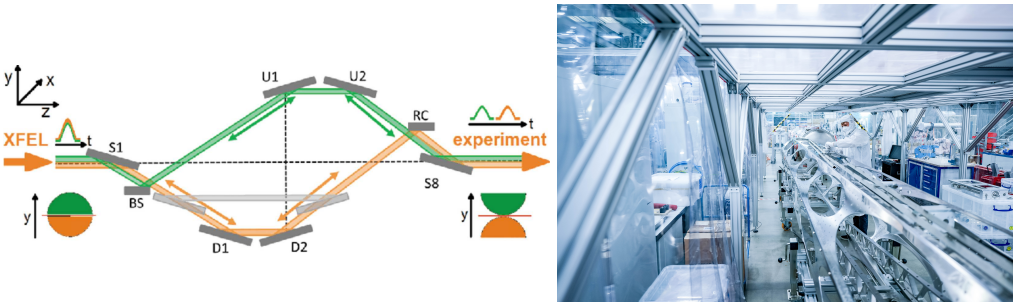

Figure 4.3: Split delay unit (SDU) for HED. **Left**: Optical concept from [104]. **Right**: Current photo in clean tent at theEuXFEL.

The HED SDU, based on multilayer Bragg mirrors, enables time-resolved two-pulse correlated hard X-ray experiments at full transmission of the SASE bandwidth and allows for intense X-ray pumping experiments (Fig. 4.3).

The project was delayed several times due to contamination of the components, which ultimately need to be ultrahigh vacuum clean, due to their installation in the photon tunnels. Also, control system standards and machine safety protocols (end switches, redundancy requirements) have evolved at EuXFEL during the time of construction and now need to be retrofitted. The vacuum vessel and the interior are currently at the EuXFEL in a shaft building, where work led by HED engineer Batchelor in a clean tent progresses. The qualification of all disassembled, cleaned, and reassembled parts into the vacuum chamber is still outstanding. In parallel, the mirrors and their deformations due to mounting have been evaluated. We currently aim for installation of the device during the long 2025 shutdown into the photon tunnel.

4.2.2 Advanced stochastic SASE spectroscopy

Self-amplified spontaneous emission (SASE) pulses are not suitable to resolve plasmon resonances due to their 0.2% bandwidth. Traditional approaches probe with seeded beam and monochromators that reduces FEL pulse energy and that require special tuning. However, collection times and experiment strategies are considerably improved when exploiting the unique stochastic spike structure of the full SASE spectrum.

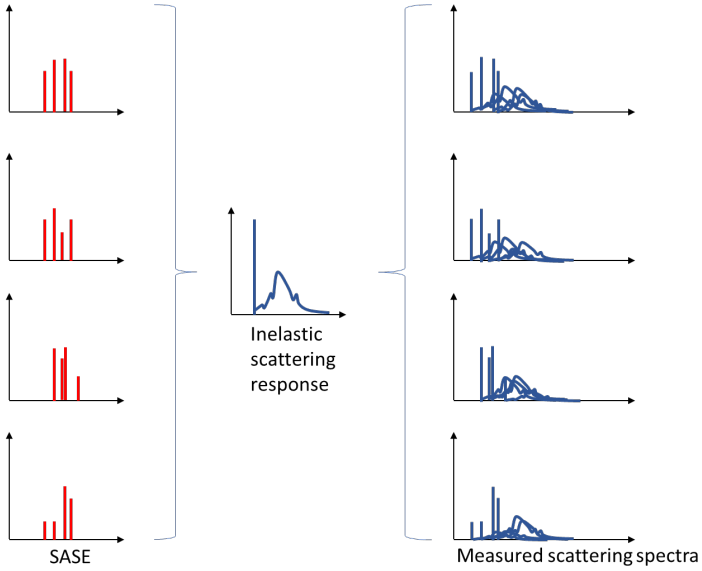

Figure 4.4: Illustration of the stochastic approach: Each SASE spectrum consists of a number of narrow spikes, < 1 eV broad. They vary in position and intensity stochastically from shot to shot. The response of the target (and the spectrometers) is, on the other hand, static. The measured scattered spectra are therefore a convolution of the incident spikes with the inelastic response by the plasma, yielding unique scattering spectra. Using an inverse matrix approach, it is possible to unwrap the inelastic scattering response from a sufficiently large dataset, as we have been able to show numerically.

This work was pioneered in cooperation with scientists from the FXE instrument (Milne et al.), and we started a joint project in 2022 involving a Ph.D. student from the University di Camerino (Italy) from the group of A. Di Cicco. During the first phase of this project, we have computationally put to a test an approach [105; 106; 107] that produces a matrix of response functions from measured SASE spectra and X-ray emission spectroscopy data (reconstructed RXES plane from XES spectra in Refs. [105; 106; 107]), respectively (Fig. 4.4). In particular, we have verified that, under suitable conditions of noise and number of SASE pulses, reliable high-resolution XES spectra can be obtained (Fig. 4.5).

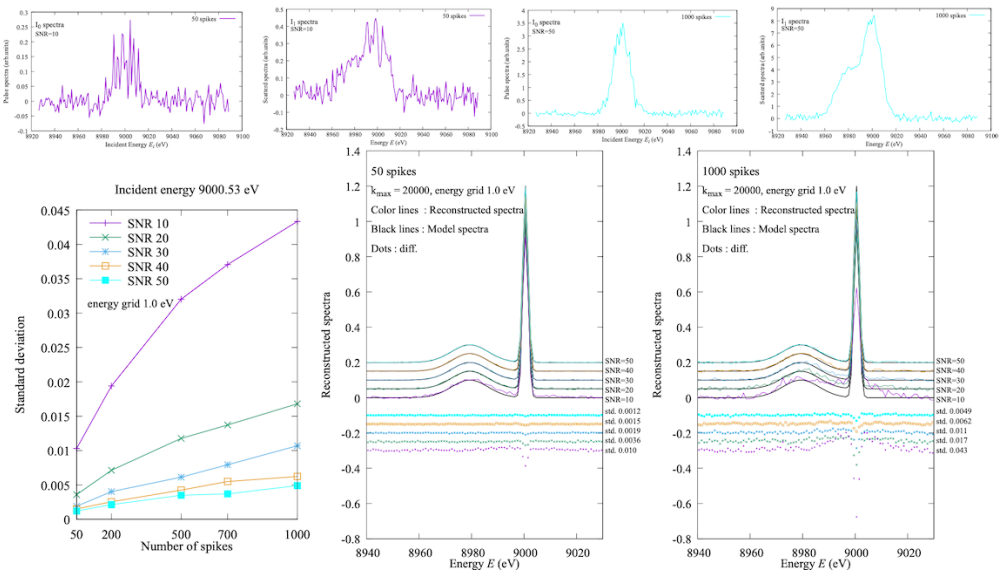

Figure 4.5: Numerical work by the HED Ph.D. student N. Hara over the last year has evaluated the necessary conditions for reconstructing the IXS signal: The upper panel shows a single incident and scattered spectra with (left, purple) 50 spikes and (right, cyan) with 1000 spikes in the SASE pulse. These are two extremes to demonstrate the limits of the method. The spectral resolution is 1eV. In the bottom panel, we illustrate that a low S/N ratio can be tolerated only if few spikes are present; a higher S/N ratio is necessary to reconstruct the IXS from a more densely populated SASE pulse. The number of spectra used for the analysis is 20 000 shots, which at 10 Hz translate into to 33 min acquisition time.

The next aim of our project is to demonstrate 1 eV-resolved measurements of the plasmonic feature or Al and Fe, both cold and X-ray heated, using the full SASE spectrum and reconstructing the data with an inverse matrix approach. From this IXS data, using Kramers-Kronig relations, the dielectric function could be reconstructed for frequencies down to the optical range.

4.2.3 Spectroscopy of dynamically compressed matter

X-ray scattering and emission spectroscopy methods are widely applied at synchrotrons to study properties of condensed matter. They provide unique information on the interplay between electronic configurations and crystallographic structures and are therefore particularly relevant for extreme conditions studies.

However, most of these methods are *photon hungry* and their application for dynamic compression experiments, investigating extreme pressure and temperature states, e.g. comparable to the interior of planets or during industrial processes, is challenging.

Usually, those conditions can be reached only very transiently in the laboratory, and the data quality has so far been limited by the low repetition rate technology driving the samples. Thus, providing the required data accumulation for sufficient photon statistics for photon-hungry spectroscopy techniques has not been possible for dynamic compression experiments up to now.

Pioneering experiments at optical laser facilities using laser-driven X-ray sources could demonstrate some of the principal capabilities, e.g. for spectrally resolved X-ray scattering [108]. However, the shot number is very limited at such facilities, and the achieved signal quality is often insufficient for advanced X-ray spectroscopy. The advent of ultrabright X-ray FEL sources has substantially improved the spectral, spatial, and temporal resolution for this class of experiments [109; 110; 111]. However, the total number of available photons per shot at X-ray FELs is similar to X-ray sources driven by large optical lasers, and thus accumulation of spectra is required to substantially improve data quality.

For this purpose, the DiPOLE laser now available at HED-HIBEF is a game changer: it raises the repetition rate in comparison to drive lasers of similar pulse energy by up to 1000×. At the same time, the temporal pulse shape of this laser is of exceptional stability due to diode pumping.

For 2024-II, Kraus (U Rostock) and Preston (EuXFEL) have submitted a community proposal to commission a new standard platform for X-ray spectroscopy in IC1. The proposed methods are IXS, such as plasmon dispersionn Al to determine collision rates and benchmark models, Compton and Raman scattering on (hydro-)carbons to resolve the local electronic structure, RIXS to study the high-pressure behaviour of nickel's 3d electrons, XES on Fe to observe the spin-state sensitive shape of Kβ line, and a test of stochastic correlation X-ray spectroscopy on shock-compressed samples (Section 4.2.2).

4.2.4 Ion temperature measurements

The ion temperature comprises a very difficult-to-measure parameter. In high-temperature (keV) plasma studies, streaked optical pyrometry (SOP) is usually employed, but it fails below the nanosecond timescale. Additionally, the signal level drastically drops when the temperature is lower at only some eV (warm dense matter), as the emissivity scales with T^4 [112; 113]. Also, SOP contains no information about the volumetric conditions. Nevertheless, we have recently successfully fielded, for the first time, an SOP during a ReLaX experiment.

Starting from the other end of the temperature range, the Debye-Waller effect is often used but requires the knowledge of the Debye temperature, which unfortunately changes with pressure and temperature itself. In addition, the diffraction intensity is also dependent on the micro structure of the sample, which can change in unpredictable ways when a shock wave passes through the material [114]. This makes the method even more unreliable in laser shock experiments. Lastly, it fails for non-crystalline samples or when the sample melts.

We use our meV inelastic X-ray scattering platform to deduce temperature from bound electrons, co-moving with the atoms as previously reported [115]. This work was started by Ph.D. student Wollenweber [116] and continues with Ph.D. student Bespalov. Experiments at HED-HIBEF have focused so far on collective scattering from phonons in crystalline solids or ion acoustic modes in amorphous materials. Spectrally resolving the scattered radiation on a meV scale gives rise to Stokes and anti-Stokes peaks, which correspond to the creation and annihilation of a phonon, respectively. The intensity ratio of these two features is a direct measurement of the temperature via the detailed balance principle [117]. This measurement can yield additional information about the sample system, like speed of sound or thermal diffusivity, too. We plan to perform a community experiment in 2025-I with his technique.

The second approach to measure temperature with IXS is to go to higher momentum transfers into the non-collective regime and measure the Doppler broadening of the individual atomic motion. If the sample system follows a Maxwell-Boltzmann distribution, the measurement of the velocity distribution is directly connected to a temperature. The spectral broadening due to the thermal motion for warm dense matter states lies similarly to the phonons and ion acoustic modes in the tens of meV range. The HED group has taken part in such experiments at the LCLS (also proving instrumentation), and proposals to perform such experiments at HED are currently under review.

Recently, X-ray photon correlation spectroscopy (XPCS) was proposed by G. Gregori (U Oxford, UK) to measure ion temperature. It could become a technique to determine temperature in dynamically excited matter states. In XPCS, the coherence property of the X-ray FEL radiation is used to generate a speckle pattern on an area detector in the far field. Changes in the structure of the sample will produce a change in the speckle pattern. Calculating the intensity auto-correlation function between these states enables conclusions on the motion of the atoms and thus, possibly temperature. XPCS is itself is already a well-established method at X-ray FELs, but it is mainly used with slower dynamics. The challenge for this technique will be whether it is possible to achieve the necessary spatial and temporal resolution, and whether

long-lasting plasma emission reduces the contrast of the XPCS signal on the detector. The HED group is involved in an experimental campaign at LCLS to test this method for HED science.

4.2.5 Detecting transient magnetic fields

The irradiation of solid matter with high-intensity lasers leads to strong electron heating and acceleration, and subsequently generates strong currents propagating through the solid density plasma. These currents are prone to instabilities and will, as a result, limit the efficient acceleration of secondary radiation sources, e.g. ion/proton acceleration. A deep understanding of the electron transport properties with solids is paramount to the optimization of such secondary radiation sources and the benchmarking of predictive computational capabilities. While the density modulations of the hot electron currents might be negligible compared with the plasma bulk density, and limited details are expected to be resolved by density sensitive X-ray diagnostics such as SAXS and PCI, plasma Faraday polarimetry could bridge the gap by enabling direct measurements of the magnetic field strength.

The Faraday effect has been proposed as a method to detect the predicted ultrastrong transient magnetic fields present in relativistic laser plasmas [118; 119]. A highly linearly polarized X-ray pulse would experience a rotation of the polarization plane by about ± 0.1 mrad when co- or counter-propagating with a strong magnetic field line. This approach thus requires the preparation of a highly linearly polarized beam, and the means to detect slight changes in its polarization plane, and will benefit from the polarimetric developments for vaccum birefringence detection.

Improving the flux before the analyser by reducing the mismatch between the SASE bandwidth and the energy acceptance of the polarizers by a seeded X-ray FEL will be an important next step for applications with highly polarized X-rays. Recently, an asymmetric Si channel-cut crystal was tested at HED, a promising candidate for widening the bandwidth. Such a setup could soon be combined with the ReLaX laser in a first attempt to detect the transient magnetic fields (Fig. 4.6 left).

As strong currents are ubiquitous in relativistic plasma, a strong community interest was expressed during the Workshop “High Intensity Laser Matter Science at the HED Instrument at the European XFEL” organized in April 2017 at EuXFEL, where a multitude of science cases driven by Faraday-polarimetry were presented (https://indico.desy.de/event/16772/). Therefore, we are making the development of such a platform within HED-HIBEF a priority, due to the immediate impact on expanding the ReLaX science case.

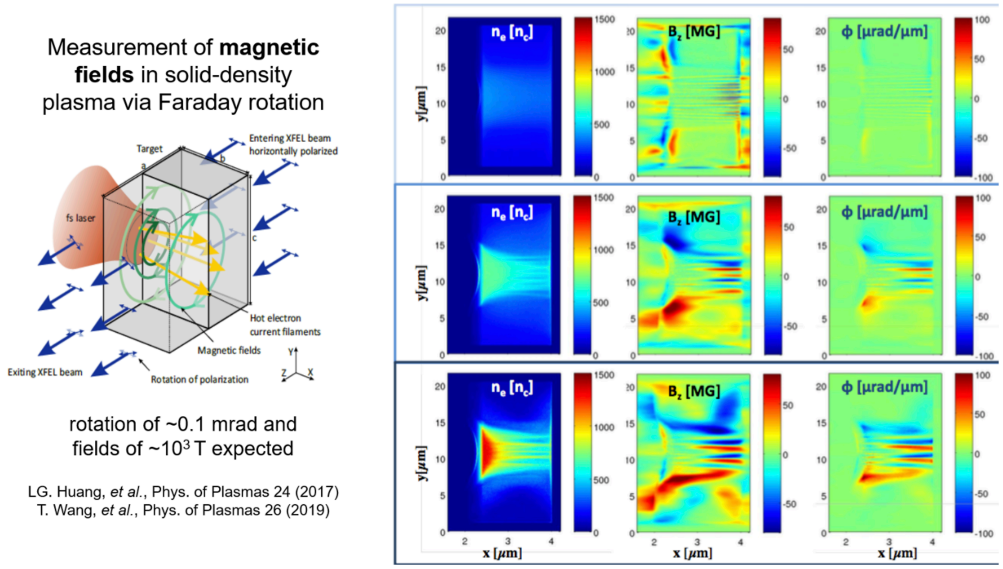

Figure 4.6: Left: Detection of transient magnetic fields using the Faraday effect. **Right:** Visualization of magnetic field generation on a laser irradiated foil.

4.2.6 Shocked diamond anvil cells

Ideal shock waves drive matter to states on the Hugoniot line. One way of achieving higher densities at finite temperatures is ramp compression. Another alternative, especially for gases and low-density liquids, is to use pre-compressed targets. For example, a shock wave can be driven into a pre-loaded diamond anvil cell (DAC) as shown in Fig 4.7.

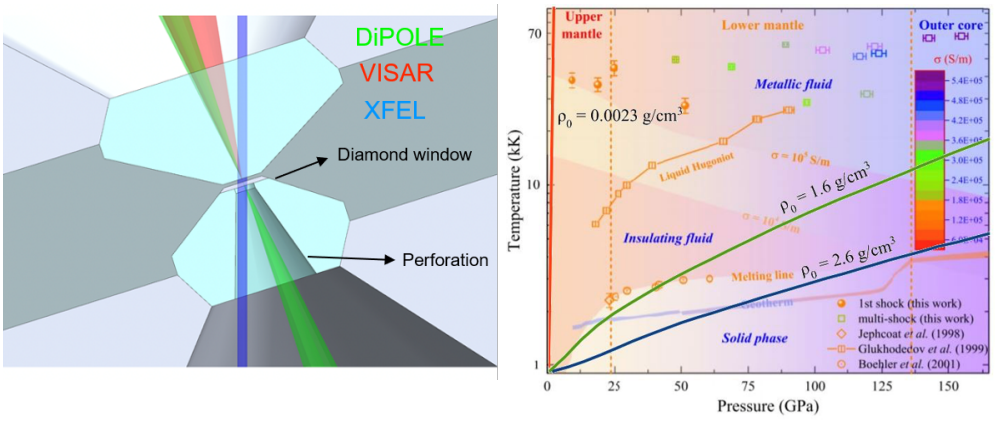

Figure 4.7: Left: CAD representation of the sDAC with a DiPOLE shock laser, X-ray beam path, and VISAR. **Right:** Example on krypton. Red line on the left: Hugoniot line in gas, and blue and green at precompressed to 0.1 and 0.5 GPa. Adapted from Wang et al.: PRB **103**, 014109 (2021).

The shocked DAC (sDAC) has been developed at the EuXFEL under the R&D/Ph.D. project S-278, “Towards Higher Densities of Matter”, specifically to be used with gaseous and liquid samples with the shock setup in IC2. It is now almost finished and followed up in close collaboration with V. Cerantola (U Milano), a former HED instrument scientist. The design of the sDAC uses a perforated anvil with an opening angle between 40° and 60° on top of which a thin (30–50 µm) diamond window is glued. The shock laser and the X-rays are envisioned to be directed through the perforated anvil and focused directly on the thin diamond window glued on top of the perforation. The VISAR system faces the opposite side and looks at the full diamond anvil, which is a modified Boehler-Almax anvil with an 80° opening. An sDAC holder, compatible with the shock setup in IC2, has been designed and can hold three cells at a time. At present, 10 sDACs belongs to HED instrument and are available to the user community.

4.2.7 Grazing-incidence surface science

Grazing-incidence small-angle X-ray scattering (GISAXS), or grazing-incidence diffraction (GID), is a powerful tool to determine the nanoscale morphology as well as the atomic structure around the surface up to ~ 100 nm depth. As summarized in Section 3.4, this technique was successfully demonstrated at the HED instrument.

At the EuXFEL, such grazing-incidence experiments are feasible also at the FXE and MID instruments. FXE offers an ambient or He environment with a large pixel detector (LPD) that can be combined with their von-Hámos XES spectrometer. MID offers a 1M AGIPD detector at variable distance that allows both a GISAXS and GIWAXS geometry. HED provides high-intensity lasers with a large vacuum chamber where one can perform simultaneous GISAXS, GID, and potentially XES, but with a limited q-coverage.

Users should choose the optimal platform based on their scientific needs, and more coordination between instruments across the facility is required to optimize the use of this technique. Therefore, in a satellite workshop, “Grazing-incidence X-ray techniques for X-ray FEL science”, during the 2024 Users’ Meeting, we will discuss our experimental capabilities with future potential users and will collect feedback and new ideas. We will also ask experts from several selected scientific fields to identify key scientific questions that should be potentially investigated.

From the technical point of view, one of the important challenges we should overcome in the coming years is to establish the 10 Hz repetition rate for this type of experiment, as mentioned in the previous section. This requires ensuring μm level sample

positioning precision while scanning at 10 Hz. Also, X-ray, laser, sample motors, and detectors should be fired or triggered with train IDs in a deterministic way.

4.2.8 Science in pulsed magnetic fields

High magnetic fields enable the stabilization of otherwise inaccessible new quantum states of matter, and scattering techniques are essential for a thorough microscopic understanding of these exotic high-field phases. The user community proposes a first experiment on one key representative system from two research areas, respectively, at the forefront of condensed matter physics to demonstrate the potential of this new setup for high magnetic field science at FELs: superconducting cuprates and magnetoelectrics. Currently, this seminal experiment could not be performed at any other facility, as it requires the unprecedented combination of the unique bunch-train structure of the EuXFEL in combination with fields exceeding 50 T. For the long term, we expect the installation of a split coil with panoramic access, polarization control and analysis for dichroism, and $\pi - \sigma/\sigma - \pi$ scattering as well as ultralow temperature inserts exploiting the “diffract and heat approach” (collaboration with TU Dresden).

4.3 kJ-class laser and fusion science-long term development strategy

The shock-compression laser at MEC (LCLS) and EuXFEL’s DiPOLE 100X laser do not differ much from the point of view of achievable pressure conditions. As soon as 2018, plans to bring a multi-kJ laser to the EuXFEL have been discussed to extend the pressure range.

Scientifically, this would make it possible to study the nature of solids at above 10 Mbar. Reaching 20–25 Mbar would enable us to study the formation of the BC8 phase. At even higher pressures, ion–electron demixing happens in Fe at 2 TPa and maybe at several TPa in Li. Further effects include phase transition kinetics and uniaxial effects as transverse stress or strain components. Large sample volumes allow a high degree of uniformity of a material following a shock and to approach thermodynamic equilibrium. Such a driver would also allow us to access highly compressed fluids, including the generation of electride-like states in Fe and Li. Further, all energy sinks are very interesting to study, like viscosity, phase transitions, chemical reactions, and mixing/demixing. Finally, a kJ laser would allow *in situ* probing of phonon and electronic band structure at high pressures.

Technically, for $\sim$ 10 ns ramp compressed targets, their thickness must increase to

avoid release wave problems. Pulse durations of 25 ns would require even thicker samples and larger phase plate spots.

There was a proposal by CAEP (China) to provide such a laser—based on regular low repetition rate technology—and the necessary staff to the EuXFEL premises (not necessarily to the HED-HIBEF instrument). In a conceptual design report (CDR), the baseline performance specifications were drafted. The system was designed to achieve a baseline performance of 1 kilojoule at 2ω within 2 nanosecond square pulses. It was intended to support variable pulse shapes ranging from 2 to 25 ns duration with a high resolution of 200 picoseconds. The specifications further included a 5% root mean square (RMS) energy stability and a 20 picosecond RMS jitter to the X-ray FEL pulse. The repetition rate was limited to 50 minutes, reflecting the required cooling time. The entire system was offered as a comprehensive package, encompassing beam transport, second harmonic generation (SHG), final optics, and a diagnostic package. Moreover, the package incorporated maintenance costs and provisions for an operational crew for several years. Additionally a new building tailored to the laser and including a standalone target area for laser-only experiment optimization, upfront of X-ray beamtimes, was financed by the HIBEF UC. However, political reasons and high-level government decisions prevented us from implementing this plan.

Since January 2023 and continuing for four years, the THRILL project provides new schemes and devices for pushing forward the limits of research infrastructures of European relevance and ESFRI landmarks. This project has received funding by the European Union's HORIZON-INFRA-2022-TECH-01 call under grant agreement number 101095207.

Eight partners joined forces not only to work on advancing technology in the field of high-energy high-repetition-rate lasers but also to train a highly skilled workforce for tomorrow's challenges in research infrastructures and industry:

- Amplitude Inc.
- CNRS – Centre national de la recherche scientifique
- ELI Beamlines Facility – The Extreme Light Infrastructure ERIC
- European XFEL – European X-Ray Free-Electron Laser Facility GmbH
- FAIR – Facility for Antiproton and Ion Research in Europe GmbH
- GSI – Helmholzzentrum für Schwerionenforschung GmbH
- HZDR – Helmholz-Zentrum Dresden-Rossendorf
- LLE – Laserlab-Europe AISBL

The THRILL project is built on six work packages, as shown in Fig. 4.8, to develop kJ-class laser technology with a repetition rate that will make it possible to efficiently drive samples coupled to the EuXFEL and bring multi-Mbar science into the repetition-rate era. At the end of October 2023, a three-day workshop was held to define the laser parameter space of scientific interest.

Figure 4.8: THRILL project is built on six work packages

In particular WP3 of THRILL will develop a CDR of a kJ laser adapted to the scientific needs and particularities of the EuXFEL. The laser blueprints should be the base of a future commercialization strategy. It will allow both the generation of kJ at ns-pulse duration and ps output at Petawatt power.

The work to be completed includes the following:

- Front-end strategies for generation of both ns and fs pulse duration
- Main amplifier strategies drawing on the results of WP4
- Beam transport and beam quality, in particular for the long paths
- Optical compression strategy for the short-pulse option
- Infrastructure and facility integration strategy

During the last few years, several fusion startup companies have emerged, most of them following an inertial confinement and laser- or impact-compression approaches. These systems operate in ns to µs timescales and could benefit greatly from a hard X-ray probe, potentially with MHz imaging capability.

For example, the fusion startup **Focused Energy GmbH** has expressed interest

in building a kJ-class fusion laser at, or close to, a large research infrastructure. In Germany, these could be GSI in Darmstadt or the EuXFEL.

Internationally, fusion science is also getting more attention at EuXFEL. In the USA, LCLS has planned an academic programme, “Inertial Fusion Energy Priority Research”, which should receive 50% of the beamtime at the MEC instrument.

The qualifying topics are:

- Imaging relativistic plasma coupling
- Multi-pulse studies of ablator material
- Viscosity/diffusivity of ablator materials
- Development of high repetition rate plasma experiments
- Radiation damage of fusion reactor walls

These research directions can also be followed at HED-HIBEF, partially with better experimental possibilities. However, the academic university–based community for this field exists only rudimentarily and would need to grow. University access can also go through research using high energy lasers at synchrotrons, such as ID-24 at ESRF, or a future installation at PETRA IV.

In 2023, the German ministry for education and research (BMBF) has released a statement [120] that it supports fusion research to help develop a future green energy source. Considerable funds have been granted to two German fusion companies, Focused Energy GmbH and Marvel Fusion GmbH. We are convinced that fundamental research in this area is crucial, and a central suitable laboratory where experiments with a multi-kJ laser in combination with an X-ray FEL probe can be performed would be more beneficial than scattered attempts. Such a facility would, of course, require long-term planning, considerable funding, and a long-term operation concept beyond a development and startup phase.

Already with the present equipment, HED-HIBEF could serve the following scientific directions:

- **Ablators:** Use XRD and SAXS for equation of state (EOS) studies in the few-Mbar regime, CHG and diamond ablators, and develop mass-producible ablators
- **Shock ignition:** Combine DiPOLE and ReLaX lasers at moderate intensities to influence pre-heating
- **Fast ignition:** Generate particle beams with ReLaX; study stopping power and non-local transport in shock-compressed matter

- **Opacity:** X-ray imaging and ionization dependence; study the spatial scales of instabilities

4.4 Strategy

The central strategic goals of EuXFEL, summarized in the next paragraph, aim to

- Improve X-ray and user operation
- Reach and maintain scientific excellence
- Develop and operate enabling technologies
- Increase the facility scope
- Develop the company further

In particular, after more than a decade dedicated to construction, commissioning, and exploratory experiments, the central goal is to put emphasis on scientific harvesting, which requires the stability and reliability of mature operations. As outcome better-quality data and publications will be obtained through a more efficient use of the time of our staff. Priorities will shift from “problem solving exploratory” experiments towards “science-driven” ones, designed to exploit well-established methods; robust, reliable and efficient experimental platforms; and streamlined data reduction and analysis. At the same time, EuXFEL will maintain its capacity to develop, innovate, and remain a leader in X-ray FEL science and technology, thereby attracting the best minds worldwide, both as staff and users. Enabling inexperienced users to perform successful experiments is key to widen our user community, and the relevance of our scientific output is vital for our long-term sustainability.

We at the HED-HIBEF instrument fully acknowledge and and strive toward the above-summarized strategic mission. We envision to enter, or have already entered, the harvesting phase and produce excellent results under stable operation conditions. Here, aim is to find a good balance between routine experiments in standard configurations and complex new discovery-class experiments, by attracting both experienced and novel groups as users of our instrument.

HED-HIBEF should conduct worldwide-unique research by exploiting our strengths, which are hard X-rays in combination with the MHz pulse train from the X-ray delivery point of view. Another strength is that the HED-HIBEF instrument serves a wide range of science cases and research fields with its broad range of excellent drivers (XFEL, pp-laser, DAC, ReLaX, DiPOLE, PMF), many of which have many parameters exceeding what is available at other X-ray FELs. Due to this variety, we can fully utilize the complete range of X-ray energies from 6 to 24 keV and special modes,

such as long train, single pulses, HXRSS, or two-colour. Thus, we should make use of a large amount of beamtime (compared to LCLS and SACLA) to use these capabilities.

HED offers many drivers for different scientific fields, which can be handled by the large HED-HIBEF group covering the required expertise. The associated HIBEF UC complements EuXFEL beamline expertise with international specialists in their field. The main UC stakeholders HZDR and DESY contribute not just dedicated human resources to operate the experiment drivers and but these also participate in general user operation.

We can accommodate frequent and complex setup changes between these drivers within available beamtime slots by grouping similar experiment, ideally using a standard setup, which allows us to keep a setup constant for several beam weeks. This also allows us to account for non-ideal X-ray delivery conditions that can mitigated by adding contingency in the beamtime schedule for such grouped experiments. To minimize downtime due to setup changes, community and campaign-style experiments are seen as an appropriate provision and are encouraged by the facility and also by the HIBEF UC. This also has the advantage that less experienced user groups and Ph.D. students can benefit from the more experienced community partners.

In addition to the described setups, the interior of the IC1 chamber and the Interaction Area 2 are flexible in the way they host other user-provided setups, which make HED-HIBEF also attractive to new user groups and science fields. But integration of such additional instrumentation bounds additional human resources and budgets. Therefore, careful evaluation on a case-to-case basis has to be done in order to weight risks and the success of such user-provided setups. Here, the user takes a major part of the responsibility towards execution and preparation of the experiment setup.

On the other hand, the fact that we can perform unique experiments often leads to unexpected and complex results, and it can take several years between an experiment and its publications. As long as the data is of good quality, we have to keep interacting closely with the users until publication. Overall, this means that only a limited fraction of the beamtime should be dedicated to high-risk non-standard experiments, in order to balance “harvesting” and “innovation”. As an opportunity with still great potential for improvement, we feel that development of new methods must be accompanied by development of data analysis tools provided and supported by the facility in cooperation with user groups. This will speed up to process from data evaluation to publication, and will also benefit another users.

We have also analysed the current threats to efficient programmes at HED-HIBEF. First: Operation of the complex EuXFEL sometimes causes unstable X-ray delivery, such as low pulse energy, drift, and jitter. Second: We also find that, in order to make efficient use of our many and excellent drivers, we need to change setups frequently, which is time-consuming and requires re-commissioning. Third: Specific drivers might not be scheduled for a longer period of time due to schedule optimizations. As a result, the hands-on experience of the operators will fade and users will have to wait several months for a certain capability to become available. Fourth: A long-term risk is that the contract duration of the HIBEF UC agreement is currently 10 years, and corresponding measures to secure beamline operation and maintain experience onsite on a longer term scale must be taken quite in advance.

To minimize potential weaknesses and avoid threats, we have to schedule contingency and avoid the temptation to schedule too many user experiments. Also, experiments have to be technically similar to each other to reduce setup changes.

To sustain HED-HIBEF's position as a world leading instrument, long-term developments are foreseen, especially in the field of laser-driven science. As an example, the THRILL project, funded by EU-INFRATEC, is focusing on a conceptional design report on a kJ laser. Such a project should not be constrained by the limitation of the HED-HIBEF instrument in view of available beamtime and space, but discussed at the facility level.

It is our current aim to ease setup changes by introducing standard configurations. We also strive to make the currently complex operation of the instrument simpler and more reliable, so users can be more directly involved in the experiments. The further increase of the instrument's capabilities beyond its current scope has to be balanced with the already large suite of drivers and scientific opportunities. Here, re-evaluation will become necessary long term, which potentially will result in discontinuing certain programmes in favor of other existing and new ones.

5 User statistics

HED has accepted early users since May 2019 for X-ray only and DAC experiments. During the COVID-19 pandemic, EuXFEL was shut down for several months in 2020, and we worked at a reduced pace in 2020 and 2021 due to severe restrictions on onsite presence, social distancing, etc. This required the development of tools for remote access, which, in some cases, have been working well. ReLaX came online in 2021. Since 2022, operation has been back to normal with most users on site, and the backlog of postponed experiments has been cleared.

5.1 Countries and institutions

From the start of operation in 2019 until the end of 2023 (5 years), HED-HIBEF has welcomed 593 users representing 21 different countries, as shown in Fig. 5.1. All 12 member countries of EuXFEL have had user visits at HED. For comparison, our sister instrument MID welcomed 366 different users from 20 countries in the same period, i.e. 63% of HED users.

Country	Users
Austria	1
China	3
Czech Republic	10
Denmark	9
Finland	1
France	47
Germany	169
Hungary	3
India	1
International	48
Israel	3
Italy	16
Japan	6
Portugal	4
Russia	13
Slovakia	3
South Korea	24
Spain	6
Sweden	3
Switzerland	4
United Kingdom	75
United States	144
Grand Total	593

(a)

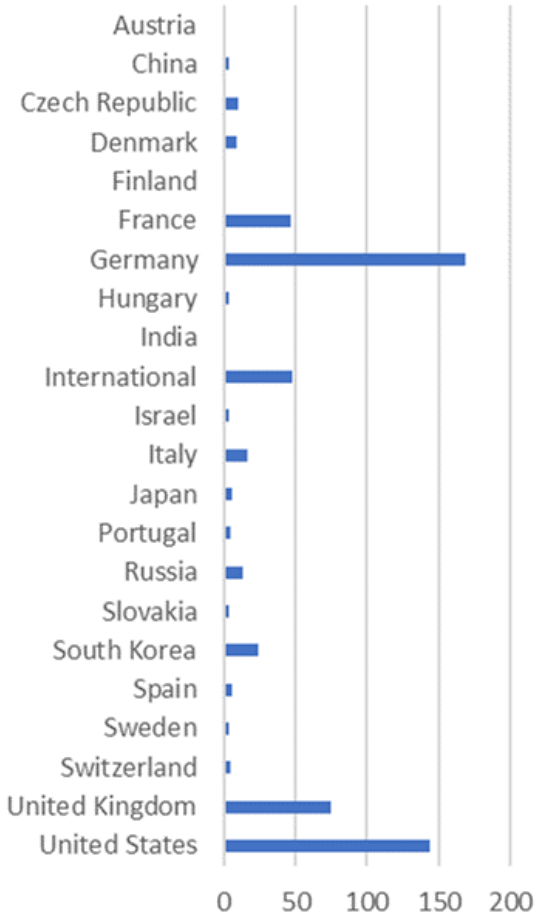

(b)

Figure 5.1: Individual amount of users sorted by country performing experiments at HED (registered in A-form) from 2019–2023, in table (a) and graphical (b) representation. Top three are: Germany (169 users – 28%), USA (144 users – 24%), and UK (75 users – 13%). *International* refers to institutions like EuXFEL or ESRF, which count according to their member states.

5.2 Proposal statistics

HED started operation in May 2019 and has been operating ever since, for a total of almost five years.

Proposals are usually submitted two times per year when the calls are open. However, there was an interruption in user operation due to the Cov19 pandemic between spring 2020 and spring 2021, and the resulting backlog of approved experiments forced us to skip two spring call for proposals.

After a feasibility scrutiny by a subgroup of the HED-HIBEF staff, the proposals are reviewed by the Peer Review Panel (PRP; see Appendix B) and ranked according to scientific merit with justifying comments by the panel. Based on this input, the EuXFEL Management Board decides on the actual allocation and schedule, with input from the group leader and the HIBEF coordination board.

We have received a varying amount of proposals:

Call no.	Allocation period	Submitted	Executed	Fraction
3	2019-I	11	3	27%
4	2019-II	13	5	38%
5	2020-I	10	5	50%
6	2020-II & 2021-I	14	4	29%
7	2021-II & 2022-I	27	19	70%
8	2022-II	27	8	30%
9	2023-I	33	9	27%
10	2023-II	31	7	23%
11	2024-I	22	11	50%
12	2024-II	16	In progress	

Here, *executed* accounts also for the fact that some proposals were initially scheduled but were canceled later for various reasons (pandemic, EuXFEL technical failure, such as cryogenic linac problems or insufficient lasing performance). Also, these numbers only account for user proposals that were submitted and reviewed by the PRP and do not reflect commissioning beamtimes or technical tests.

After reaching a peak of submissions for the allocation period 2023-I, the number has since kept decreasing. However, details of the call matter: from 2023-I, we allow submission of DAC and DiPOLE proposals only in alternating calls, which are

both highly demanded standard configurations. On top of that, Call 12 has seen the submission of four large community proposals, which otherwise could be easily equivalent to two to three separate proposals.

Besides a single heroic effort to get rid of the backlog from the pandemic, the fraction of executed over submitted proposals is between 25 and 50%, which translates into an over-subscription rate of two to four.

Regarding the demand for and relative distribution of the various drivers, only the last calls are relevant when most drivers were offered for user experiments:

Call	Allocation	ReLaX	DiPOLE	DAC	PP laser	X-ray only	PMF
9	2023-I	10	-	8	8	5	-
10	2023-II	8	7	6	4	5	-
11	2024-I	5	-	9	3	5	-
12	2024-II	5	6	-	2	2	1

We see that the request for the three drivers ReLaX, DiPOLE, and DAC are the largest. To accommodate more of these experiments, we implemented standard configurations. Slightly less demanded but still significant are experiments requiring the pump–probe (PP) laser and X-ray only experiments. The latter also comprise X-ray polarization experiments, Axion search, and X-ray pump, X-ray probe two-colour experiments.

The available and delivered number of hours for new experiments have been fluctuating a lot since the first half of 2019, when HED started operation. This is caused by the startup phase of SASE 2 in 2019–2020, when experiments were longer and often performed as user-assisted commissioning (UAC), but, of course, also due to the COVID-19 pandemic in which operation was ceased from March to August 2020. For the remainder of 2020 and 2021, there were fewer experiments and only with limited access of users to the EuXFEL site (remote access preferred). Several proposals were delayed but finally there were no complete cancellations. Until February of 2022, HED was still catching up with postponed proposals from the COVID-19 period. In 2022, a special call for “water research” was issued in parallel with Call 9 to highlight and promote this branch of science. HED received three water proposals (all DAC), out of which one was accepted. The water proposals are integrated in the statistics shown here.

For HED, the total requested hours is 12 924 (MID: 8608 h). These were associated with 206 proposals, making an average request of 63 h or 2.6 24 h-days per proposal.

Call No.	Submitted proposals to HED per call	Withdrawals after deadline	Requested hours per call @ HED	Finished experiments *per call* of submission	Delivered hours to proposals *per call*	Allocated/ finished experiments *per run* of execution	Delivered hours *per run* of execution	Run / allocation period
#3	12		648	4	312	3	276	Run 3 / 2018-II Nov 2018_June 2019
#4	13		924	5	444	4	216	Run 4 / 2019-I July-Nov 2019
#5	10		696	2	252	1	96	Run 5 / 2020-I (interrupted March 2020)
#6	15		1032	8	828	2	264	Run 2020-II Aug-Nov 2020 (only 5 instruments in this call)
NA						2	248	Run 2021-I March-June 2021 (lockdown postponements, COVID priority BT till April 2021)
#7	27		1104	13	1072	7	736	Run 2021-II (w. postponed proposals from call 6)
						12	928	Run 2022-I (w. postponed proposals e.g. from call 7)
#8	27		1608	8	816	8	816	Run 2022-II July-Nov 2022
#9 reg. / water science	30		1744	8	696	9	840	Run 2023-I Feb-June 2023 (regular & water science + 1 LTP submitted 203-I & scheduled 2023-II below)
#9 Long-Term Projects	*2*	*1*	*440*	*1*	*96*	*see 2023-II*		*Run 2023-I LTP submission - to date 1 LTP max 60 shifts / 480 hours over max 5 following semesters*
#10	31		2032	7	688	7	784	2023-II July-Nov 2023 (including LTP 1st part)
#11 (*)	23		1360	10	TBC	11		2024-I Feb-June 2024 (scheduled)
#12 (**)	16		1336		TBC	TBC		2024-II Aug-Dec 2024 (review/allocation phase)
	206		**12.924**	**66**	**5.204**	**66**	**5.204**	

(*) including 3 HIBEF Priority Access Proposals

(**) including HIBEF Priority Access Proposals

Figure 5.2: Submitted proposals, resulting requested, and accepted hours for user experiments per call, compared to the delivered hours

The total number of delivered user hours is 5204 distributed over 66 experiments (MID: 3264 h for 38 experiments), corresponding to 79 h per experiment (MID: 69). The average demand per experiment is only 63 h, meaning that HED provides about 14 h (22%) extra time per experiment on average. This “extra time” is proposal dependent and estimated during the technical feasibility assessment. The extra time is used for experiment specific setup and preparations, particularly for HXRSS, detector calibration, optical laser alignment, and tests of user contributed equipment. The 5204 delivered user hours are also corrected for unforeseen severe downtime (more than one lost 8 h shift) due to linac or instrument malfunctioning.

The use of internal time for startup/commissioning and in-house research, for instance to support student and postdoc projects, is not easily distinguishable for user experiment setup, as we try to combine all these efforts and execute the tasks in parallel. Typically, since 2022, three days per run are used to commission the instrument after a maintenance period (72 h). Until 2023, the management allocated two weeks per run to advanced (re-)commissioning, method development, and research; since 2024, this is handled more flexibly. HED-HIBEF typically allocated one week per run for commissioning and method developments, e.g. one week in 2023-I for commissioning the DiPOLE laser with X-rays. In 2023-II, one day was allocated to test asymmetric channel cut crystals for polarimetry. In 2024-I, two days will be allocated to commission the pulsed magnetic field setup.

In addition to the regular proposal cycles, a call for long-term proposals (LTPs) was issued in 2022. For HED, one project on pair distribution function and total scattering has been accepted. It will receive ~360 h distributed over five semesters, two experiments at HED, but up to three more at FXE and MID.

In-house research at HED-HIBEF is done in the framework of regular user proposals. These proposals are initiated and led by members of the HED and HIBEF groups, but typically include external co-proposers, they are submitted as regular competitive proposals, and they are subject to PRP review. If they are not scheduled as regular proposals, we can allocate up to one week per run for these proposals, and the final choice is made by the HED-HIBEF coordination board.

5.3 Publication output

Fig. 5.3 illustrates the timeline of executed proposals and the time it takes until ultimately a peer-reviewed article is published in a journal. At the time of writing, 21 green dots indicate that 21 publications with HED data have been published. Several more are submitted, and the number of drafts is typically of the order of one

per experiment.

The timeline in Fig. 5.3 also shows that, by now, all experiments from 2019 and 2020 have produced one or even several articles each, except for two that are still in a draft state. These are 15 articles from a total of 21 published so far, indicating a time between experiment and publication of 2–4 years. Only results from three experiments in 2021 and only one from 2022 are published so far.

Figure 5.3: Graphical representation of the timeline of executed experiments (blue dots), indication of failed experiments (red dots), indication of a first paper draft (gray dot), and publication of a peer-reviewed article (green dot)

We are awaiting the publication of the bulk of high-impact science in the next two years. One article in **Nature Astronomy** by Frost et al. (2844) is currently in print. This research was conducted in 2022-I in a 48 h DAC standard configuration beamtime, which suffered from beam loss on the second day. Nevertheless, the data the users acquired on the first day was groundbreaking. This case proves that also short, focused experiments in a standard configuration can yield excellent results.

The red dots indicate the experiments that completely failed to generate scientific dataexperiments!failed.

Reasons for these failures are

- Non-available Si (111) monochromator and failure of a user-provided backup solution (3048), which was not tested beforehand
- Too complex setup resulting in not enough time (3071)
- Failure of a major IT switch in SASE 2 (3449)

- Cancellation of beam delivery due to insufficient performance (3996)

Many other experiments were affected partially (e.g. by failure of the cryogenic cooling of the linac or by power outages), but at least a part of the user programme could be executed. We have implemented procedures to minimize the risk of complete failures by demanding that users bring only tested equipment (characterized crystals) and schedule more time for setups.

Since 2015, the HED-HIBEF group itself has published about 110 peer-reviewed articles and 13 proceedings, also containing data from other facilities as well as computational studies.

6 HED-HIBEF instrument publications

PDF copies of publications describing the technical and scientific capabilities of the HED-HIBEF instrument can be downloaded in a zip file here:
https://syncandshare.xfel.eu/index.php/s/HftD6oQYgm7w9Ly

General overview of the HED instrument:

- "The High Energy Density Scientific Instrument at the European XFEL"
  Zastrau, Appel, Baehtz et al.: J. Synchrotron Radiat. **28**, 1393–1416 (2021)
  https://doi.org/10.1107/S1600577521007335

DAC research:

- "Diffraction from Diamond Anvil Cell platform at HED - overview"
  Liermann et al.: J. Synchrotron Radiat. **28**, 688-706 (2021)
  https://doi.org/10.1107/S1600577521002551

- "MHz XFEL XRD and modeling of pulsed laser heated DAC"
  N. Jaisle et al., J. Appl. Phys. **134** (9), 095904 (2023)
  https://doi:10.1063/5.0149836

- "MHz XRD set-up for dynamic compression experiments in the diamond anvil cell (dDAC)"
  R.J. Husband et al.: J. Synchrotron Radiat. **30** (4), 671–685 (2023)
  https://doi:10.1107/S1600577523003910

- "Dynamic optical spectroscopy and pyrometry (SOP) under optical and x-ray laser"
  O.B. Ball et al.: J. Appl. Phys. **134** (5), 055901 (2023)
  https://doi:10.1063/5.0142196

Optical lasers:

- "ReLaX: the HIBEF high-intensity short-pulse laser driver"
  A. Laso Garcia et al.: High Power Laser Sci. Eng. (2021)
  https://doi.org/10.1017/hpl.2021.47

Monochromators, spectrometers, and analyser crystals:

- “Design and performance of the meV high resolution setup”
  Wollenweber et al.: Rev. Sci. Instrum. **92**, 013101 (2021)
  https://doi.org/10.1063/5.0022886

- “Design and performance of the HAPG von-Hamos spectrometers”
  Preston et al.: J. Instrum. **15** (2020)
  https://doi.org/10.1088/1748-0221/15/11/P11033

- “A von Hámos spectrometer for diamond anvil cell experiments”
  Kaa et al., J. Synchrotron Radiat. ***30*** *(4), 822–830 (2023)*
  https://doi:10.1107/S1600577523003041

- “Design and performance of the SAXS HAPG mirror”
  Smid et al.: Rev. Sci. Instrum. **91**, 123501 (2020)
  https://doi.org/10.1063/5.0021691

7 Acknowledgements

The HED group presently comprises Karen Appel, Michal Andrzejewski, Mohammedredza Banjafar, Lewis Batchelor, Bernard Baranasic, Dmitrii Bespalov, Khachiwan Buakor, Thomas Feldmann, Christiana Franke, Sebastian Goede, Oliver Humphries, Zuzana Konôpková, Daniel Loureiro, Eike-Christian Martens, Mikhail Mishchenko, Motoaki Nakatsutsumi, Thomas Preston, Lisa Randolph, Rahul Sripati Venkata, Sven Wagner, and Ulf Zastrau. We also explicitely thank Erik Brambrink, member of the Lasers group.

The HIBEF group presently comprises Carsten Baehtz, Alejandro Laso Garcia, Samuele Di Dio Cafiso, Jens Hauser, Hauke Hoeppner, Rachel Husband, Alexander Pelka, Masruri Masruri, Björn Näser, Michael Röper, Marlit Looden, Georgiy Shoulga, Jan-Patrick Schwinkendorf, Cornelius Strohm, Monika Toncian, and Toma Toncian.

Many thanks to Kurt Ament for proof-reading, Silvia Bertini for input to the report regarding user statistics and to Christiana Franke for assistance in organizing the review meeting.

We acknowledge the continuous support from EuXFEL management and thank all groups and services at EuXFEL for excellent collaborations and help in construction, commissioning, and operation of the SASE 2 beamline and HED instrument. The DESY groups supporting EuXFEL, particularly those responsible for detector development and linac operation, are acknowledged for their important contributions. Special thanks goes to former HED design engineer Ian Thorpe for his contributions to designing, engineering, and commissioning of the instrument.

We acknowledge contributions to HED's instrumentation and staff from the German Bundesministerium für Bildung und Forschung (BMBF) through funding via grants 05K19PE2, 05K10PM2, 05K13PM1, and 05K16PM. We acknowledge funds for research, instrumentation, and Ph.D. students from the Deutsche Forschungsgemeinschaft DFG via grants via the research unit FOR2440 and AP262/2-1/-2 and the research unit CarboPat through grant AP262/1-1/-2.

Finally, many thanks to all our scientific collaborators and users for walking the extra mile with us.

Bibliography

[1] U. Zastrau, K. Appel, C. Baehtz, O. Baehr, L. Batchelor, et al.: "The High Energy Density Scientific Instrument at the European XFEL", Journal of Synchrotron Radiation **28**, 1393–1416 (2021) doi:10.1107/S1600577521007335

[2] M. Nakatsutsumi, T. Tschentscher: "Technical Design Report: Scientific Instrument High Energy Density Physics (HED)" (2013) doi:10.3204/XFEL.EU/TR-2013-003

[3] M. Nakatsutsumi, K. Appel, G. Priebe, I. Thorpe, A. Pelka, et al.: "Conceptual Design Report: Scientific Instrument High Energy Density Physics (HED)" (2014) doi:10.3204/XFEL.EU/TR-2014-001

[4] T. Tschentscher, C. Bressler, J. Grünert, A. Madsen, A. P. Mancuso, et al.: "Photon Beam Transport and Scientific Instruments at the European XFEL", Applied Sciences **7** (2017) doi:10.3390/app7060592

[5] W. Decking, S. Abeghyan, P. Abramian, A. Abramsky, A. Aguirre, et al.: "A MHz-repetition-rate hard X-ray free-electron laser driven by a superconducting linear accelerator", Nature Photonics **14**, 391–397 (2020) doi:10.1038/s41566-020-0607-z

[6] M. Störmer, F. Siewert, C. Horstmann, J. Buchheim, G. Gwalt: "Coatings for FEL optics: preparation and characterization of B_4C and Pt", Journal of Synchrotron Radiation **25**, 116–122 (2018) doi:10.1107/S1600577517016095

[7] H. Sinn, M. Dommach, B. Dickert, M. Di Felice, X. Dong, et al.: "The SASE1 X-ray beam transport system", Journal of Synchrotron Radiation **26**, 692–699 (2019) doi:10.1107/S1600577519003461

[8] A. Koch, J. Risch, W. Freund, T. Maltezopoulos, M. Planas, et al.: "Operation of photon diagnostic imagers for beam commissioning at the European XFEL", Journal of Synchrotron Radiation **26**, 1489–1495 (2019) doi:10.1107/S1600577519008737

[9] S. Casalbuoni, J. Baader, G. Geloni, V. Grattoni, D. La Civita, et al.: "TOWARDS A SUPERCONDUCTING UNDULATOR AFTERBURNER FOR THE EUROPEAN XFEL" (2021) doi:10.18429/JACoW-IPAC2021-WEPAB132

[10] T. Maltezopoulos, F. Dietrich, W. Freund, U. F. Jastrow, A. Koch, et al.: "Operation of X-ray gas monitors at the European XFEL", Journal of Synchrotron Radiation **26**, 1045–1051 (2019) doi:10.1107/S1600577519003795

[11] N. Kujala, W. Freund, J. Liu, A. Koch, T. Falk, et al.: "Hard x-ray single-shot spectrometer at the European X-ray Free-Electron Laser", Review of Scientific Instruments **91**, 103101 (2020) doi:10.1063/5.0019935

[12] H. Sinn, M. Dommach, X. Dong, D. La Civita, L. Samoylova, et al.: “Technical Design Report: X-Ray Optics and Beam Transport”, Technical Report (2012) doi:10.3204/XFEL.EU/TR-2012-006

[13] I. Petrov, U. Boesenberg, V. A. Bushuev, J. Hallmann, K. Kazarian, et al.: “Performance of a cryo-cooled crystal monochromator illuminated by hard X-rays with MHz repetition rate at the European X-ray Free-Electron Laser”, Opt. Express **30**, 4978–4987 (2022) doi:10.1364/OE.451110

[14] K. R. Tasca, A. Madsen, I. Petrov, A. Rodriguez-Fernandez, R. Shayduk, et al.: “Performance simulation of a diamond channel cut monochromator operating under high heat load at the European X-Ray Free-Electron Laser Facility”, X-Ray Free-Electron Lasers: Advances in Source Development and Instrumentation VI, ed. by T. Tschentscher, L. Patthey, K. Tiedtke, M. Zangrando, vol. 12581, International Society for Optics and Photonics, 125810L (SPIE 2023) doi:10.1117/12.2669178

[15] D. Shu, S. Narayanan, A. Sandy, M. Sprung, C. Preissner, et al.: “Precision mechanical design of an UHV-compatible artificial channel-cut x-ray monochromator”, New Developments in Optomechanics, ed. by A. E. Hatheway, vol. 6665, International Society for Optics and Photonics, 66650O (SPIE 2007) doi:10.1117/12.733101

[16] X. Dong, D. Shu, H. Sinn: “Design of a cryo-cooled artificial channel-cut crystal monochromator for the European XFEL”, AIP Conference Proceedings **1741**, 040027 (2016) doi:10.1063/1.4952899

[17] E. A. Schneidmiller, M. V. Yurkov, DESY: “Photon Beam Properties at the European XFEL (December 2010 Revision).”, Red Report (2011)

[18] B. Lengeler, C. Schroer, J. Tümmler, B. Benner, M. Richwin, et al.: “Imaging by parabolic refractive lenses in the hard X-ray range”, Journal of Synchrotron Radiation **6**, 1153–1167 (1999) doi:10.1107/S0909049599009747

[19] F. Seiboth, A. Schropp, M. Scholz, F. Wittwer, C. Rödel, et al.: “Perfect X-ray focusing via fitting corrective glasses to aberrated optics”, Nature Communications **8**, 14623 (2017) doi:10.1038/ncomms14623

[20] S. Makarov, M. Makita, M. Nakatsutsumi, T. Pikuz, N. Ozaki, et al.: “Direct LiF imaging diagnostics on refractive X-ray focusing at the EuXFEL High Energy Density instrument”, Journal of Synchrotron Radiation **30** (2023)

[21] S. Makarov, S. Grigoryev, N. Inogamov, E. Filippov, T. Pikuz, et al.: “Damage threshold of LiF crystal irradiated by femtosecond hard XFEL pulse sequence”, Optics Express **31**, 26383–26397 (2023)

[22] T. Pikuz, A. Faenov, T. Matsuoka, S. Matsuyama, K. Yamauchi, et al.: “3D visualization of XFEL beam focusing properties using LiF crystal X-ray detector”, Scientific Reports **5**, 17713 (2015)

[23] P. Heimann, N. J. Hartley, I. Inoue, V. Tkachenko, A. Antoine, et al.: “Non-thermal structural transformation of diamond driven by x-rays”, Structural Dynamics **10** (2023)

[24] O. de La Rochefoucauld, P. K. Cook, G. Dovillaire, F. Harms, L. Huang, et al.: “Hard X-Ray Hartmann Wavefront Sensor for Beamline Optimization”, Synchrotron Radiation News **35**, 3–7 (2022)

[25] T. Preston, S. Göde, J.-P. Schwinkendorf, K. Appel, E. Brambrink, et al.: “Design and performance characterisation of the HAPG von Hámos Spectrometer at the High Energy Density Instrument of the European XFEL”, Journal of Instrumentation **15**, P11033–P11033 (2020) doi:10.1088/1748-0221/15/11/p11033

[26] J. M. Kaa, Z. Konôpková, T. R. Preston, V. Cerantola, C. J. Sahle, et al.: “A von Hámos spectrometer for diamond anvil cell experiments at the High Energy Density Instrument of the European X-ray Free-Electron Laser”, Journal of Synchrotron Radiation **30** (2023)

[27] M. Harmand, M. Cammarata, M. Chollet, A. G. Krygier, H. T. Lemke, et al.: “Single-shot X-ray absorption spectroscopy at X-ray free electron lasers”, Scientific Reports **13**, 18203 (2023)

[28] G. Palmer, M. Kellert, J. Wang, M. Emons, U. Wegner, et al.: “Pump-probe laser system at the FXE and SPB/SFX instruments of the European X-ray Free-Electron Laser Facility”, Journal of Synchrotron Radiation **26**, 328–332 (2019) doi:10.1107/S160057751900095X

[29] M. Pergament, G. Palmer, M. Kellert, K. Kruse, J. Wang, et al.: “Versatile optical laser system for experiments at the European X-ray free-electron laser facility”, Opt. Express **24**, 29349–29359 (2016) doi:10.1364/OE.24.029349

[30] A. L. Garcia, H. Höppner, A. Pelka, C. Bähtz, E. Brambrink, et al.: “ReLaX: the Helmholtz International Beamline for Extreme Fields high-intensity short-pulse laser driver for relativistic laser–matter interaction and strong-field science using the high energy density instrument at the European X-ray free electron laser facility”, High Power Laser Science and Engineering **9**, e59 (2021)

[31] P. J. Phillips, P. Mason, K. Ertel, J. Smith, M. De-Vido, et al.: “A kW-class nanosecond DPSSL operating at 100 J, 10 Hz for high energy density research at the European XFEL (Conference Presentation)”, High Power Lasers for Fusion Research V, ed. by A. A. S. Awwal, C. L. Haefner, vol. 10898, International Society for Optics and Photonics (SPIE 2019) doi:10.1117/12.2505605

[32] J. P. Phillips, S. Banerjee, P. Mason, J. Smith, J. Spear, et al.: “Second and Third harmonic conversion of a high energy, 1 KW average power diode-pumped, Yb:YAG amplifier in phase-matched Lithium Triborate”, To be submitted in optics letters, 2021

[33] Paul Scherrer Institute: *Jungfrau detectors* https://www.psi.ch/en/lxn/jungfrau

[34] Linac Coherent Light Source (LCLS): *ePIX100 detectors* https://lcls.slac.stanford.edu/detectors/ePix100

[35] A. Allahgholi, J. Becker, A. Delfs, R. Dinapoli, P. Göttlicher, et al.: "Megapixels @ Megahertz – The AGIPD high-speed cameras for the European XFEL", Nuclear Instruments and Methods in Physics Research Section A: Accelerators, Spectrometers, Detectors and Associated Equipment **942**, 162324 (2019) doi:https://doi.org/10.1016/j.nima.2019.06.065

[36] J. Kim, S. Göde, S. Glenzer: "Development of a cryogenic hydrogen microjet for high-intensity, high-repetition rate experiments", Review of Scientific Instruments **87**, 11E328 (2016)

[37] L. Obst, S. Göde, M. Rehwald, F.-E. Brack, J. Branco, et al.: "Efficient laser-driven proton acceleration from cylindrical and planar cryogenic hydrogen jets", Scientific reports **7**, 1–9 (2017)

[38] S. Göde, C. Rödel, K. Zeil, R. Mishra, M. Gauthier, et al.: "Relativistic electron streaming instabilities modulate proton beams accelerated in laser-plasma interactions", Physical review letters **118**, 194801 (2017)

[39] B. Heisen, D. Boukhelef, S. Esenov, S. Hauf, I. Kozlova, et al.: "Karabo: An integrated software framework combining control, data management, and scientific computing tasks", 14th International Conference on Accelerator & Large Experimental Physics Control Systems, ICALEPCS2013. San Francisco, CA (2013)

[40] H. Fangohr et al.: "Data Analysis Support in Karabo at European XFEL", Barcelona, Spain, Proc. of International Conference on Accelerator and Large Experimental Control Systems (ICALEPCS'17), Barcelona, Spain, 8-13 October 2017, International Conference on Accelerator and Large Experimental Control Systems 16, https://doi.org/10.18429/JACoW-ICALEPCS2017-TUCPA01, 245–252 (JACoW, Geneva, Switzerland 2018) doi:https://doi.org/10.18429/JACoW-ICALEPCS2017-TUCPA01

[41] N. Otsu: "A threshold selection method from gray-level histograms", IEEE transactions on systems, man, and cybernetics **9**, 62–66 (1979)

[42] M. Schölmerich: "Dynamic compression experiments of SiO_2 and GeO_2 at synchrotron-and X-ray free electron laser (XFEL) light sources", PhD thesis (Universität Rostock 2020)

[43] N. Biedermann: "Carbonate-silicate reactions at conditions of the Earth's mantle and the role of carbonates as possible trace-element carriers", PhD thesis (Universität Potsdam 2020)

[44] C. Plückthun: "Investigating the effect of the compression rate on the kinetic response of diamond anvil cell experiments", PhD thesis (Universität Rostock 2022)

[45] M. Banjafar: “Dynamical evolution of a high-density plasma surface upon high-intensity laser-solid interaction”, PhD thesis (Dissertation, Dresden, Technische Universität 2022)

[46] J. Kaa: “Electronic spin state studies of iron-bearing minerals contained in an X-ray heated diamond anvil cell”, PhD thesis (Dissertation, Dortmund, Technische Universität 2023)

[47] M. O. Schoelmerich, T. Tschentscher, S. Bhat, C. A. Bolme, E. Cunningham, et al.: “Evidence of shock-compressed stishovite above 300 GPa”, Scientific Reports **10**, 10197 (2020)

[48] L. Randolph, M. Banjafar, T. R. Preston, T. Yabuuchi, M. Makita, et al.: “Nanoscale subsurface dynamics of solids upon high-intensity femtosecond laser irradiation observed by grazing-incidence x-ray scattering”, Physical Review Research **4**, 033038 (2022)

[49] D. Kraus, J. Vorberger, N. Hartley, J. Lütgert, M. Rödel, et al.: “Indirect evidence for elemental hydrogen in laser-compressed hydrocarbons”, Physical Review Research **5**, L022023 (2023)

[50] J. Lütgert, J. Vorberger, N. Hartley, K. Voigt, M. Rödel, et al.: “Measuring the structure and equation of state of polyethylene terephthalate at megabar pressures”, Scientific reports **11**, 12883 (2021)

[51] L. Gaus, L. Bischoff, M. Bussmann, E. Cunningham, C. B. Curry, et al.: “Probing ultrafast laser plasma processes inside solids with resonant small-angle x-ray scattering”, Physical Review Research **3**, 043194 (2021)

[52] L. B. Fletcher, J. Vorberger, W. Schumaker, C. Ruyer, S. Goede, et al.: “Electron-ion temperature relaxation in warm dense hydrogen observed with picosecond resolved x-ray scattering”, Frontiers in Physics **10**, 139 (2022)

[53] A. K. Schuster, K. Voigt, B. Klemmed, N. J. Hartley, J. Lütgert, et al.: “Recovery of release cloud from laser shock-loaded graphite and hydrocarbon targets: in search of diamonds”, Journal of Physics D: Applied Physics **56**, 025301 (2022)

[54] T. Gawne, T. Campbell, A. Forte, P. Hollebon, G. Perez-Callejo, et al.: “Investigating mechanisms of state localization in highly ionized dense plasmas”, Phys. Rev. E **108**, 035210 (2023) doi:10.1103/PhysRevE.108.035210

[55] J.-W. Lee, M. Kim, G. Kang, S. M. Vinko, L. Bae, et al.: “Investigation of nonequilibrium electronic dynamics of warm dense copper with femtosecond x-ray absorption spectroscopy”, Physical Review Letters **127**, 175003 (2021)

[56] J. Krása, T. Burian, V. Hájková, J. Chalupskỳ, Š. Jelınek, et al.: “Ion emission from warm dense matter produced by irradiation with a soft x-ray free-electron laser”, Matter and Radiation at Extremes **9** (2024)

[57] E. Stavrou, A. A. Maryewski, S. S. Lobanov, A. R. Oganov, Z. Konôpková, et al.: “Ethane and methane at high pressures: Structure and stability”, The Journal of Chemical Physics **155** (2021)

[58] N. Biedermann, E. Bykova, W. Morgenroth, I. Efthimiopoulos, J. Mueller, et al.: “Equation of state and high-pressure phase behaviour of $SrCO_3$”, European Journal of Mineralogy **32**, 575–586 (2020)

[59] G. Serghiou, H. J. Reichmann, N. Odling, K. Spektor, A. Pakhomova, et al.: “An unexpected cubic symmetry in group IV alloys prepared using pressure and temperature”, Angewandte Chemie International Edition **60**, 9009–9014 (2021)

[60] R. J. Husband, E. F. O’Bannon, H.-P. Liermann, M. J. Lipp, A. S. Méndez, et al.: “Compression-rate dependence of pressure-induced phase transitions in Bi”, Scientific reports **11**, 14859 (2021)

[61] M. Schoelmerich, A. Mendez, C. Plueckthun, N. Biedermann, R. Husband, et al.: “In situ x-ray diffraction study of dynamically compressed α-cristobalite using a dynamic diamond anvil cell”, Physical Review B **105**, 064109 (2022)

[62] C. Albers, R. Sakrowski, N. Thiering, L. Libon, G. Spiekermann, et al.: “High-efficiency X-ray emission spectroscopy of cold-compressed Fe 2 O 3 and laser-heated pressurized FeCO 3 using a von Hámos spectrometer”, Journal of Analytical Atomic Spectrometry **38**, 1097–1107 (2023)

[63] A. R. Thomson, R. O. Piltz, W. A. Crichton, V. Cerantola, I. S. Ezad, et al.: “Incorporation of tetrahedral ferric iron into hydrous ringwoodite”, American Mineralogist: Journal of Earth and Planetary Materials **106**, 900–908 (2021)

[64] M. Campione, M. Murri, V. Cerantola, D. Bessas, A. Rosenthal, et al.: “Magnetic Ordering of Magnetite Inclusions in Olivine at Mantle Depths in Subduction Zones”, ACS Earth and Space Chemistry **6**, 2755–2759 (2022)

[65] V. Cerantola, C. J. Sahle, S. Petitgirard, M. Wu, S. Checchia, et al.: “Tetracarbonates in silicate melts may be at the origin of a deep carbon reservoir in the deep Earth”, Communications Earth & Environment **4**, 67 (2023)

[66] C. Bernert, S. Assenbaum, F.-E. Brack, T. E. Cowan, C. B. Curry, et al.: “Off-harmonic optical probing of high intensity laser plasma expansion dynamics in solid density hydrogen jets”, Scientific Reports **12**, 7287 (2022)

[67] C. Bernert, S. Assenbaum, S. Bock, F.-E. Brack, T. E. Cowan, et al.: “Transient Laser-Induced Breakdown of Dielectrics in Ultrarelativistic Laser-Solid Interactions”, Physical Review Applied **19**, 014070 (2023)

[68] M. Rehwald, S. Assenbaum, C. Bernert, F.-E. Brack, M. Bussmann, et al.: “Ultra-short pulse laser acceleration of protons to 80 MeV from cryogenic hydrogen jets tailored to near-critical density”, Nature communications **14**, 4009 (2023)

[69] G. Pérez-Callejo, V. Bouffetier, L. Ceurvorst, T. Goudal, S. Klein, et al.: “Phase imaging of irradiated foils at the OMEGA EP facility using phase-stepping X-ray Talbot-Lau deflectometry”, High Power Laser Science and Engineering, 1–11 ()

[70] M. Valdivia, G. Perez-Callejo, V. Bouffetier, G. Collins, C. Stoeckl, et al.: “Current advances on Talbot–Lau x-ray imaging diagnostics for high energy density experiments”, Review of Scientific Instruments **93** (2022)

[71] T. Dornheim, M. Böhme, D. Kraus, T. Döppner, T. R. Preston, et al.: “Accurate temperature diagnostics for matter under extreme conditions”, Nature Communications **13**, 7911 (2022)

[72] G. Pérez-Callejo, V. Bouffetier, L. Ceurvorst, T. Goudal, M. Valdivia, et al.: “TIA: A forward model and analyzer for Talbot interferometry experiments of dense plasmas”, Physics of Plasmas **29** (2022)

[73] T. Dornheim, Z. A. Moldabekov, K. Ramakrishna, P. Tolias, A. D. Baczewski, et al.: “Electronic density response of warm dense matter”, Physics of Plasmas **30** (2023)

[74] N. Medvedev, Z. Kuglerová, M. Makita, J. Chalupskỳ, L. Juha: “Damage threshold in pre-heated optical materials exposed to intense X-rays”, Optical Materials Express **13**, 808–822 (2023)

[75] T. Dornheim, M. P. Böhme, D. A. Chapman, D. Kraus, T. R. Preston, et al.: “Imaginary-time correlation function thermometry: A new, high-accuracy and model-free temperature analysis technique for x-ray Thomson scattering data”, Physics of Plasmas **30** (2023)

[76] F. Paschke-Bruehl, M. Banjafar, M. Garten, L. Huang, B. E. Marré, et al.: “Heating in multi-layer targets at ultra-high intensity laser irradiation and the impact of density oscillation”, New Journal of Physics **25**, 043024 (2023)

[77] V. Cerantola, A. D. Rosa, Z. Konôpková, R. Torchio, E. Brambrink, et al.: “New frontiers in extreme conditions science at synchrotrons and free electron lasers”, Journal of Physics: Condensed Matter **33**, 274003 (2021) doi:10.1088/1361-648X/abfd50

[78] U. Zastrau, C. Fortmann, R. Fäustlin, L. Cao, T. Döppner, et al.: “Bremsstrahlung and line spectroscopy of warm dense aluminum plasma heated by xuv free-electron-laser radiation”, Physical Review E **78**, 066406 (2008)

[79] “Turning solid aluminium transparent by intense soft X-ray photoionization”, Nature Physics **5**, 693–696 (2009)

[80] S. Vinko, O. Ciricosta, B. Cho, K. Engelhorn, H.-K. Chung, et al.: “Creation and diagnosis of a solid-density plasma with an X-ray free-electron laser”, Nature **482**, 59–62 (2012)

[81] K. Voigt, M. Zhang, K. Ramakrishna, A. Amouretti, K. Appel, et al.: “Demonstration of an x-ray Raman spectroscopy setup to study warm dense carbon at the high energy density instrument of European XFEL”, Physics of Plasmas **28** (2021)

[82] D. Ranjan, K. Ramakrishna, K. Voigt, O. Humphries, B. Heuser, et al.: “Toward using collective x-ray Thomson scattering to study C–H demixing and

hydrogen metallization in warm dense matter conditions", Physics of Plasmas **30** (2023)

[83] O. Ball, C. Prescher, K. Appel, C. Baehtz, M. Baron, et al.: "Dynamic optical spectroscopy and pyrometry of static targets under optical and x-ray laser heating at the European XFEL", Journal of Applied Physics **134** (2023)

[84] N. Jaisle, D. Cébron, Z. Konôpková, R. J. Husband, C. Prescher, et al.: "MHz free electron laser x-ray diffraction and modeling of pulsed laser heated diamond anvil cell", Journal of Applied Physics **134** (2023)

[85] R. J. Husband, C. Strohm, K. Appel, O. B. Ball, R. Briggs, et al.: "A MHz X-ray diffraction set-up for dynamic compression experiments in the diamond anvil cell", Journal of Synchrotron Radiation **30** (2023)

[86] H. Hwang, T. Kim, H. Cynn, T. Vogt, R. J. Husband, et al.: "X-ray Free Electron Laser-Induced Synthesis of ε-Iron Nitride at High Pressures", The Journal of Physical Chemistry Letters **12**, 3246–3252 (2021)

[87] M. Frost, R. S. McWilliams, E. Bykova, M. Bykov, R. J. Husband, et al.: "Diamond precipitation dynamics from hydrocarbons at icy planet interior conditions", Nature Astronomy, 1–8 (2024)

[88] J. M. Kaa, C. Sternemann, K. Appel, V. Cerantola, T. R. Preston, et al.: "Structural and electron spin state changes in an x-ray heated iron carbonate system at the Earth's lower mantle pressures", Phys. Rev. Res. **4**, 033042 (2022) doi:10.1103/PhysRevResearch.4.033042

[89] M. Šmıd, C. Baehtz, A. Pelka, A. Laso Garcıa, S. Göde, et al.: "Mirror to measure small angle x-ray scattering signal in high energy density experiments", Review of Scientific Instruments **91**, 123501 (2020)

[90] S. V. Roth: "A deep look into the spray coating process in real-time - The crucial role of x-rays", Journal of Physics Condensed Matter **28** (2016) doi:10.1088/0953-8984/28/40/403003

[91] A. Rudenko, A. Abou-Saleh, F. Pigeon, C. Mauclair, F. Garrelie, et al.: "High-frequency periodic patterns driven by non-radiative fields coupled with Marangoni convection instabilities on laser-excited metal surfaces", Acta Materialia **194**, 93–105 (2020) doi:https://doi.org/10.1016/j.actamat.2020.04.058

[92] J. Bonse, S. Höhm, S. V. Kirner, A. Rosenfeld, J. Krüger: "Laser-Induced Periodic Surface Structures— A Scientific Evergreen", IEEE Journal of Selected Topics in Quantum Electronics **23** (2017) doi:10.1109/JSTQE.2016.2614183

[93] J. Vorberger, K. Plageman, R. Redmer: "The structure in warm dense carbon", High Energy Density Physics **35**, 100737 (2020)

[94] D. Kraus, J. Vorberger, J. Helfrich, D. Gericke, B. Bachmann, et al.: "The complex ion structure of warm dense carbon measured by spectrally resolved x-ray scattering", Physics of Plasmas **22** (2015)

[95] S. M. Sharma, S. J. Turneaure, J. Winey, Y. Gupta: “Transformation of shock-compressed copper to the body-centered-cubic structure at 180 GPa”, Physical Review B **102**, 020103 (2020)

[96] T. Yamaji, K. Tamasaku, T. Namba, T. Yamazaki, Y. Seino: “Search for Axion like particles using Laue-case conversion in a single crystal”, Physics Letters B **782**, 523–527 (2018)

[97] F. Karbstein, E. A. Mosman: “X-ray photon scattering at a focused high-intensity laser pulse”, Physical Review D **100**, 033002 (2019)

[98] H.-P. Schlenvoigt, T. Heinzl, U. Schramm, T. E. Cowan, R. Sauerbrey: “Detecting vacuum birefringence with x-ray free electron lasers and high-power optical lasers: a feasibility study”, Physica Scripta **91**, 023010 (2016)

[99] K. S. Schulze, B. Grabiger, R. Loetzsch, B. Marx-Glowna, A. T. Schmitt, et al.: “Towards perfectly linearly polarized x-rays”, Physical Review Research **4**, 013220 (2022)

[100] F. Karbstein, H. Gies, M. Reuter, M. Zepf: “Vacuum birefringence in strong inhomogeneous electromagnetic fields”, Physical Review D **92**, 071301 (2015)

[101] S. Liu, C. Grech, M. Guetg, S. Karabekyan, V. Kocharyan, et al.: “Cascaded hard X-ray self-seeded free-electron laser at megahertz repetition rate”, Nature Photonics, 1–8 (2023)

[102] M. Prasciolu, K. T. Murray, N. Ivanov, H. Fleckenstein, M. Domarackỳ, et al.: “On the use of multilayer Laue lenses with X-ray free electron lasers”, International Conference on X-Ray Lasers 2020, ed. by D. Bleiner, vol. 11886, International Society for Optics and Photonics, 118860M (SPIE 2021) doi:10.1117/12.2592229

[103] V. Kärcher, S. Roling, L. Samoylova, A. Buzmakov, U. Zastrau, et al.: “Impact of real mirror profiles inside a split-and-delay unit on the spatial intensity profile in pump/probe experiments at the European XFEL”, Journal of Synchrotron Radiation **28**, 350–361 (2021)

[104] S. Roling, K. Appel, S. Braun, A. Buzmakoc, O. Chubar, et al.: “A hard x-ray split-and-delay unit for the HED experiment at the European XFEL”, Spie Proceedings **9210**, 92100B–1 (2017)

[105] Y. Kayser, C. Milne, P. Juranić, L. Sala, J. Czapla-Masztafiak, et al.: “Core-level nonlinear spectroscopy triggered by stochastic X-ray pulses”, Nature communications **10**, 4761 (2019)

[106] F. D. Fuller, A. Loukianov, T. Takanashi, D. You, Y. Li, et al.: “Resonant X-ray emission spectroscopy from broadband stochastic pulses at an X-ray free electron laser”, Communications chemistry **4**, 84 (2021)

[107] W. Błachucki, Y. Kayser, A. Wach, R. Fanselow, C. Milne, et al.: “Resonant X-ray Emission Spectroscopy with a SASE Beam”, Applied Sciences **11**, 8775 (2021)

[108] S. H. Glenzer, R. Redmer: “X-ray Thomson scattering in high energy density plasmas”, Reviews of Modern Physics **81**, 1625 (2009)

[109] L. Fletcher, H. Lee, T. Döppner, E. Galtier, B. Nagler, et al.: “Ultrabright X-ray laser scattering for dynamic warm dense matter physics”, Nature photonics **9**, 274–279 (2015)

[110] U. Zastrau, E. Gamboa, D. Kraus, J. Benage, R. Drake, et al.: “Tracking the density evolution in counter-propagating shock waves using imaging X-ray scattering”, Applied physics letters **109** (2016)

[111] T. Preston, K. Appel, E. Brambrink, B. Chen, L. Fletcher, et al.: “Measurements of the momentum-dependence of plasmonic excitations in matter around 1 Mbar using an X-ray free electron laser”, Applied Physics Letters **114** (2019)

[112] J. Stefan: “Über die Beziehung zwischen der Wärmestrahlung und der Temperatur”, Sitzungsber. Kaiserl. Akad. Wiss. Math. Naturwiss. Cl. II. Abth. **79**, 391–428 (1879)

[113] L. Boltzmann: “Ableitung des Stefan’schen Gesetzes, betreffend die Abhängigkeit der Wärmestrahlung von der Temperatur aus der electromagnetischen Lichttheorie”, Annalen der Physik **258**, 291–294 (1884) doi:10.1002/andp.18842580616

[114] S. M. Sharma, Y. M. Gupta: “Inherent issues regarding the use of *in situ* x-ray diffraction measurements to determine temperature in shock-compressed metals”, Physical Review B **104** (2021) doi:10.1103/physrevb.104.064113

[115] A. Descamps, B. Ofori-Okai, K. Appel, V. Cerantola, A. Comley, et al.: “An approach for the measurement of the bulk temperature of single crystal diamond using an X-ray free electron laser”, Scientific Reports **10**, 14564 (2020)

[116] L. Wollenweber, T. R. Preston, A. Descamps, V. Cerantola, A. Comley, et al.: “High-resolution inelastic x-ray scattering at the high energy density scientific instrument at the Free-Electron Laser”, Review of Scientific Instruments **92**, 013101 (2021) doi:10.1063/5.0022886

[117] T. Scopigno, G. Ruocco, F. Sette: “Microscopic dynamics in liquid metals: The experimental point of view”, Reviews of Modern Physics **77**, 881–933 (2005) doi:10.1103/revmodphys.77.881

[118] L. Huang, H.-P. Schlenvoigt, H. Takabe, T. Cowan: “Ionization and reflux dependence of magnetic instability generation and probing inside laser-irradiated solid thin foils”, Physics of Plasmas **24** (2017)

[119] T. Wang, T. Toncian, M. Wei, A. Arefiev: “Structured targets for detection of Megatesla-level magnetic fields through Faraday rotation of XFEL beams”, Physics of plasmas **26**, 013105 (2019)

[120] *Positionspapier Fusionsforschung - BMBF*, 2023

A User institutions and countries

Table A.1: HED user institutions

Institution	Country
Aarhus University	Denmark
AGH University of Science and Technology	Poland
Aix-Marseille Université	France
ALBA Synchrotron Light Source	Spain
Albert-Ludwigs University of Freiburg	Germany
Argonne National Laboratory (ANL)	United States
Arizona State University (ASU)	United States
Atomic Weapons Establishment (AWE)	United Kingdom
Brigham Young University	United States
Bundesanstalt für Materialforschung und -prüfung (BAM)	Germany
California Institute of Technology (Caltech)	United States
Central Laser Facility (CLF)	United Kingdom
Charles University	Czech Republic
Chinese Academy of Sciences (CAS)	China
CNR - Consiglio Nazionale delle Ricerche	Italy
CNRS - DSI Meudon	France
CNRS - Université de Bordeaux	France
Commissariat a L'Energie Atomique (CEA)	France
Consiglio Nazionale delle Ricerche Bari	Italy
Coventry University	United Kingdom
Czech Academy of Sciences (CAS)	Czech Republic
DESY Deutsches Elektronen-Synchrotron	Germany
Diamond Light Source Ltd	United Kingdom
Durham University	United Kingdom
Ecole Normale Superieure (ENS)	France
Ecole Polytechnique Federale de Lausanne (EPFL)	Switzerland
Ecole Polytechnique, Palaiseau	France
ELI Beamlines	Czech Republic
ETH Zurich	Switzerland
European Synchrotron Radiation Facility - ESRF	International
European XFEL GmbH	International
Friedrich-Alexander-Universitaet Erlangen-Nuernberg	Germany

Friedrich-Schiller-Universität Jena	Germany
FSRC “Crystallography and Photonics” RAS	Russia
Geophysical Laboratory	United States
Georgia Institute of Technology	United States
Goethe University Frankfurt	Germany
GSI Helmholtzzentrum für Schwerionenforschung	Germany
Gwangju Institute of Science and Technology	South Korea
Hanyang University	South Korea
HB11 Energy Holdings Pty Ltd	Australia
Heinrich-Heine-Universität Düsseldorf (HHU)	Germany
Helmholtz-Zentrum Berlin ... GmbH (HZB)	Germany
Helmholtz-Zentrum Dresden-Rossendorf (HZDR)	Germany
Helmholtz-Zentrum Potsdam (GFZ)	Germany
Hochschule Mittweida, University of Applied Sciences	Germany
Horia Hulubei National Institute (IFIN-HH)	Romania
HPSTAR	China
Immanuel Kant Baltic Federal University	Russia
Imperial College London	United Kingdom
Indian Institute of Science	India
Institut Minéralogie, de Physique ... (IMPMC)	France
Institute for High pressure Physics (HPPI RAS)	Russia
Instituto de Plasmas e Fusão Nuclear	Portugal
ISIS Neutron and Muon Source	United Kingdom
Istituto Nazionale di Fisica Nucleare (INFN)	Italy
Johannes Gutenberg University Mainz (JGU)	Germany
Joint Institute for High Temperatures (JIHT RAS)	Russia
Joint Institute for Nuclear Research (JINR)	Russia
Korea Research Institute of Standards and Science (KRISS)	South Korea
KTH Royal Institute of Technology	Sweden
Lawrence Berkeley National Laboratory (Berkeley Lab)	United States
Lawrence Livermore National Lab. LLNL	United States
Lebedev Physical Institute (LPI RAS)	Russia
Los Alamos National Laboratory	United States
Lund University	Sweden
Massachusetts Institute of Technology	United States
Max Planck Institut für Kohlenforschung	Germany
Max Planck Institute (MPI) for Polymer Research	Germany
Max Planck Institute for Nuclear Physics (MPIK)	Germany
Moscow Steel & Alloys Institute	Russia
MTC - Manufacturing Technology Centre	United Kingdom

NASA Ames Research Center	United States
National Research Centre (NRC) “Kurchatov Institute”	Russia
National University - NUST MISIS	Russia
Nevada National Security Site (NNSS)	United States
Nikolaev Institute of Inorganic Chemistry SB RAS (NIIC)	Russia
Osaka University	Japan
Paul Scherrer Institut (PSI)	Switzerland
Pavol Jozef Safarik University in Kosice (UPJS)	Slovakia
Pohang Accelerator Lab.	South Korea
Pohang Accelerator Laboratory	South Korea
Polish Academy of Sciences	Poland
Princeton University	United States
Queen Mary University of London	United Kingdom
Queen’s University Belfast	United Kingdom
Rensselaer Polytechnic Institute (RPI)	United States
RIKEN Harima Institute	Japan
RWTH Aachen University	Germany
Sandia National Laboratories	United States
SLAC National Accelerator Laboratory	United States
Slovak Academy of Sciences	Slovakia
Sobolev Institute of Geology and Mineralogy SB RAS	Russia
Sogang University	South Korea
Sorbonne University	France
Southwest Jiaotong University	China
Stanford University	United States
Stanford University and SLAC	United States
Stony Brook University	United States
Synchrotron SOLEIL	France
Technical University of Denmark (DTU)	Denmark
Technische Universität (TU) Dortmund	Germany
Technische Universität Darmstadt	Germany
Technische Universität Dresden (TUD)	Germany
Technische Universität Kaiserslautern	Germany
The Peac Institute of Multiscale Sciences	China
The Pennsylvania State University (Penn State)	United States
The University of Chicago	United States
The University of Edinburgh	United Kingdom
The University of Texas at El Paso - UTEP	United States
TU Bergakademie Freiberg	Germany
UKAEA	United Kingdom

Universidad Autónoma de Madrid (UAM)	Spain
Universidad de Oviedo	Spain
Universidad de Valencia - UV	Spain
Universidad Politecnica de Madrid	Spain
Università degli Studi dell'Insubria	Italy
Università degli Studi di Milano Bicocca	Italy
Università degli Studi di Padova	Italy
Università di Camerino	Italy
Università di Pavia	Italy
Università di Trento	Italy
Universität Duisburg-Essen (UDE)	Germany
Universität für Bodenkultur Wien (BOKU)	Austria
Universität Potsdam	Germany
Universität Rostock	Germany
Universität Siegen	Germany
Universität zu Köln	Germany
Université de Bourgogne (uB)	France
Université de Lille, CNRS	France
Université Grenoble Alpes	France
Université Rennes 1	France
University Bayreuth	Germany
University College London (UCL)	United Kingdom
University of Alberta	Canada
University of California - Berkeley	United States
University of California San Diego - UCSD	United States
University of Cambridge	United Kingdom
University of Copenhagen (UCPH)	Denmark
University of Fribourg	Switzerland
University of Hamburg (UHH)	Germany
University of Helsinki	Finland
University of Massachusetts Amherst	United States
University of Michigan	United States
University of Nevada, Las Vegas	United States
University of Nevada, Reno	United States
University of Oxford	United Kingdom
University of Plymouth	United Kingdom
University of Rochester	United States
University of South Florida - USF	United States
University of Strathclyde	United Kingdom
University of Toronto	Canada

University of Toyama	Japan
University of Valladolid	Spain
University of Warwick	United Kingdom
University of Washington - UW	United States
University of York	United Kingdom
University of Zurich	Switzerland
Washington State University	United States
Weizmann Institute of Science	Israel
Westfälische Wilhelms-Universität (WWU) Münster	Germany
Wigner Research Centre for Physics	Hungary
Yonsei University	South Korea

B Proposal Review Panels

The Proposal Review Panel (PRP) meets two times per year to discuss and rank the incoming proposals. Table **??** shows the current and past members of the HED PRP.

Table B.1: PRP members as of January 2023.

Name	**Affiliation**
Ryszard Sobierajski	Polish Academy of Sciences
Chair	Warsaw, Poland
Michael Armstrong	Lawrence Livermore National Laboratory
	Livermore,USA
Alessandra Benuzzi	Laboratoire pour l'Utilisation des Lasers Intenses, LULI
	Paris, France
Zahirul Islam	Argonne National Laboratory
(future chair)	Lemont, USA
Paul Loubeyre	CEA
	Arpajon, France
Stuart Mangles	Imperial College
	London, UK
Emma McBride	Queen's University
	Belfast, Ireland
Paul Neumayer	GSI Helmholtzzentrum für Schwerionenforschung
	Darmstadt, Germany
Luca Volpe	Centro de Láseres Pulsados, CLPU
	Salamanca, Spain
Matt Zepf	Friedrich Schiller University
	Jena, Germany
	Former members
Guillaume Fiquet	IMPMC, Paris, France
Mattias Marklund	Chalmers University, Gothenburg, Sweden
David Neely	Central Laser Facility, Didcot, United Kingdom
Norimasa Ozaki	Osaka University, Osaka, Japan
Sakura Pascarelli	European Synchrotron Radiation Facility
	Grenoble, France *(Chairwoman)*
Sergey Pikuz	Joint Institute for High Temperatures, Moscow, Russia
	(Membership suspended from May 2022)
Klaus Sokolowski-Tinten	University Duisburg-Essen, Germany

Index